UNIVERSITÀ DI PARMA

UNIVERSITA' DEGLI STUDI DI PARMA

DOTTORATO DI RICERCA IN
" *Scienza e Tecnologia dei Materiali* "

CICLO XXXVII

Low-friction Silane-based Coating on Pharmaceutical Glass Vials: Development of Alternative Solutions to Standard Industrial Process

Coordinatore:
Chiar.mo Prof. Enrico Dalcanale

Tutore:
Dott.ssa Giovanna Trevisi

Dottoranda: Tiziana Pastore

Anni Accademici 2021/2022 – 2023/2024

Summary

Abstract

The pharmaceutical packaging industry faces a fundamental challenge in preserving the strength of glass containers, requiring coatings to ensure smoothness and functionality along production and filling lines. Current coating processes involve the application of a metal oxide primer and a subsequent lubricating layer in two stages (hot-end and cold-end coating), the first of which requires a dedicated equipment to manage toxic fume emissions. This PhD research, conducted in collaboration with Bormioli Pharma S.p.A., aims to develop a sustainable lubricant coating for glass vials as an alternative to the current hot-end coating. Organosilane-based solutions were explored for their environmental and economic advantages. In particular, an aqueous-based aminosilane as adhesion promoter for lubricant anchoring and an alternative organosilane in water as one-component coating were investigated. Both approaches were initially tested with dip coating deposition, followed by spray application on soda-lime-silica vials and pieces of vials to evaluate their industrial scalability. The coated surfaces were analysed with morphological, chemical and mechanical characterisations. The results show that the organosilane primer effectively promotes lubricant adhesion, protects the vial surface and can be successfully deposited with spray systems, thus fulfilling the requirement of industrial scalability. Mechanical tests, consisting in tribological and scratch resistance tests, confirmed lubrication, particularly for the primer-lubricant spray mixture. The one-component organosilane solution showed promising protective qualities during spray application, although further studies are needed to confirm its full potential. Overall, replacing the traditional hot-end process with a silane primer offers several industrial advantages, including greater sustainability and the possibility of combining primer and lubricant in a single spray application step, which is also cost-effective. This innovative approach offers the possibility to reduce the environmental impact and production costs of pharmaceutical vials, facilitating large-scale commercial implementation. Future research will focus on optimising the molecular interaction between primer and lubricant, improving the functionality of single-component lubrication, and refining mechanical testing methods to more accurately simulate the movement of vials on production and filling lines.

1. Introduction

1.1 Glass for Pharma Packaging

Glass has historically been used in the production of containers for storing products considered precious. Early civilisations used glass vessels for storing and transporting 'sacred' liquids, such as oils and perfumes in Egypt, wine and funerary materials among the Greeks and Romans. In the 17th century, new moulding equipment enabled the mass production of glass bottles mainly used to hold wines. From the 18th century onwards, glass began to be used for transporting and storing medicines in both dry and liquid form, until the present day, the 21st century, when it still remains the material of choice for storing and preserving pharmaceutical products [1]. *Figure 1.1* shows some examples of glass containers and their evolution over time.

Figure 1.1 Evolution of pharmaceutical container shape, size, color, and glass composition from 1600s through today. From left to right: (a) manually free-blown soda-lime bottle circa 17th century, (b) manually mold-blown soda-lime bottle circa 18th century, (c) manually mold-blown soda-lime vial circa 1840 –1860, (d) manually mold-blown soda-lime bottle circa 1865–1915, (e)semi-automatically mold blown soda-lime bottle circa 1880 –1920, and (f) borosilicate vials: mold blown amber and tubular converted clear circa 2013–2016. Objects a– e are from the collection of the Corning Museum of Glass, Corning, NY [1].

Thanks to the remarkable progress in glass production over the last two centuries, despite the introduction of alternatives such as plastic, no new material has been developed that can compete with glass in terms of effectiveness in preserving these precious substances [2]. In 2012, approximately 98% of injectable products were stored in glass containers [3]. The reason lies in the fact that it possesses a combination of properties that surpass those of other materials:

i. not- porosity and high density
ii. high transparency for content inspection or coloured for light protection
iii. impermeability to liquids and gases
iv. excellent chemical durability
v. moldability into various shapes

Unlike ceramics, glass is not porous, which eliminates the risk of evaporation losses or contamination by substances trapped in the pores. Substances that are introduced in the glass melt to act as colorants, refiners, stabilizers are strongly bounded to the vitreous network and may migrate to a minimum extent. Its transparency allows the contents to be easily inspected for signs of degradation or contamination, while coloured glass offers additional functionality, such as protection from light-induced degradation [4]. In addition, glass is a perfect barrier for liquids and gases, preventing oxidation or other forms of degradation of the contents. It can also be remoulded by heating into complex shapes with thin walls without compromising its structural integrity, thanks to its high elastic modulus, which prevents deformation under applied loads [1]. Chemically, glass is more durable than metals and other crystalline materials and offers superior resistance to a wide range of solutions, thus minimising the impact of the container on its contents [5].

The choice of packaging material in the pharmaceutical industry is primarily based on its physico-chemical properties, which must be compatible with the type of dosage form, the method of application, and the formulation's characteristics. Commercial glass, an inorganic material primarily composed of silicates, is widely used for this purpose. It is produced by heating various materials to a molten state and then cooling them without allowing crystallization (see *Fig. 1.2*). Several metal oxides, such as SiO_2, B_2O_3, P_2O_5 and GeO_2, possess the ability to cool without crystallising and these serve as the foundation of glass, hence they are called network-forming

oxides [6]. Among them, SiO_2 is the most commonly used in pharmaceutical applications, due to its excellent resistance to chemical corrosion (notably from acids), minimal electrical conductivity (5.5×10^{-7}/°C), very low thermal expansion coefficient, and effective transparency to ultraviolet (UV) light [7].

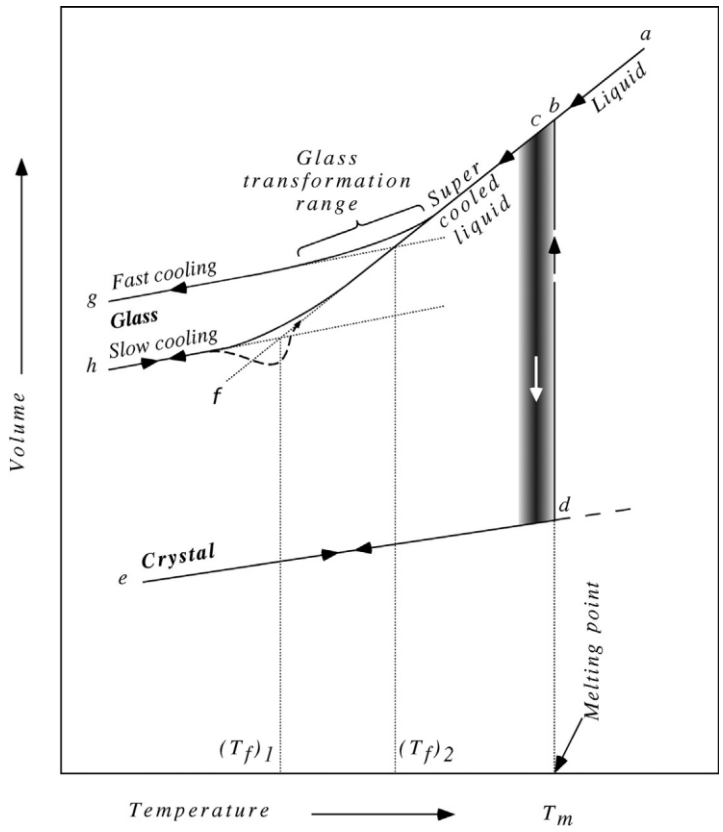

Figure 1.2 The volume-temperature diagram for a glass-forming liquid [8].

Silicate glass is composed of SiO_4 tetrahedra, where each silicon atom forms covalent bonds with four oxygen atoms, creating a three-dimensional network. This arrangement leads to a rapid increase in viscosity during cooling, preventing the glass from transitioning to a crystalline structure [6], [9]. However, the high manufacturing cost—since melting high-purity quartz or refined sand requires temperatures above or higher than 2000°C—restricts the use of vitreous silica alone, mainly to specialized products (such as astronomical mirrors, optical fibers, crucibles for melting high-purity silicon, and high-performance lamp envelopes). For this reason, a widely used technique for engineering the physical properties of glass is to incorporate various minerals

into the molten SiO_2 glass. In this way, silica-based glasses are obtained, in which, in addition to silica, other main constituents may be alkalis, alkaline earths, alumina, boric oxide, and lead oxide [7]. Alkali metal oxides (Na_2O, K_2O, Li_2O), alkaline earth metal oxides (MgO, CaO), and zinc oxide (ZnO) are referred to as network modifiers because they are incorporated into a network-forming oxide, disrupting its continuity and thus weakening the structure, leading to significant changes in the physical properties of silica glass. Specifically, they reduce the viscosity at high temperatures, enabling the production of a glass that can be refined and worked at significantly lower temperatures. Alumina, on the other hand, is classified as an intermediate oxide; it integrates into the glass network through AlO_4 tetrahedra but requires the presence of network modifiers to facilitate glass formation [10]. Based on specific additives, pharmaceutical glasses can be classified into two main types: soda-lime-silicate glass and borosilicate glass (see *Fig. 1.3*).

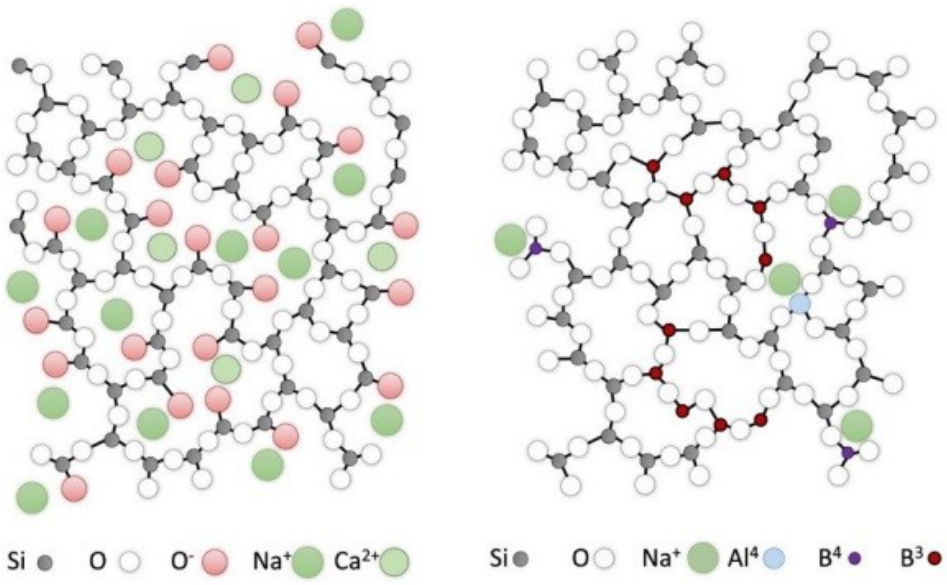

Figure 1.3 Glass structure of soda-lime glass (left) and borosilicate glass (right) [11].

Soda-lime-silicate glass is made by adding sodium carbonate (soda ash) and calcium carbonate (limestone) as sources of sodium and calcium oxides, which account for approximately 25% of the glass's weight [6]. Additional oxides like magnesium and potassium are added to further reduce the melting point. However, soda-lime glass is susceptible to thermal shock failure due to its high coefficient of thermal expansion (~ 100 x 10^{-7}/°C) and has a limited chemical durability. The latter

is due to the high leaching potential of sodium and potassium ions, a property that can be somewhat improved by adding Al_2O_3, which forms stronger covalent bonds. In amber glasses, Fe_2O_3 is included to enhance light protection by effectively absorbing ultraviolet radiation. Generally, large-scale continuous melting of low-cost raw materials such as sodium carbonate (Na_2CO_3), limestone ($CaCO_3$), and sand (SiO_2) at temperatures of 1400–1500°C enables the economical and high-productivity formation of containers [7]. Consequently, soda-lime silicate glass remains the most widely used type among commercial glasses, though it has specific end-use limitations in pharmaceutical applications.

Borosilicate glass is produced by introducing boron oxide (B_2O_3) as a lattice former in addition to silica, with a small amount of alkali ions. This type of glass offers superior chemical durability and high resistance to thermal shock and rapid temperature changes, due to its low coefficient of thermal expansion (~ 30–60 x 10^{-7}/°C) [7]. Additionally, Fe_2O_3, Ti_2O_3, or MnO can be added to create an amber glass for increased ultraviolet protection. Borosilicate glasses can be commercially produced in a manner similar to soda-lime glasses, but require higher melting temperatures (1550–1650°C) and more expensive raw materials. However, due to its stability in harsh thermal processes such as depyrogenation, freeze-drying, and sterilization, borosilicate is the glass of choice for parenteral containers [12].

To date, soda-lime and borosilicate are the commonly accepted glass materials in the European Pharmacopoeia, although studies have been underway for several years for the inclusion of aluminosilicate glasses that appear to show excellent qualities from both a chemical and mechanical point of view.

The long history that led to the modern production of glass bottles for pharmaceutical use is an example of materials science and engineering and is still evolving. It highlights how a thorough understanding of the structure, properties, processing methods and final performance of a material are closely intertwined, demonstrating the critical role of material knowledge in achieving the high standards required for pharmaceutical applications [4]. In fact, despite the above-mentioned excellent qualities that characterize glass as a material, there are still many scientific and technological challenges to be addressed. Numerous issues have historically been associated with pharmacopoeial compendial glasses, some so critical that they have led to costly

recalls of non-compliant products. The following sections will delve deeper into these challenges, exploring the specific issues surrounding glass containers in pharmaceutical contexts, with a focus on ongoing research and innovations addressing specifically the issue of mechanical resistance.

1.1.1 Issues and Challenges

In the pharmaceutical packaging sector, glass is a key material since the healthcare container must ensure the safe and effective storage of drugs. However, it faces several complex challenges that can affect its performance, safety and sustainability. These challenges can be broadly categorised as follows:

i. Glass-drug interactions: Chemical interactions between glass and medicines can compromise the integrity of the container and the stability of the drug. Key issues include:
    - Chemical durability: Leaching of ions from the glass surface, which may contaminate the drug.
    - Precipitation: Formation of unwanted precipitates due to interactions between the glass and pharmaceutical compounds.
    - Delamination: Separation or flaking of the inner glass layers, which can introduce particles into the drug solution.

ii. Mechanical strength: Pharmaceutical glass containers are susceptible to mechanical stresses, which can result in fractures or cracks that compromise container integrity and safety.

iii. Environmental impact: The production and disposal of pharmaceutical glass containers pose environmental concerns. Issues include the energy-intensive manufacturing process and the challenges associated with recycling materials contaminated by pharmaceutical residues.

Each of these areas presents distinct hurdles that must be addressed to optimize the performance and sustainability of pharmaceutical glass containers. The following paragraphs will explore these challenges in detail, analysing the current research and technological advancements aimed at improving the quality and safety of glass used in pharmaceutical packaging.

Glass-drugs Interaction

First of all, there is the still open problem of the interaction between drug products and glass surface of the container. This contact can lead to the leaching and dissolution of inorganic substances, which may subsequently react with the drug formulation and result in the formation of sub-adducts and precipitates, potentially posing risks to patient safety [4]. The occurrence of *flakes* or *lamellae*, thin inorganic particles, typically less than 1 µm in thickness and exceeding 50 µm in width [13], can cause serious complications when administered subcutaneously. These particles are often the result of low-durability, precipitation and delamination [14] phenomena. In the late 1800s, when parenteral products were first being developed, the only available glasses were soda-lime silicates, which had relatively poor durability compared to modern borosilicate glasses. These glasses were easily corroded by drug products, including pure water, and often led to the generation of flakes [3]. Over time, leaching from the *low-durability glass* results in the formation of a silica-rich gel layer, which, once thick enough, detaches from the underlying glass into the solution [15]. Chemical durability remains the primary attribute of pharmaceutical glasses, based on this the Pharmacopoeia has classified three Types of glass containers [*EP7- 3.2.1 European Pharmacopeia 7.0 – 3.2.1. Glass containers for pharmaceutical use*]:

1. Type I glass containers: They are made of borosilicate glass (Type I glass) and have a high hydrolytic resistance and a high thermal shock resistance due to their inherent chemical composition; they are intended for any purpose.
2. Type II glass containers: They are in soda-lime glass (Type III glass) with high hydrolytic resistance obtained through an appropriate treatment of the internal surface, which gives them, for a thickness of a few microns, surface properties equivalent to those of Type I. Suitable for most acidic and neutral aqueous preparations, whether or not for parenteral administration.
3. Type III Glass Containers: They are made of untreated soda-lime-silica glass (Type III) have a moderate hydrolytic resistance due to their inherent chemical composition. Suitable for nonaqueous preparations, for parenteral and more generally for non-parenteral use.

Regulatory authorities require distinct tests to evaluate both the stability of the drug and its compatibility with its primary-packaging, which must be fully assessed prior to distribute the drug preparation. To ensure this, tests on extractables and leachables, and stability evaluations are conducted under stress conditions, including variations in pH, temperature, and time. These tests are designed to quantify the migration of foreign substances into the drug product, confirming the stability of the drug under both accelerated and standard storage conditions [16].

Another process that can result in the formation of solid flakes is *precipitation*, which occurs when the components of a solution surpass their solubility limit [17], [18], [19]. This may happen due to interactions between leachables from containers and the drug or excipients, leading to the formation of insoluble solid phases [20]. These precipitates can take various forms, including flat sheets on the container walls, which may eventually detach and appear as solid flakes. Other than precipitation and poor-durability mechanisms, there is another phenomenon specific to the formation of glass flakes, *delamination* (*Figure 1.4*), usually cited as a weakness of glass containers. The term "delamination" refers to the detachment of glass lamellae from the inner surface of glass containers, caused by the interaction between the glass and the solution in contact with it. The formation of flakes in borosilicate glass differs from the behavior observed in soda-lime glass, a phenomenon known since the 1940s [19]. Due to its significance, this issue was the cause of several major vial recalls in 2010, prompting the Food and Drug Administration to issue a warning to the pharmaceutical industry in 2011. Additionally, the International Commission on Glass (ICG) established a technical committee (TC12 – Pharma Packaging), bringing together experts from both the glass and pharmaceutical industries to collaborate and share knowledge in order to address this problem collectively. Delamination in pharmaceutical glass vials is a rare yet complex phenomenon, with multiple contributing factors and no single identified cause. The main contribution is the manufacturing process, and is in fact a typical problem for tube containers. The tubular conversion process at high temperatures leads to inhomogeneities in the composition of the vial surface due to evaporation and redeposition of low-melting components [13], [21], [22], [23].

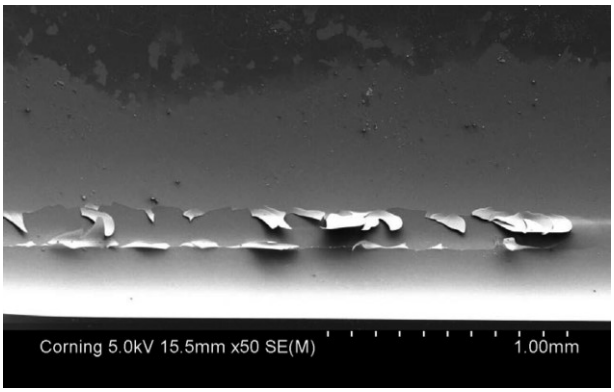

Figure 1.4 Electron microscope image of the interior heel region of a vial which exhibited delaminated flakes after exposure to a liquid solution. The figure shows several thin flakes that were not yet released from the container surface and regions where the flakes have already been released [1].

Sulphate treatments, although intended to limit the release of alkalis, can paradoxically increase the risk of delamination by making treated surfaces more susceptible to corrosion [24]. Finally, the duration and conditions of storage are also involved in this mechanism and in particular room temperature storage increases the risk of delamination compared to cold storage [12]. Current research focuses on developing effective tests for delamination propensity and refining corrosion resistance assessments [25].

Mechanical Strength

Mechanical resistance issues in glass containers, specifically cracks and breakage, arise from the inherent fragility of glass and its sensitivity to surface damage. A breakage is defined as a fracture that extends fully through the wall of a glass container [26]. Cracks can form during high-temperature manufacturing or result from handling during filling, transport, or distribution. Glass is especially prone to breakage when applied loads create tensile stresses that act on existing surface flaws, causing them to propagate. Additionally, contact with materials of similar or greater hardness (such as other glass containers) can introduce or aggravate surface damage, further compromising the strength of the glass and increasing the likelihood of future breakage [1].

The pharmaceutical industry faces significant challenges from breakage in glass containers, as it can contaminate aseptic filling areas, raise production costs and waste, and lead to drug shortages and product recalls. Cracks pose particular risks because they compromise the sterile barrier, creating pathways that allow: (i) microbes and contaminants to enter the product, (ii) potential leakage of the drug product, and (iii) changes in the gas composition within the headspace. The headspace refers to the area inside the container above the drug and typically contains gases like nitrogen or oxygen [27] essential to ensure drug stability, particularly for oxygen-sensitive formulations. When cracks allow gases to escape or contaminants to enter, the product's efficacy and safety are compromised. In severe cases, undetected contamination could lead to the administration of compromised doses, resulting in serious consequences such as sepsis or even death [28].

To address these risks, two approaches are possible: reducing the likelihood of crack formation by avoiding glass-to-glass contact and increasing inspection during production and filling; or directly enhancing the mechanical strength of containers. Section 1.2 will discuss in more detail the problem of surface damage and current methods of dealing with cracked containers.

Environmental Impact

Glass constitutes approximately 20% of the total weight of all packaging materials and is the only packaging material recognized as "Generally Regarded as Safe" (GRAS) by the US Food & Drug Administration [29]. Despite its inherent fragility and the higher costs associated with transportation [30], consumer preference for glass remains strong, even with the wide array of packaging alternatives available today [31]. As global population continues to rise, the demand for glass containers used in packaging for food, beverages, pharmaceuticals, and other products has similarly increased [32]. A report from the Freedonia Group (2021) predicts that the use of glass in pharmaceutical packaging will continue to grow, driven by increased investment in research and development. Additionally, a forecast by the Technavio Research Institute anticipates that the pharmaceutical glass packaging market will expand by $7.73 billion between

2024 and 2028 [9] (*Figure 1.5*), highlighting the increasing significance of this material in the pharmaceutical industry.

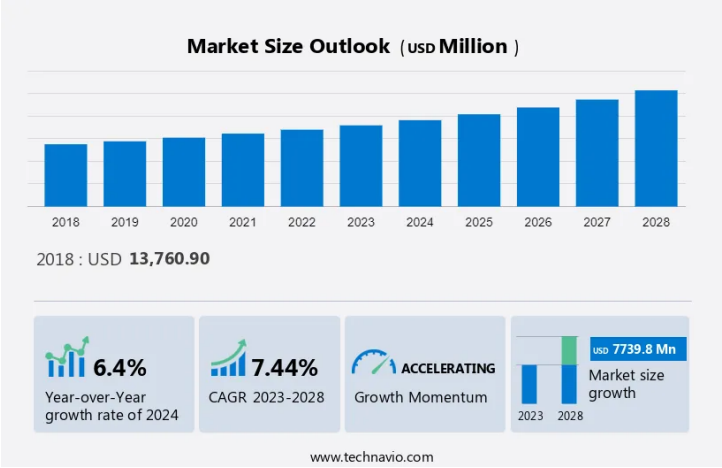

Figure 1.5 Pharmaceutical glass packaging market size report during the forecast period [33].

To meet the increasing demand for glass packaging, the rise in glass production inevitably leads to greater consumption of natural resources and higher emissions. The manufacturing process for glass is resource- and energy-intensive, contributing significantly to the emission of carbon dioxide (CO_2) emissions and other pollutants [30] . Consequently, the environmental impact of glass packaging production, is a key consideration as the industry continues to expand. Despite the energy-intensive nature of its production, glass is widely regarded as an environmentally friendly packaging material due to its ability to be easily reused and recycled into new containers, which helps reduce its overall environmental impact [34]. In the glass bottle industry, recycled glass cullet has become the primary component of production batches (*Figure 1.6*). For example, soda-lime green glass can contain up to 95% cullet, amber glass between 60% and 80%, and flint (clear) glass between 50% and 70%. This extensive use of cullet is made possible by effective colour separation during collection and the removal of contaminants. The inclusion of cullet accelerates the melting process, leading to energy savings—approximately 3% less energy for every 10% cullet added—and significantly reduces CO_2 emissions and the need for raw materials [4].

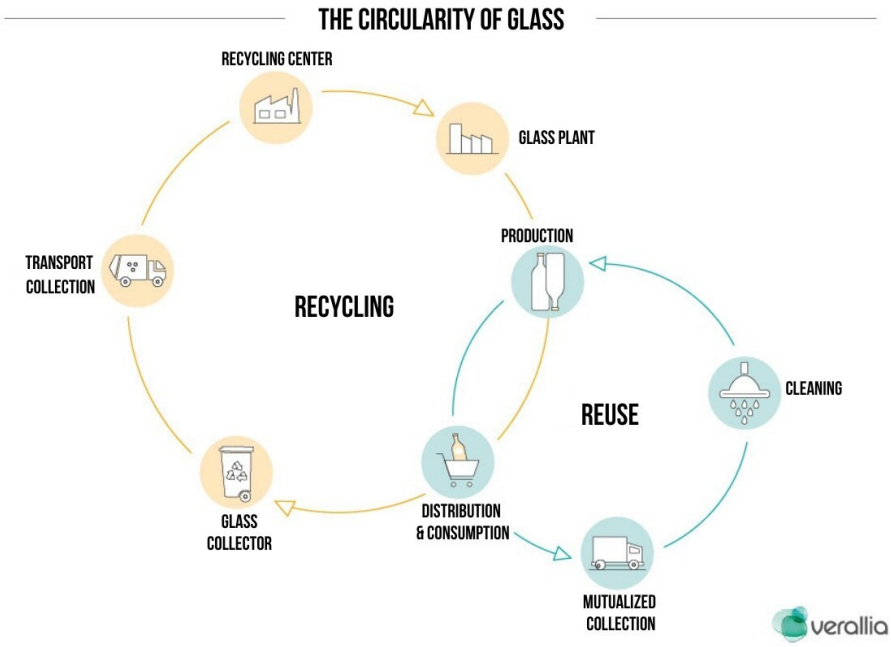

Figure 1.6 The circular economy possibility of glass packaging [35].

Once used, glass pharmaceutical containers are typically classified as municipal waste, except when they come from infected areas. In these cases, they are usually sterilised before being disposed of by incineration. From an environmental point of view, glass presents far fewer risks than polymers. Composed mainly of inorganic materials, including common oxides found in the earth's crust, glass that is dispersed into the environment gradually degrades without threatening ecosystems or the environment itself. In contrast, plastic decomposes into microplastics, which are known to infiltrate the food chain and pose significant environmental risks [36].

Investing in recycled materials, enhancing the efficiency of production processes, and adopting innovative technologies, such as hydrogen-compatible furnaces, are essential strategies to reduce the environmental impact of glass while maintaining the safety and effectiveness of pharmaceutical products. These combined efforts help pave the way for a more sustainable future in the glass pharmaceutical industry, benefiting both the environment and public health.

1.2 The Issue of Surface Damage

1.2.1 Glass Surface and the Problems of Flaws

Glass containers, including both borosilicate and soda-lime silicate types, face a significant challenge in maintaining mechanical strength due to damage introduced during the forming and handling processes. One critical form of damage is breakage, defined as a "*fracture that penetrates completely through the wall of the glass [container]"* [26]. Cracks, however, are considered "critical" defects because they present a "probable" risk of causing personal injury or patient harm. These defects can also *"compromise the integrity of the container*, potentially leading to *microbiological contamination of a sterile package"* [26] as shown in *Figure 1.7*. Cracks are essentially small slits or cuts in the container, which can create pathways for liquids, gases, or microorganisms to penetrate.

Cracks can occur even after thermal annealing, a process applied after forming that reduces most residual stresses within the glass, but may not completely eliminate them. These defects can also form or worsen at other stages of production and filling, representing a significant concern for the pharmaceutical industry that has faced recalls due to cracked or broken containers [4]. Cracks most commonly appear in the body, heel, and base (footprint) areas of a vial following shock inspection—a quality control procedure where vials are subjected to controlled mechanical stresses or impacts to identify structural weaknesses. Although less frequent, high-risk cracks, such as those occurring in the neck or the edge of the base (footprint), can also develop and are more difficult to detect [5] (see *Figure 1.7*- right).

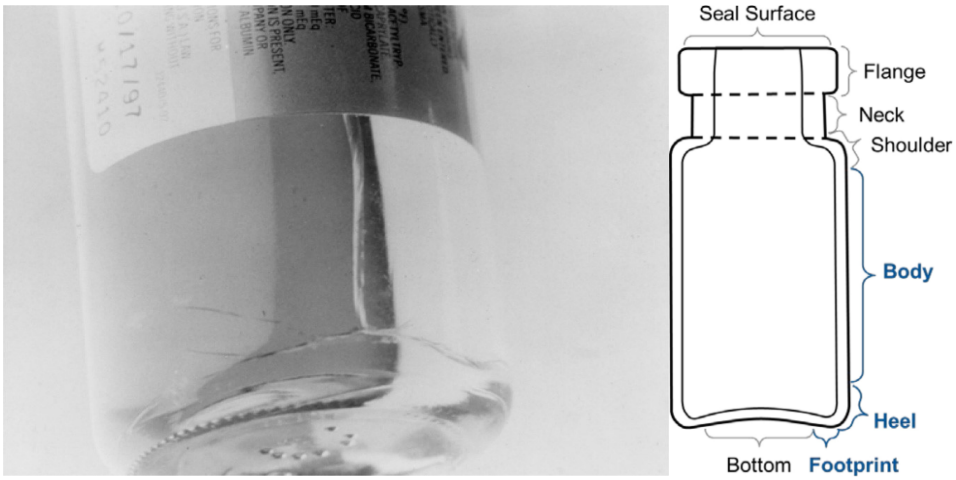

Figure 1.7 Left - Cracked borosilicate vial of contaminated human albumin, which upon injection resulted in blood stream infections for patients[37]. Right - Vial schematic labelled with common locations. The highlighted regions (Body, Heel, & Footprint) show where more than 90% of cracks are introduced [5].

The susceptibility of glass containers to cracking can be attributed to three factors: i) the presence of initial surface flaws caused by damage during forming, handling, and shipping; ii) the significant tensile forces experienced during filling and handling, which can cause these flaws to evolve into cracks; and iii) the lack of sufficient surface compression within the glass, which would otherwise help prevent the spread of cracks and ultimately the breakage of the container.

Brittle materials, such as glass, exhibit considerable strength under compressive forces but are prone to failure when subjected to tensile stress. In theory, pristine glass is an exceptionally strong material, with a tensile strength depending on interatomic bonding forces estimated to be around 6500 MPa. However, when used as a practical engineering material, its strength is significantly lower, with typical values around 1200 MPa for glass fibers and only 30-40 MPa for containers [38]. This reduction in glass tensile strength was first explained by Griffith in 1920 [39], who attributed it to the presence of submicrometric flaws—tiny discontinuities or breaks in the atomic bonds on the glass surface. These flaws range in size from approximately 10^{-6} to 10^{-8} cm, compared to larger flaws on the order of 10^{-1} to 10^{-3} cm. Consequently, the mechanical strength of glass is not an intrinsic property of its composition but is heavily influenced by handling practices. When stress is applied, these surface defects propagate, serving as focal points that amplify the forces, eventually leading to potential fracture [40]. As flaws enlarge, fatigue develops

throughout the period of applied stress, a phenomenon not accounted for in earlier brittle solid strength theories prior to Griffith's work. Griffith revised the theoretical framework for calculating the fracture strength of glass (Equations 1-2) by incorporating the concept of elliptical defects (see *Fig.1.8*):

$$\sigma_{yy} = \sigma_f\sqrt{1 + 2c/b} = \sigma_f\sqrt{1 + 2\left(\frac{c}{\rho}\right)} \quad (1)$$

$$\sigma_f = \sqrt{2E\gamma/\pi c^*} \quad (2)$$

where σ_{yy} is the stress at the tip of an assumed elliptical hole or flaw, σ_f is the mechanical stress needed to trigger fracture (frequently indicated in MPa) in conventional glasses, c^* is the critical flaw length for crack growth, $\rho = b^2/c$ is the radius of curvature at the tip of elliptical flaw, E is the Young modulus (in MPa) and γ is the fracture surface energy [40].

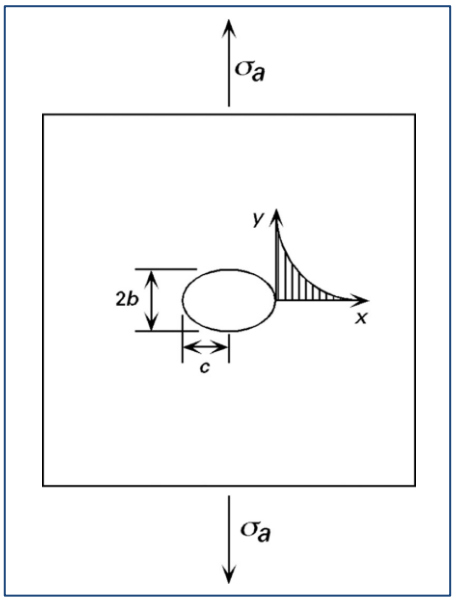

Figure 1.8 Elliptical flaw in a glass plate under tension. Where σ_a is an applied stress; 2b is the minor axis and 2c is the major axis of the elliptical flaw. $\sigma_f = [\sigma_a]_{failure}$ [40].

The shape, size, and distribution of these flaws are crucial in determining the energy necessary to initiate fracture. Exceeding the value c^* the energy decreases and the defect widens, thereby influencing the overall strength of the glass.

Flaws typically appear on free surfaces and have a wide range of lengths; however, fractures begin at the position of the most severe flaw. In particular, the applied load focuses on the tips of the defects, such as cracks, scratches or breaks, leading to their propagation only when the localised stress exceeds the strength of the individual atomic bonds. The growth of these defects may stop if the applied load decreases over time or if the defect forms in an area subject to less stress (see *Figure 1.9*). Conversely, if the applied load remains sufficiently uniform and persists longer than the time required for the defect to propagate, the defect will continue to extend through the thickness of the wall or away from its origin, eventually causing the container to fail [5], [40].

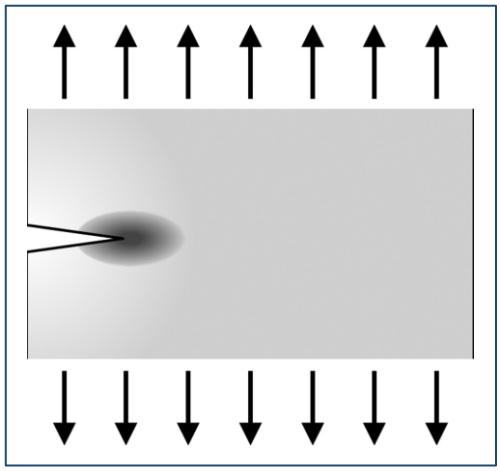

Figure 1.9 Cross-sectional schematic of a glass article under uniform applied tension, showing low level stress (grey shading) throughout the part and high stress concentration (dark grey shading) near the flaw tip [5].

Initial surface defects in glass containers are mainly introduced during the forming process, when the tensile stress exceeds the hydrostatic yield strength—the maximum pressure that molten or semi-solid glass can withstand uniformly from all directions without deforming or cracking [40]. Subsequently they can be exacerbated by contact with other surfaces during handling, transport and filling. Cracks can develop or worsen during loading and unloading, particularly when glass comes into contact with sharp objects, such as other glass surfaces. As a result, surface damage to glass containers is inevitable during handling, especially after the forming process, when vials are exposed to applied stress. The likelihood of defect formation depends on both the duration of the stress and the alignment of the originating flaw with the direction of the applied force.

These defects are more likely to occur in specific areas of the vial and can evolve into cracks or fractures over time [5].

1.2.2 Methods to Improve Mechanical Strength

Minimizing surface damage plays a key role in maintaining the structural integrity and mechanical performance of the vials throughout their use. Therefore, it is evident that any method capable of reducing surface damage is essential for preserving such failures. Over the years, various approaches have been employed to address this issue. One strategy is to minimise the risk of defects by preventing glass-to-glass contact and, for example, some pharmaceutical manufacturers designed new type of filling lines to achieve this purpose. For example, Stevanato Group developed the EZ-fill® platform, which uses pre-sterilized containers in nest-and-tub or tray configurations to minimize container contact during filling [41]. However, this is not always practical on an industrial scale, as the need for specialized production lines, where vials move without touching, may not always be compatible with existing factory processes. A second, equally important approach is to enhance quality control efforts through the use of advanced inspection technologies, including sophisticated equipment and data management systems, to reduce the risk of releasing products with undetected defects [4]. Practical application of these techniques is not trivial, for instance optical inspection methods for glass containers are dependent on the precise alignment of the detector, light source, and crack, which increases the likelihood of false negatives. As a result, these methods can often be ineffective in reliably detecting cracks and, despite significant investments in inspection technology by the pharmaceutical manufacturing industry, injectable drugs are still frequently recalled or re-evaluated due to sterility concerns linked to cracks. Recent updates to the US Pharmacopeia chapters on package integrity testing [27] highlight that traditional methods are probabilistic and cannot consistently guarantee container integrity. Therefore, they are still insufficient to completely eliminate material waste and the residual risk of a damaged product reaching the consumer.

A promising approach to improving the mechanical strength of glass containers involves applying post-processing techniques. In the production of glass for different applications, it is well established that strengthening methods can inhibit both the initiation and propagation of defects while also controlling fracture behavior when breakage occurs, such as the number and shape of fragments. For instance, thermally toughened (i.e. thermally tempered) safety glass, commonly used in automotive and architectural contexts, is designed to create a surface layer of compressive stress, which prevents damage initiation and limits defect propagation. Compressive stresses on glass surfaces are beneficial for strengthening, as any external stress must first overcome this compression before subcritical crack growth can begin. When this type of glass fractures, it does so at a higher load as compared to non-toughened glass, and the resulting fragments are small and cubic, reducing the risk of injury from sharp, dagger-like shards typical of annealed glass [42]. The specific fracture behavior of toughened glass is achieved only when the strengthening process generates sufficient strain energy to impact defect propagation [43].

A similar method used for pharmaceutical glass containers is ion-exchange (i.e. chemical tempering), which strengthens the glass and prevents stable crack formation. Compared to thermal tempering, chemical tempering through ion-exchange is suitable in strengthening containers with thin walls, complex geometries, and low thermal expansion glass compositions, while still providing the necessary strain energy threshold [44]. This strengthening technique aim to retain the original strength of the glass or to increase the force required for breakage by introducing compressive stresses that counteract the applied tensile stresses, thus enhancing the practical strength of the container. The ion-exchange process works by replacing small alkali ions such as sodium and lithium, representing typical “modifiers” in the glass structure with larger potassium ions (see *Figure 1.10*) from an external salt bath where the glass is held at high temperature for a certain time [44], [45], [46].

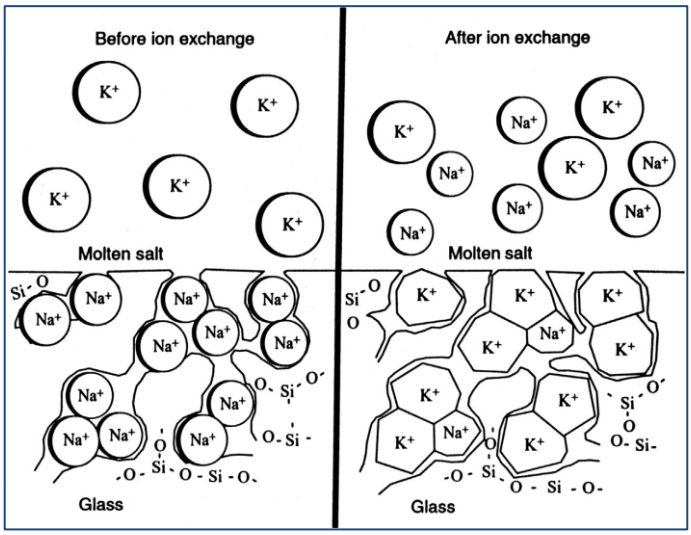

Figure 1.10 Schematic representation of the ion exchange process used to make chemically strengthened glass [47].

This exchange creates a compressive stress on the surface of the container and a balancing tensile stress throughout the thickness of the glass wall, as illustrated in *Figure 1.11*. Since this stress profile is generated by ion interdiffusion, the exposure time and temperature during the process can be carefully controlled to ensure that the strain energy remains above the minimum threshold necessary for preventing cracks.

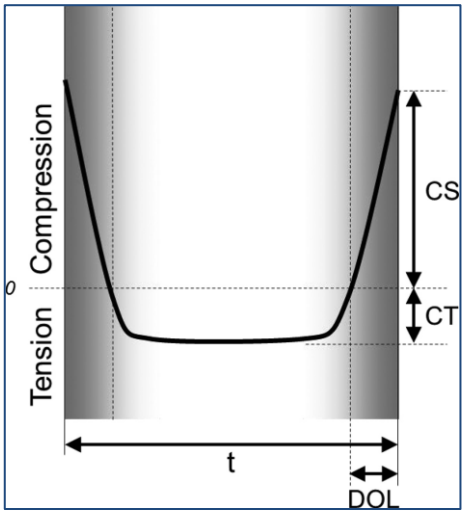

Figure 1.11 Illustration of the engineered stress profile resulting from ion-exchange of a thin-walled glass article, where the abscissa is the wall thickness (t, radial direction) and stress is the ordinate. High compressive stress (CS) is installed at the surfaces, and it decreases to the depth of the compressive stress layer (DOL-Depth Of Layer). The compressive strain energy induced by this ion-exchange process is balanced by tensile strain energy, measurable as central tension (CT) [5].

Since the process relies on diffusion, treatments take place at relatively high temperatures for several hours to complete [48]. Although current research is exploring ways to make the process more efficient and reduce the required times [49], it remains unsuitable for widespread application in most industrial production settings especially for glass containers.

Chemical tempering directly increases the intrinsic strength of the glass, improving its resistance to stress, but does not prevent the external forces to which the vials are subjected during handling. Another approach, particularly interesting for the glass-packaging industry, is to develop surface coatings to reduce the impact of these external stresses, thus indirectly preventing the formation of surface defects. These coatings aim to improve the smoothness of the vials, minimising friction and potential damage during the manufacturing and filling processes, offering an effective way to reduce stress-related defects in pharmaceutical containers.

Standard Method in Use and Industrial Requirements

The traditional method used to preserve the strength of the glass container consists in the application of two successive treatments called hot-end and cold-end coating (see *Fig. 1.12*). This method has been widely studied [50], [51], [52], [53], [54] and is still the most used method in the glass container industry especially in food packaging. The first treatment, known as *hot-end coating*, is applied to the surface of glass containers immediately after forming and prior to annealing. This process involves vapor-phase deposition at atmospheric pressure, where a thin tin oxide film is applied while the containers are still at elevated temperatures, typically between 520 °C and 650 °C. The oxide coating helps maintain the pristine strength of the glass, offers high transparency to visible light, and exhibits high hardness [52], [55], [56]. It is usually deposited using organometallic precursors, such as mono-butyl-tin-trichloride (n-$C_4H_9SnCl_3$) [57], [58] for the deposition of SnO_2. Hot-end treatment requires a dedicated hood on the production line for toxic fumes, such as HCl, released during this deposition process. The second treatment, *cold-end coating*, is applied afterward through the spray deposition of an organic, water-based formulation (such as polyethylene, waxes, or oleic/stearic acid) immediately after annealing, when container

temperature ranges from 80 °C to 160 °C [53], [54]. It is widely accepted that the tin oxide film serves as a coupling agent, bonding both the glass and the polymer [50], [54], [59].

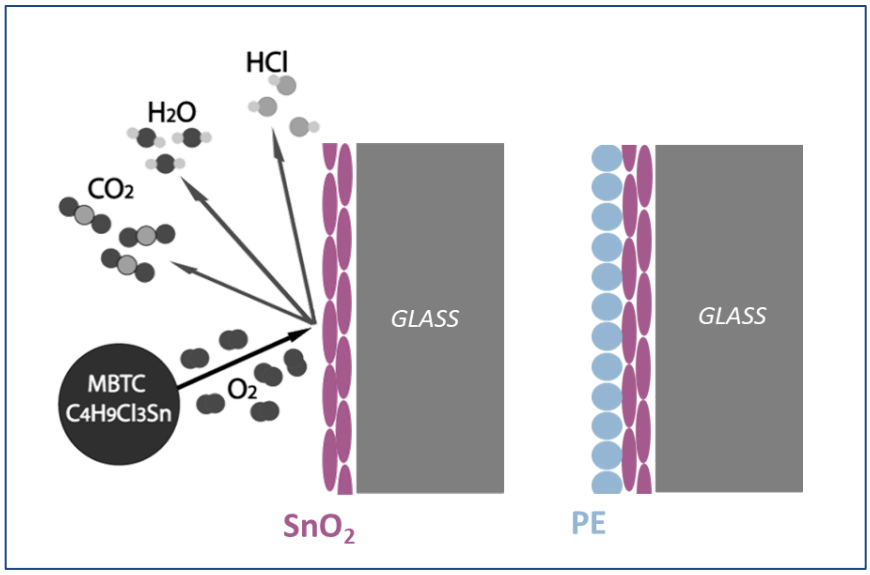

Figure 1.12 Hot-End and Cold-End systems, adapted from [60].

The polymer coating significantly reduces the coefficient of friction during glass-to-glass contact, enhances lubricity, and minimizes surface damage that could weaken the glass. The anchoring function of oxide has been extensively studied [50] and is believed to arise from its ability to enhance the bond strength between organic coatings and glass. The presence of stronger Brönsted acid sites and strong Lewis acid sites, due to metal cations, explains why tin oxide primers interact more effectively with both polar and non-polar organic molecules compared to soda-lime silica glass. This enhanced interaction is attributed to the more covalent nature of tin dioxide, which leads to stronger acid-base interactions between the primer and polymer, a result of the oxide's cationic polarizability [61]. However, the tin dioxide deposit roughens the glass surface, suggesting that the anchoring function of the primer may also have a mechanical effect [60]. Optimal mechanical properties are generally reported as a result of the combined effects of tin dioxide thickness and the amount of deposited polymer [52]. This indicates that both the surface roughness and chemical properties of SnO_2 play a role in stabilizing the polymer coating [54]. Although these methods have proven their effectiveness over the years, they cannot be

considered a definitive solution. While hot- and cold-end coatings provide some degree of surface protection, their impact and durability are often limited and may not fully meet all supply chain requirements, from production to filling, up to the end user (schematically in the *Figure 1.13*).

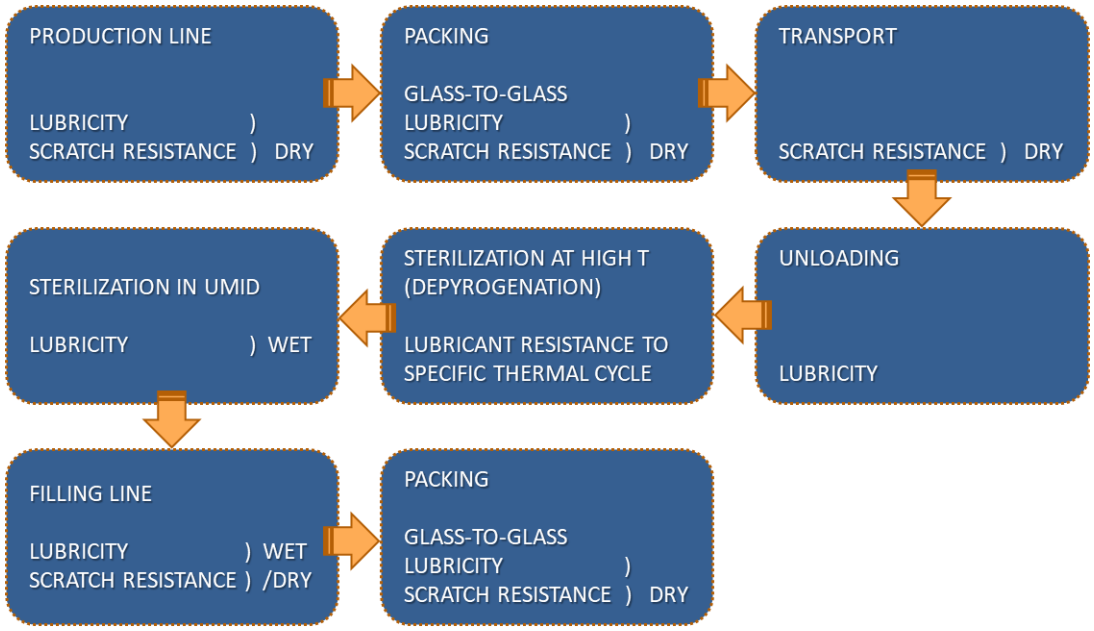

Figure 1.13 Outline of manufacturing and filling line processes and associated surface treatments requirements, adapted from [38].

The primary requirement for manufacturers is that glass containers have high resistance to scratching in the dry state, ensuring they retain as much of their original strength as possible during production. This is especially critical for modern high-speed production and filling lines, where the smooth and efficient movement of containers is essential to avoid costly breakages. The glass surface must also be protected without compromising its aesthetic appearance with visible scratches, a key marketing factor. Adequate lubrication is required to ensure that the containers pass smoothly through inspection and packaging processes, but excessive lubrication should be avoided to prevent handling issues [38]. From the viewpoint of pharmaceutical clients, there is a need for sufficient dry lubrication to ensure the containers flow smoothly during in-line filling and packaging for transport. Specific requirements, such as wet lubrication that can withstand washdowns or sterilization processes like depyrogenation (where containers are

exposed to rapid thermal cycles at high temperature), may also be demanded by pharmaceutical clients. For end users, key requirements include safe containers without any type of contaminations and free from visible defects, such as scratches or abrasion marks [38].
Historically, safety was achieved through thicker-walled, heavy containers, but with the growing trend toward lighter containers, protective coatings have become increasingly important. These coatings play a crucial role in maintaining container durability and performance while supporting the transition towards lighter and more sustainable packaging solutions [62].

1.3 Aim and Outline of the Work

The aim of this PhD project is to develop a lubricant coating for the external surface of pharmaceutical vials, in collaboration with Bormioli Pharma, a leader in pharmaceutical packaging. The primary objective is to replace the current hot-end coating process, (*Fig. 1.14*), which involves a dedicated manufacturing step and specialized equipment to manage the release of toxic fumes, with a more sustainable and cost-effective alternative. Specifically, the project focuses on introducing a water-based organosilane primer that can be applied via spray deposition, while retaining the lubricant currently used in the factory. This approach aims to eliminate the costly and environmentally harmful aspects of the existing process, while maintaining the required surface protection and performance of the vials.

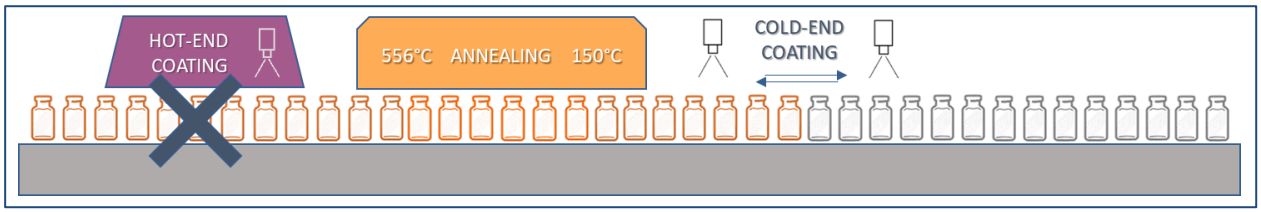

Figure 1.14 A schematic representation of the industrial application of hot and cold-end coatings, together with the initial concept of my work to replace the hot-step.

Initially, the silane primer was studied using the dip-coating method, applied directly to glass vial samples, to assess the influence of deposition parameters on the formation of the primer film

through morphological and chemical characterizations. The effectiveness of the primer in promoting lubricant adhesion was evaluated through mechanical testing on both vial samples and whole vials. Subsequently, the industrial feasibility of the coating process was investigated by testing airbrush and spray systems to demonstrate scalability from laboratory to industrial production. Mechanical performance of the coating was further tested using these alternative deposition methods.

In parallel, a preliminary study was conducted on a single-component organosilane coating, exploring the possibility of combining both adhesion promotion and lubricant functionality within a single molecule. As with the silane primer, deposition was first studied via dipping, followed by tests of industrial scalability using spray techniques.

The work focused on transparent soda-lime glass vials, aiming to improve the surface lubrication treatment on the least expensive glass type. The development of these coatings was designed to alter only the surface layer of the containers, targeting commercial applications for mass-produced vials, with an emphasis on lowering production costs and minimizing environmental impact.

1.4 Structure of the Thesis

The Thesis is organized as follow.

Chapter 1 provides an introduction to glass as a material for pharmaceutical containers, discussing why it is the material of choice, alongside the main challenges and issues associated with glass containers in the pharmaceutical industry. This includes a specific focus on the problem of mechanical strength and surface damage, methods to address these issues, the current industrial strategies adopted, and the approach undertaken in this research to protect the external surface

of soda-lime glass vials. The primary objective is to eliminate environmentally unsustainable and costly processes within industrial applications.

Chapter 2 describes the materials and methods used in developing a surface coating, focusing on aqueous silane-based solutions, primarily used as primers to anchor lubricants. It includes a literature review on silanes as adhesion promoters and the main associated challenges, along with the importance of surface pretreatment. The chapter further explores the lubrication mechanisms of organic lubricants and the specific requirements in the pharmaceutical industry. A sub-chapter is dedicated to a description of the experimental techniques, theoretical foundations and instrumentation used.

Chapter 3 details the first experimental phase, examining the deposition of an aminosilane-based aqueous primer and a potential single-component silane solution via dipping. The results of morphological, chemical, and mechanical characterisations are presented.

Chapter 4 covers the second experimental phase, which investigated the application of these formulations through spray systems to assess their industrial applicability. The characterisation results are provided, with a particular focus on mechanical performance.

Finally, Chapter 5 presents conclusions and future perspectives, summarising the most significant findings and highlighting areas requiring further investigation. The chapter also emphasises the industrial benefits of this research.

2. Development of a Surface Coating

2.1 Silane Adhesion Promoters

2.1.1 Description and Applications

Adhesion promoters, also known as coupling agents, are chemicals that improve adhesion between dissimilar materials such as organic polymers and inorganic surfaces by acting at their interface. Significant differences between organic and inorganic materials, such as compatibility, chemical reactivity, surface properties and thermal expansion, often make it difficult to form strong adhesive bonds between them. An effective adhesion promoter addresses this challenge by chemically and physically binding organic and inorganic materials, creating a cohesive and durable bond structure. In addition to improving adhesion, these promoters also act as a 'compatibility bridge', altering the physical and chemical forces at the interface and providing resistance to environmental factors such as heat and humidity that can weaken adhesive strength [63].

Historically, organosilanes have been the most commonly used type of coupling agents for promoting adhesion due to their ability to integrate both inorganic and organic reactivity within one molecular framework [63]. This hybrid nature allows them to react with both polymers and inorganic surfaces[64], making them the most interesting molecules in surface engineering science for decades. Their use spans in different industrial sectors from biomaterials to semiconductors and construction technology, but the most important applications regard the coating industry [65], [66] where they are especially employed in adhesion promotion. Their popularity in the industrial context is due not only to their hybrid nature, but also to their relative safety compared to other chemical coupling agents. In particular, the ability to use them in aqueous solutions is a significant advantage in all those applications that prohibit or require a reduced release of volatile organic compounds [67].

Specifically, in glass surface modification, studies on organosilanes range from imparting hydrophilicity/hydrophobicity [68], [69], [70], [71] to glass reinforcement [72], [73], [74], [75], [76], [77]. Regarding the latter, an objective very close to that of the present work, organosilanes are used both as adhesion promoters for polymer coatings and as crosslinking agents. When used in coating formulations, two approaches are typically followed: either as a primer – a thin layer of organosilane primer is deposited onto the substrate before the polymeric coating is applied – or as an additive – a silane organo-compound is added directly into the coating formulation before being deposited onto the substrate [78]. Numerous studies have employed silanes as coupling agents with both synthetic [77] and natural [72] reinforcement polymers, often aimed at improving the abrasion resistance of glass surfaces [79]. When the specific focus regards glass strengthening, organosilanes are frequently used as additives in coating formulations [76] or as cross-linking agents to facilitate crack-bridging mechanisms [75]. Most of these applications are focused on flat and/or float glass.

Today there is a large variety of organosilanes with different functionalities that can be deposited on inorganic substrates by different methods such as liquid phase deposition by dip coating or spray coating, sol-gel reactions, chemical vapour deposition – CVD and plasma enhanced CVD - which exhibit different advantages and disadvantages [80], [81], [82], [83], [84], [85]. Unless differently stated, in the following we will refer specifically to the liquid phase deposition via dip coating, the technique mainly used to carry out the present research activity.

2.1.2 Chemistry and Reactions

Organosilanes coupling agents are silicon-based chemicals that typically feature a structure with four substituents attached to a single silicon atom, some for the interaction with inorganic material and some for the interaction with the organic material. To qualify as an organosilane, at least one of the substituents attached to the silicon atom must be an organic group (carbon-based), which is directly connected to the silicon via a Si-C bond. The general formula (3) for this type of compounds could be expressed as:

$[R_nSiX_{(4-n)}]$ (3)

Where R represents the non-hydrolysable organic portion, which can be: i) non-reactive alkyl or aryl groups such as methyl, butyl, octyl, or phenyl; ii) organofunctional, incorporating a terminal reactive group (such as amino, epoxy, methacrylate, sulphidic or isocyanato) separated from the silicon atom by an organic chain (as showed in *Fig. 2.1*); iii) a combination of them. This portion ensures compatibility with organic materials, allowing silanes to form interpenetrating polymer networks (IPNs) or, in the case of reactive organofunctional silanes, to interact with the polymer coating. Alkyl and aryl groups are also used to create hydrophobic surfaces.

The X group represents the hydrolysable portion. In the most common organosilanes X are represented by three alkoxy groups (such as methoxy or ethoxy), which react with hydroxyl groups, releasing methanol or ethanol in the process. In this way, alkoxy groups can bond with inorganic substrates, thereby enhancing the integrity and adhesion of the coating [2] [54].

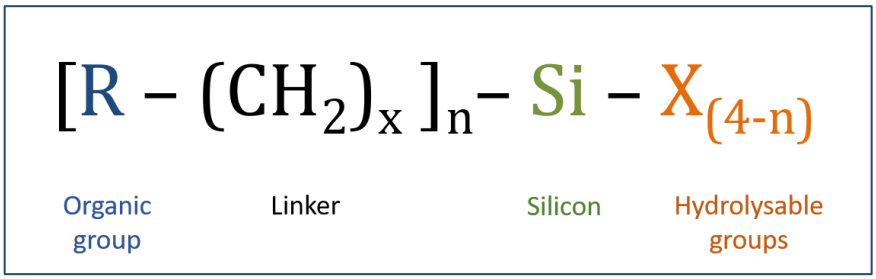

Figure 2.1 General formula of organosilane coupling agents adapted from [86].

The surface treatment process using organosilanes involves several steps detailed in the following with reference to *Figure 2.2* (from left to right). Initially, the alkoxy groups on silicon undergo hydrolysis, either through added water or residual moisture on the inorganic surface. During the hydrolysis alkoxy groups convert into silanols, with the release of the corresponding alcohol from the present alkoxys [87]. Silanol groups (Si-OH) formed are very reactive, particularly electrophilic due to the larger and more electropositive silicon atom, and condense with each other (*self-condensation*) or with metal hydroxyl groups present on the inorganic surface (*condensation*), leading to the formation of oxane bonds and the release of water. This process creates a crosslinked siloxane structure, characterized by tightly packed layers near the surface and more

diffuse layers far from the surface. The self-condensation of silanols with one another leads to the formation of a multimolecular cross-linked siloxane structure on the inorganic surface [63]. The final hydrolysed alkoxy group aligns itself with the hydroxyl sites of the substrate, forming hydrogen bonds. Upon drying or heating, covalent bonds are established at the interface, enhancing adhesion. Although these covalent bonds are hydrolysable, they can reform, allowing for tension relaxation at the organic/inorganic boundary. This leads to improved adhesion and greater durability of the coating [64] [63] [87]. This final step requires the surface of the substrate – such as glass – to be as hydrophilic as possible with exposed hydroxyl sites. This necessitates a pre-treatment step to activate the glass surface that will be discussed in the dedicated 2.2 sub-chapter.

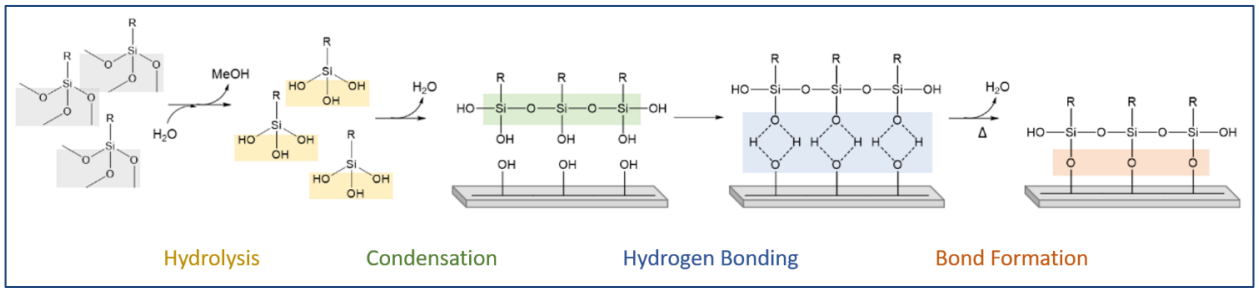

Fig 2.2 Silane deposition process- adapted from [88].

2.1.3 Relevant Factors for Silane Reactions

The deposition of silanes on solid surfaces depends on a number of factors – processes and parameters – such as surface preparation, silane concentration, choice of solvent and pH control, solution temperature, reaction time and post-deposition treatments, including washing and curing. Each of them directly affects the adhesion, structure and stability of the resulting silane coating. Research on this topic provides valuable insights into these critical factors.

Effective silane deposition depends heavily on proper *surface preparation*. This process typically involves both cleaning the surface to remove contaminants and activating it to expose hydroxyl

groups (-OH), which provide the necessary reactive sites for covalent bonding with silanes [89] [90].

The surface pre-treatment for glass substrates will be examined in detail in the subsequent section, where the specific methods of glass surface modification will be addressed.

The *concentration of silane* in the deposition solution is another determining factor. Lower silane concentrations tend to form uniform monolayers, which can enhance controlled adhesion by limiting excessive crosslinking. On the other hand, higher concentrations, particularly when using di- and tri-alkoxy-silanes, may lead to the formation of multilayers. These multilayer structures can provide additional benefits, such as enhanced mechanical strength and improved barrier properties, but may also introduce potential challenges in maintaining uniformity across the surface [91], [92], [93].

The solution temperature influences the rate of hydrolysis and condensation reactions, affecting the final structure and thickness of the silane layers. Moderate temperatures promote homogeneous monolayer formation [89], while excessively high temperatures can lead to multilayering or surface defects due to accelerated reactions [94]. Conversely, low temperatures slow the reaction, potentially resulting in incomplete coverage.

Solvent selection and *pH* control play a crucial role in the deposition process, as they influence the kinetics of the hydrolysis and condensation reactions of silane. The choice of solvent, whether organic or alcoholic, and the presence of water are essential to facilitate the hydrolysis of alkoxy groups, and this selection also depends on the specific type of organosilane used. Additionally, precise pH control is necessary to promote controlled condensation, preventing fast or irregular reactions that could result in a non-uniform coating [90], [95].

The *reaction time*, defined as the period during which the substrate is exposed to the silane solution, influences both the uniformity and the quantity of the deposited layers. This parameter directly affects the thickness and density of the silane coverage. Generally, shorter exposure times can result in incomplete coverage, while longer times tend to promote multilayer formation, particularly at higher concentrations [82], [83], [84], [85].

Post-deposition treatments, such as washing and curing performed after silane deposition, are essential for stabilising the silane layer and ensuring its long-term functionality. Washing the

silane-coated surface removes unreacted silanes, and prevents the formation of defects such as uneven areas in the silane layer[96]. Curing, typically performed by heating, promotes cross-linking within the silane layer, enhancing its mechanical stability and chemical resistance. However, over-curing can lead to degradation of the functional groups, particularly in highly cross-linked layers like those formed from tri-aminosilanes [94], [96].

A fundamental challenge in surface modification with silanes is managing the different stages of the process—hydrolysis, condensation, and phase separation of the solution—which, while sequentially dependent (as condensation cannot occur without prior hydrolysis, nor phase separation without condensation), become competitive once initiated. Phase separation occurs as distinct phases form within the solution. If these reactions are not properly controlled, they can result in poor adhesion or uneven coatings. Several factors influence each stage, some of which have already been briefly mentioned, including catalysts, the water-to-silane molar ratio, temperature, pH, and the choice of solvent. Hydrolysis must occur before surface modification, converting organo-silanes into silanol-containing species. This process releases alcohol from the hydrolysed alkoxy groups. These species are highly reactive intermediates responsible for substrate bond formation. However, premature condensation can occur, which affects performance [95]. As previously mentioned, condensation starts with the interaction between two hydroxyl (-OH) functional groups; -Si-OH in the case of glass substrate, leading to the formation of siloxane linkages (Si-O-Si) with the release of water. This occurs not only between substrate silanols and silane silanols but also between silane silanols themselves (see *Fig. 2.3*), leading to the formation of oligomeric species [87].

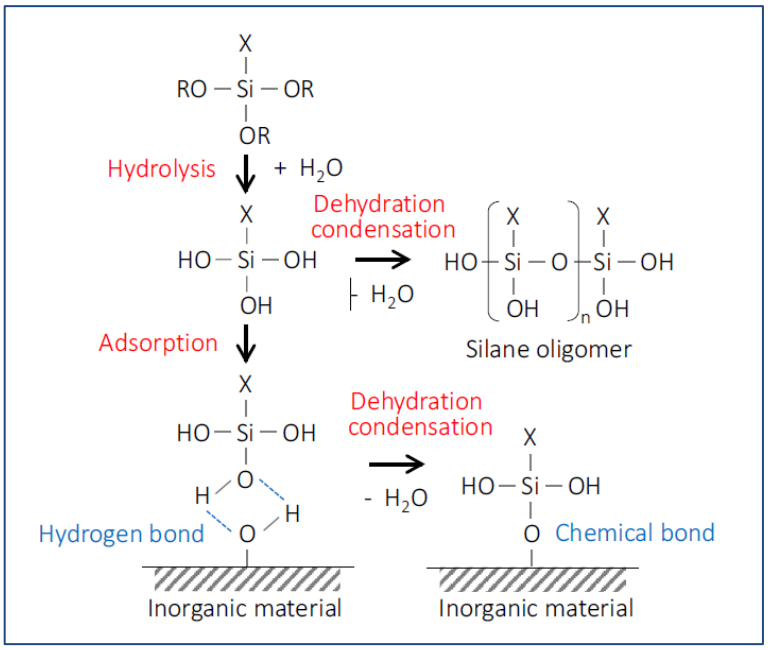

Figure 2.3 Competition between hydrolysis, adsorption and self-condensation reactions [100].

Balancing hydrolysis, condensation, and self-condensation is crucial for the surface modification process. The kinetics of hydrolysis and condensation are complex and governed by multiple parameters. The size and branching of the alkoxy group attached to the silicon directly influence the rate of hydrolysis, with smaller groups (e.g. methoxy) hydrolysing faster than larger groups such as butoxy, which has a direct effect on the thickness of the siloxane film [95]. The nature of the organic group (R group) influences the hydrolysis reaction, for example in presence of polarity the solubility increases thus promoting hydrolysis or in specific cases (e.g. amino, carbonyl or ester) affecting it directly by interacting with each other or with adjacent silicon groups [101], [102], [103]. In particular, the amino functionality tends to self-catalyse – both by hydrolysis and condensation – compared to other functionalities [104].The pH of a solution plays a critical role in controlling the rates of hydrolysis and condensation during silanization. In general, these reactions proceed very slowly in neutral conditions, necessitating the use of catalysts. Hydrolysis is typically favoured in basic environments, whereas condensation tends to proceed more rapidly under acidic conditions. Catalysts like ammonia, hydrofluoric acid, or organic acids (such as acetic acid) are often introduced to optimise reaction rates, ensuring efficient silanization [87].

In addition to hydrolysis and condensation reactions, phase separation must also be considered. As hydrolysis proceeds, a single phase containing reactive silanols is formed. With aging, the silanols condense to form siloxanes and the solution becomes rich in oligomers. Finally, as the molecular weight of these oligomers increases, phase separation and precipitation can occur. In this mechanism other important factors take place, water/silane ratio and solvent medium. In particular, the water-to-silane ratio significantly impacts the resulting oligomer characteristics – *both in the hydrolysis rate*, including their structure, shape, distribution, and molecular weight [95]. Generally, an increase in water content leads to higher molecular weights in the produced oligomers [105], [106]. Since many organosilanes exhibit poor solubility in water, it is often necessary to employ water-alcohol mixtures or organic solvents to ensure uniform polymerization. However, the use of these solvents can result in the generation of reactive, toxic, or flammable by-products, posing both safety and environmental concerns.

The deposition of silanes is a complex process due to the strong interdependence of the various parameters involved. The interaction between these variables makes it difficult to standardise the process, as altering one can significantly impact the others. This challenge highlights the need for precise control and careful optimization of processes and deposition parameters to achieve consistent and effective coatings.

2.1.4 Waterborne Silanes – Aminosilanetriols

The complexity of the silanization process presents significant obstacles for its industrial implementation. The deposition of organosilanes often requires organic or flammable solvents, prolonged hydrolysis times and often unstable products requiring freshly prepared solutions. These factors make process standardization difficult. In addition, managing reaction kinetics, catalysts and solvents to achieve consistent results adds further challenges. This complexity is enhanced by safety and environmental concerns, as industrial scale-up must also meet regulatory standards. Balancing these technical requirements with ecological and safety considerations

makes the industrial transfer of this process particularly challenging. The increased focus on environmental sustainability has also pushed the formulation of these silanes to be solvent-free and effective in industrial processes. As a result, the focus for achieving efficient and scalable industrial application of silane treatments has shifted towards the development of high silanols-content, compounds that are stable in aqueous solutions under neutral conditions.

Maximising the concentration of hydrolysed OH species is crucial in the industrial grafting processes [107], but equally important is the stability of these species in water over a reasonably long time. The hydrolysis of organosilanes produces highly reactive compounds, among which organosilanetriols $RSi(OH)_3$ stand out as a unique class [108]. Since 1959, they have been the focus of numerous studies for their preparation, stabilisation, and isolation. These compounds exhibit a strong tendency to form hydrogen-bonded networks due to the proximity of three donor and acceptor sites, with the high polarity of the Si-O bond enhancing this effect. However, this also contributes to their instability in aqueous environments. The development of *waterborne* silanes with stable silanol groups in water, has progressed significantly since the mid-20th century. Initial studies on alkoxysilanes revealed limits in industrial applications, inducing further research in the 1980s and 1990s that focused on the stabilisation of silanes in aqueous solutions [109], which led to advances in organosilane chemistry. These efforts culminated in the formulation of water-based silanes [110], which exhibit improved stability and performance. The inclusion of functional groups, such as amine, helped refine these compounds, allowing for controlled hydrolysis and improved adhesion under neutral or slightly acidic conditions. It was already known that amino functionalities are very effective in aqueous environments, thanks to the capability to act as an intramolecular catalyst [111]. They facilitate the rapid formation of silanols, with shorter reaction times than other functional groups, improve water solubility due to their polar nature and minimize self-condensation reactions [107].

Today, there are some commercially available water-based coupling agent solutions, usually free of VOCs and flammable alcohol byproducts, that consist of hydroxyl-rich silsesquioxane copolymers [112]. Some examples of commercial products are shown in Figures below, table with list of Gelest company products (*Fig. 2.4*) and chemical structures of two of these compounds *(Fig. 2.5-2.6)*.

Code	Functional Group	Mole %	Molecular weight	Weight % in solution
WSA-7011	aminopropyl	65-75	250-500	25-28
WSA-9911	aminopropyl	100	270-550	22-25
WSA-7021	aminoethylaminopropyl	65-75	370-650	25-28
WSA-6511	aminopropyl, vinyl	50-65	250-500	25-28
WSA-1511	aminopropyl, fluoroalkyl	15-20	–	15-20

Figure 2.4 Water-borne coupling agent solutions - Technical Brochure, Gelest [113].

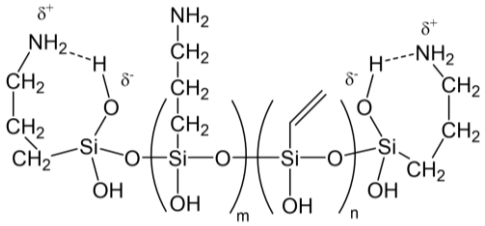

Figure 2.5 Aminopropyl/vinylsilsesquioxane in aqueous solution [114].

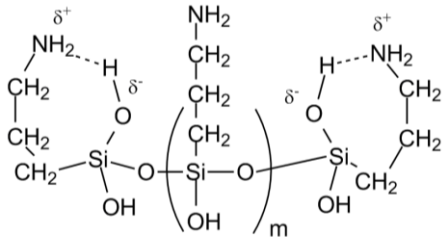

Figure 2.6 Aminopropylsilsesquioxane in aqueous solution [114].

The development of waterborne silanes, particularly *aminosilanetriols* based solutions, marks a significant advancement in industrial surface modification. These silanes offer notable improvements over traditional alkoxysilanes by addressing issues such as uncontrolled hydrolysis and the environmental concerns associated with organic solvents. Their ability to maintain stable, reactive silanol groups in aqueous and neutral environments leads to more consistent and durable coatings. This makes them ideal for pharmaceutical applications, where non-toxicity,

durability, and compliance with stringent regulatory standards are crucial. Their versatility and reliable performance represent a leap forward in creating scalable, sustainable coating solutions.

2.1.5 Structure of Siloxane Network and Interphase Region

The strength of adhesion between a film and its substrate is largely determined by the condition of the interfacial layer that forms between them. There are various types of interfaces that rely on different adhesion mechanisms [115], which are often combined to enhance overall performance, as schematically illustrated in *Fig. 2.7*.

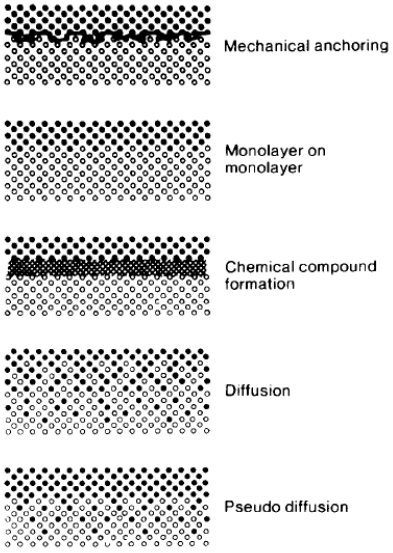

Fig 2.7 Different types of interface layers formed between film and substrate [115].

As previously mentioned, organosilanes act within the interphase region as "bonding" or "bridging" elements. This is because the interface that is formed is a combination of a chemically bonded layer to the substrate and a diffusion layer away from the surface that will allow the organic coating to bind to the substrate.

In the literature, several studies carried out by water extraction after the deposition of aminosilanes on SiO_2 surfaces have shown that film growth by this type of molecule is complicated and depends on several parameters such as the concentration of silane in solution, the immersion time, the pH of the solution, the choice of solvent and so on. Another important point is that both condensation with the hydroxylated surface and self-condensation occur during immersion, and that the latter could include horizontal and/or vertical polymerisation depending on the previously mentioned parameters [116]. All these factors influence the final structure of the siloxane network and the orientation of the molecules in the different layers of the deposited film.

From aqueous solutions, the amine groups can be deposited on the glass surface in two different orientations (*Fig. 2.8*), one with the silanols oriented towards the silanols of the glass substrate and the other with the amine groups oriented towards the glass surface [94], [117]. Furthermore, it is widely known that vertical polymerisation is favoured when the solvent used is water, and this could allow the deposition of thicker multilayer films [89], [94], [118]. In addition, the amino group can catalyse the formation and hydrolysis of intramolecular siloxane bonds through the formation of stable five-membered cyclic intermediates (*Fig. 2.9*) known as intra-amino siloxane bonds [94], [119]. This molecular rearrangement of the silanol during annealing will render many amines inaccessible [82].

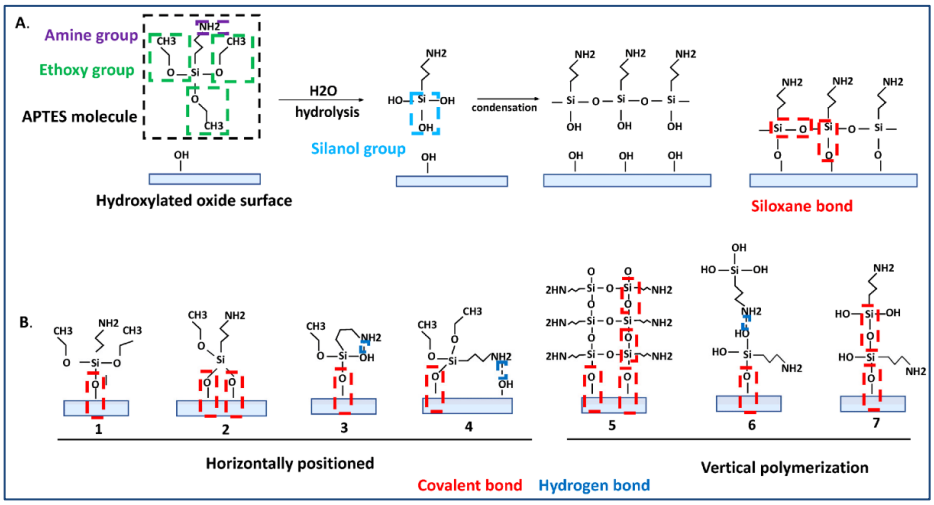

Fig 2.8 (A) Schematic representation of an APTES molecule, activation, and reaction with the hydroxylated oxide surface in an ideal situation. (B) Chemical interactions involved in APTES grafting on the hydroxylated oxide surface [94].

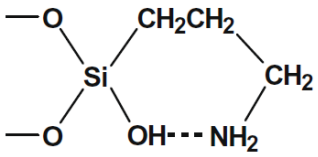

Figure 2.9 A proposed cyclic hydrogen-bonded amine structure in the hydrolytic APS Solution [119].

All these factors contribute to the complexity of determining the structure of the siloxane network formed after the deposition of aminosilanes in water. It is unlikely that this process will result in a monolayer. Instead, it is far more probable that a multilayer siloxane film will form, creating an interwoven network that may facilitate the adhesion of a subsequent organic layer.

Based on several studies, it was assumed that the siloxane network has a structure with decreasing density as one moves away from the glass surface towards the more superficial layers of the coating. This was confirmed thanks to the extraction and identification of soluble oligomeric aggregates present at the interface with the air [120]. Schematically, therefore, this network is made up of (See *Fig. 2.10*): a chemisorbed component which is the one close to the glass surface with which it has formed covalent chemical bonds; an intermediate component made up of molecules weakly linked by chemical bonds; and a physisorbed component with easily extractable oligomeric structures [120], [121]. The chemisorbed layer is characterized by a high density (cross-linked) network with a high protonated amine component and a low content of long network ends. The weakly chemisorbed layer is a cross-linked siloxane network-portion with high density of long chain network-ends in which the protonated amines are still present. Finally, the physisorbed layer is characterized by a loss of density with diffuse oligomers rich in free amine groups [117].

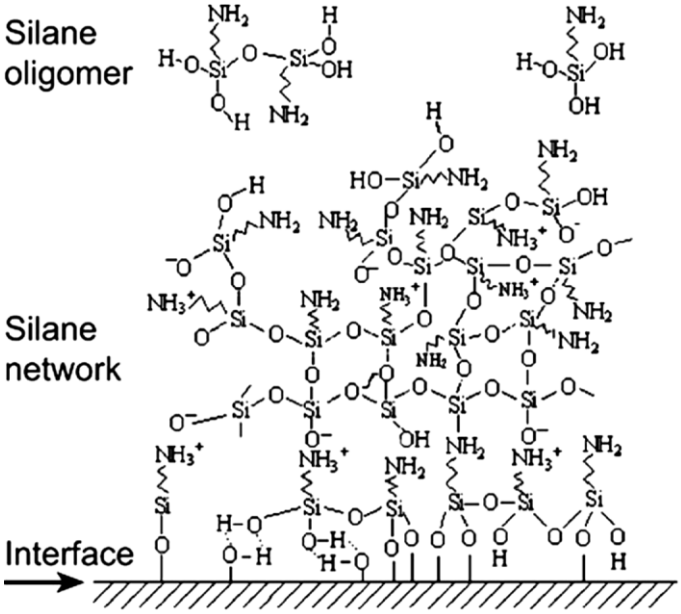

Figure 2.10 Schematic of composite interface between glass surface,, and polymeric matrix [117].

The presence of these soluble silane oligomers allows the silane deposit to diffuse into the organic polymer matrix to varying degrees. The oligomeric components may be present in the body of the deposit or as a surface-active agent adsorbed onto the siloxane film. These mobile silane oligomers diffuse into the organic layer, to varying degrees, leaving molecular-sized voids that accommodate the organic coating [100], [117]. In this manner, the role of the chemisorbed component is to facilitate the formation of molecular-sized pores, into which the organic molecules of the polymer can diffuse, thereby promoting adhesion through molecular interlocking. An interphase region, or interface, is established between the organic component of the coating and the inorganic substrate. The resulting adhesion mechanism is influenced by a combination of chemical and physical factors, including the formation of electrostatic interpenetration forces that act as adhesive agents, contributing to the final bonding process [63]. The formation of a so-called "*interpenetrating network (IPN)"* as a possible adhesion mechanism provides a mode of interaction between silanes and polymers that does not necessarily involve chemical coupling. This broadens the range of organic polymers with which organosilanes can be used as adhesion promoters [87]. In the interdiffusion process between the siloxane film and the

organic polymer, the chemical compatibility between the organic component of the coupling agent and the polymer is crucial. This compatibility facilitates strong interfacial adhesion by enabling the formation of Lewis acid-base interactions and molecular interpenetration [122]. The strength of substrate-coating adhesion is also influenced by this factor and must therefore be carefully considered to optimise silane performance and prevent debonding at the interface.

Various deposition factors will affect the formation and layering of the siloxane film, thereby influencing the structure of the interphase region between the organic coating and the glass substrate. This region will, in all cases, be characterised by an interface covalently bonded to the substrate, as well as a more or less diffuse interface, which may be defined by chemical bonding and/or interdiffusion between the siloxane and the polymer (*Fig. 2.11*).

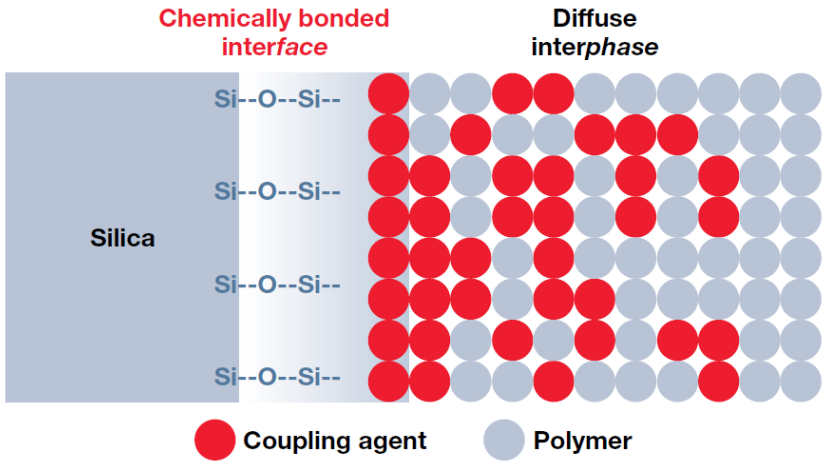

Fig. 2.11 The inter-penetrating network (IPN) bonding mechanism. Adaptation from [63].

2.2 Glass Surface Preparation

The preparation of glass surfaces for silanization is a crucial step that significantly influences the quality and functionality of silane deposition. Effective surface preparation involves thorough cleaning to remove organic contaminants and expose reactive hydroxyl groups (Si-OH) on the

glass surface, as mentioned in the previous paragraph. The concentration of hydroxyl groups on glass surfaces (Si-OH) determines the quality of silane deposition. The higher the density of hydroxyl groups on the glass substrate, the greater the uniformity and coverage of the silane layers. This improved bonding increases the structural integrity of the coating, making it more effective for applications requiring precise surface modification, such as promoting adhesion [123].

In the literature, there are numerous methods indicated for cleaning and activating the glass surface. These include various chemical cleaning procedures, HF etching, chelation and steam degreasing, as well as activation treatments with UV ozone, oxygen plasma, pyrolysis and lasers [71]. Below is presented an in-depth description of chemical cleaning, HF etching method and oxygen plasma activation which were used for the pre-treatment of the samples, as will be illustrated in the Experimental Section of this Thesis.

2.2.1 Wet Chemical Cleaning

Wet chemical cleaning methods are widely used for cleaning and activating glass surfaces prior to silanization. These methods involve the application of reactive liquids — combinations of acids, bases, and organic solvents — under controlled conditions of time, concentration, and temperature with the aim of interacting with the surface contaminants to produce soluble byproducts, which can then be removed [124]. Despite the availability of various cleaning methods, no universal protocol has been established, particularly for glass, which is a less homogeneous substrate and have received less attention compared to silica [125]. Common solvents include acetone and isopropanol, which are effective for dissolving organic contaminants. Acidic and basic solutions such as hydrochloric acid (HCl) and potassium hydroxide (KOH) are used as leaching agents of the glass surface, exposing the silanol groups necessary for silanization [125]. One of the most effective cleaning agents is the Piranha solution—a highly oxidizing mixture of concentrated hot sulfuric acid and ammonium persulfate. The resulting peroxysulphuric acid reacts with water, releasing reactive oxygen atoms, highly effective in

removing organic contaminants and exposing hydroxyl groups. However, its highly reactive nature poses significant safety risks, including potential explosions, making it unsuitable for routine use [124], [125]. An alternative often used is a combination of peroxide and ammonium compounds [82], effective in complexing surface contaminants [124]. The most common involves hydrogen peroxide/ammonium hydroxide mixture, followed by an acid rinse, and it is known as Remote Chemical Cleaning (RCA), particularly employed in the semiconductor industry [71]. Experimental studies stated that, for glass silanization, this cleaning method is versatile and less aggressive than the Piranha solution, though it is also somewhat less effective in achieving maximum cleanliness [125]. Another common procedure is methanol/hydrochloric acid washes [94] often followed by a sulfuric acid bath, which effectively removes organic contaminants and prepares a uniform, reactive surface for silanization [125]. However, it is a corrosive process and requires careful handling due to the aggressive chemicals involved. Each wet chemical cleaning method has its specific advantages depending on the type of contaminants and the surface involved. Acid cleaning is highly effective at dissolving organic residues, but its corrosive nature requires careful handling. Alkaline cleaning, using solutions like sodium or potassium hydroxide, effectively removes organic residues while being safer than acid cleaning. Solvent cleaning, using organic solvents such as acetone or isopropanol, efficiently removes oils and greases but may be less effective against inorganic contaminants. Despite their effectiveness, wet chemical cleaning methods may leave residues that can hinder silanization if not thoroughly rinsed and pose challenges in terms of safety, effectiveness, and environmental impact.

Chemical cleaning is usually done using an ultrasonic bath, making it more effective. This cleaning methodolgy utilizes ultrasonic waves (20-40 kHz) to create cavitation in a solvent-filled container. The collapse of microscopic bubbles generates localized high pressure (~1000 atm) and temperatures, producing a scrubbing action that effectively dislodges contaminants from surfaces [71], [126]. This method offers significant advantages for cleaning glass surfaces, especially for removing tough contaminants from intricate geometries. It is particularly effective for dislodging large particles like polymers, resins, and fats [127]. Ultrasonic cleaning is often paired with mild chemical solvents to enhance its overall cleaning efficiency, as the cavitation process aids in the removal of contaminants dissolved or softened by the solvent [124]. While widely used as a

routine cleaning method in laboratories, especially for glassware, ultrasonic cleaning is considered a preliminary step. To achieve full surface activation, it must be followed by more precise treatments, such as plasma or UV-ozone cleaning, to fully prepare the surface for subsequent processes [124].

2.2.2 HF etching

Chemical etching can be used to remove surface material along with the contaminants. Etching removes surface layers such as oxides, eliminates or smooths out surface cracks in brittle materials, and removes challenging contaminates. Hydrofluoric (HF) acid solution is a common etchant for silicon and is particularly potent for etching glass surface [124]. HF etches silicate glass by breaking the Si-O bonds within the silica network, involving a coordinated attack where a Lewis acid targets the bridging oxygen atom and a Lewis base interacts with the silicon atom [71]. This interaction causes a redistribution of electrons, leading to the formation of an O-H group and a Si-FH group, ultimately resulting in the formation of soluble compounds like silicon tetrafluoride (SiF_4) and hexafluorosilicic acid (H_2SiF_6) as showed in the reaction below (4):

$$SiO_2 + 6HF \rightarrow H_2SiF_6 + 2H_20 \quad (4)$$

The above mechanism for dissolving vitreous SiO_2 can also be applied to dissolving glasses with more complex compositions, but the etch rate varies widely. HF etching of soda-lime glass involves the removal not only of the silica, but also of sodium and calcium ions. HF reacts with these components to form soluble fluorides, facilitating the removal of the surface layers. The process is particularly efficient due to the presence of these alkali and alkaline earth metals, which are more easily etched than pure silica. On the other hand, borosilicate glass is more resistant to HF etching due to the strong bonding between boron atoms within the glass matrix. As a result, the etch rate of HF on borosilicate glass is reduced with respect to that on soda-lime glass [128]. Another point is that HF etching of the silicon surface can allow both hydrogen terminations and hydroxyl terminations. In the first case the surface becomes hydrophobic and in the second hydrophilic. Some studies identify different regimes for the glass etching process. After a wetting

phase, a regime occurs in which the glass surface becomes hydrophobic. This dewetting phase can be due to non-uniform etching and depends on the glass composition and surface conditions [129]. In general, cleaning methods are preferred which do not etch or otherwise chemically attack the glass object, such as for instance organic solvents, aqueous detergent solutions or strong acids. However, for some contaminants which are not attacked by these liquids, it is necessary to use a process which dissolves the glass surface and thus frees the contaminant from the surface. Aqueous HF etching is used in that case. The formation of insoluble fluorides can be avoided by adding a strong acid [128], however, it is important to perform an ultrasonic wash in water to remove insoluble byproducts [130].

2.2.3 Plasma treatment

Plasma treatments utilise reactive species, such as charged, atomic or radical species, generated in the plasma that impact the surface by releasing their ionisation or excitation energies. The interaction between reactive species and the surface leads to the formation of volatile compounds that are then removed from the treated substrate without leaving any residues. This absence of residue is an additional advantage of plasma cleaning compared to cleaning with chemical solvents [124]. During plasma treatment of a glass surface, two main processes occur, both closely related to the presence of physically and chemically adsorbed water molecules (*Fig. 2.12*). The first process involves the removal of organic contaminants, while the second leads to the formation of polar groups [131].

The energy of the plasma electrons is sufficient to first break the hydrogen bonds (0.2-0.3 eV) of the weakly adsorbed water on the glass surface. This physically bound water layer is removed, along with any overlying organic impurities. Additionally, the electron impact cleaves the O-OH bonds in the chemically adsorbed water layer, resulting in the formation of atomic oxygens and numerous OH radicals on the glass surface [132] [71] (*Fig. 2.13*). Due to the polarity of surface-exposed hydroxyl functional groups, the surface becomes more hydrophilic, leading to an

increase in surface free energy and enhanced wettability [133] that plays a crucial role especially in silanization process.

Oxygen (or air) plasmas are highly effective in removing hydrocarbons and adsorbed water vapour from surfaces, but other reactive gases like nitrogen, argon, and hydrogen are also used [131]. The choice of gas depends on the desired surface modification and the type of substrate. For hydroxylation of glass surfaces, oxygen is most commonly used [71].

This dry cleaning method compared to wet chemical methods offers several advantages, including the absence of secondary contamination, no damage to the substrate, high efficiency, and environmental friendliness [131].

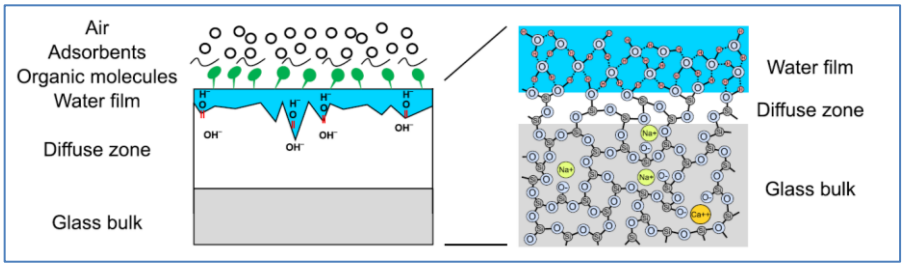

Fig 2.12 Water film adsorbed onto soda-lime glass surface [132].

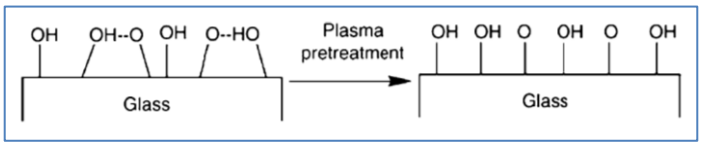

Fig. 2.13 The change of molecular structure on glass surface after plasma treatment [71].

2.3 Lubrication in Glass Container Industry

In the glass packaging industry, lubricants are usually applied to the surface of glass containers to reduce friction and improve container handling during all stages of production. Reducing the coefficient of friction is essential for the smooth movement of sliding mating surfaces, as it

prevents excessive surface damage and wear [134]. This becomes particularly mandatory in the case of pharmaceutical packaging to ensure the integrity of the vials and avoid the formation of cracks that can lead to serious safety issues as discussed in detail in paragraphs 1.2. Indeed, the lubrication mechanism involves the introduction of a layer between the sliding surfaces that has a lower shear resistance than the surfaces themselves, which is essential to ensure smoothness between contacting surfaces [135]. This thin protective layer minimizes direct contact between the external surfaces of the vials moving on the production/filling equipment or on the handling tools. This reduces the likelihood of mechanical damage, such as micro-abrasions or scratches, which can compromise the integrity of the vials and lead to contamination.

2.3.1 Lubrication Mechanism of Organic Molecules on Glass

The lubrication mechanism involving organic molecules on glass surfaces is a complex interplay of interactions among microscopic surface asperities when one solid slides against another. During this contact, attractive forces arise at the asperity boundaries, resulting in the formation of microscopic bonds between the two solid surfaces. This bonding process can lead to surface damage, particularly when forces are applied in different directions, which in turn leads to high coefficients of friction and heat generation, contributing to the welding of the asperities. This phenomenon is particularly pronounced in soda-lime glass surfaces, for which adsorbed water facilitates the extraction of sodium from the glass. The resulting alkaline solution interacts with the surface, forming a gel-like layer that solidifies under load, resembling a cement-like substance that enhances the bonding of the asperities under pressure [50].

The effectiveness of adsorbed or deposited organic molecules in reducing surface friction and preventing damage depends on several factors. These include the strength of the organic molecules' adhesion to the glass surface and the thickness of the organic lubricating layer, which can be increased by depositing multiple layers or extending the alkyl chain length. Thicker layers elevate the distance between the contacting solids, thereby decreasing the number of asperities that make contact. Surface damage typically occurs only when the organic layer is compromised.

Furthermore, the extent of intermolecular forces among the adsorbed molecules (layer cohesion) and the degree of surface coverage also significantly influences lubrication efficiency. Finally, to minimize adhesion and the coefficient of friction, the outermost end groups of the adsorbed organic molecules should possess the lowest possible surface energy, allowing the lubricated surfaces to slide against each other without being damaged [50]. Among organic compounds, the most commonly used as lubricants in the glass container industry include polyethylene (PE) and polyethylene emulsions, epoxy resins, ethyltetrafluoroethylene (ETFE), and carboxylic acids (stearic and oleic) [136]. The application of these compounds typically follows a cold-end coating treatment that is widely utilized in industrial processes, occurring after an initial hot-end coating treatment. This hot-end treatment involves the deposition of a metal oxide layer, usually tin oxide (SnO_2), as discussed in the first chapter.

2.3.2 Lubricants for Pharma

In the pharmaceutical sector, all materials involved from the production to the end-use of containers must meet specific requirements. These requirements are outlined in the guidelines of the European Pharmacopoeia (EP), Good Manufacturing Practice (GMP), European Medicines Agency (EMA) regulations, and applicable ISO standards. Although these do not specifically address lubricants, they establish general standards that influence the selection of materials, including coatings for pharmaceutical containers [EP Chapters 3.1 - Materials used for the manufacture of containers, 3.2 – Containers, 3.2.1 – Containers for Pharmaceutical Use]. Therefore, when considering the use of lubricants for the surface treatment of pharmaceutical containers, it is essential to adhere to these strict regulations that ensure both the safety and functionality of the product throughout its life cycle. These requirements can be outlined as follows:

Safety, biocompatibility, and chemical inertness: According to EudraLex Volume 4 and European Pharmacopoeia (EP) Chapter 3.1, materials applied to pharmaceutical containers must meet strict biocompatibility standards, ensuring that no harmful substances leach into the drug product,

thereby preserving its stability and integrity. Also, lubricant must adhere to the high purity standards set by the regulation EP Chapter 3.2.1: Containers for Pharmaceutical Use, which help prevent chemical, physical, or microbiological contamination during the manufacturing process (EudraLex Volume 4, Annex 1). In addition to biocompatibility and high purity, lubricants must demonstrate chemical inertness. These materials must undergo thorough compatibility testing with the pharmaceutical product to ensure no adverse chemical interactions occur. The lubricant must not interact with the container materials, such as glass, nor cause any chemical degradation. Furthermore, the lubricant must not migrate into the pharmaceutical product in amounts that could compromise the drug safety, quality, or efficacy. These stringent requirements ensure that no contamination or adverse reactions take place between the lubricant and the vial contents, thus preserving the drug's therapeutic integrity.

Sterility and Thermal Stability: Lubricants and coatings applied to glass vials must withstand the rigorous sterilization and depyrogenation processes commonly carried out by the pharmaceutical customer before filling the vials, which often involve temperatures exceeding 250°C to 300°C. The European Pharmacopoeia (EP) mandates that lubricants remain stable under these conditions without degrading or degrading without leaving residues that could compromise the sterility of the containers [EP Chapter 3.2.9]. EudraLex Volume 4, Annex 1 also addresses the requirements for maintaining the integrity of materials during high-temperature sterilization. It must not introduce particulate contamination, microorganisms, or other impurities during the sterilization process. In addition, biocompatibility testing should be conducted to confirm that, also after sterilization, the lubricant does not elicit any toxic or irritant effects, and that it is safe for use in the pharmaceutical environment [EudraLex, Vol. 4, Annex 1; EP Chapter 3.2.9].

To date, the most widely used products for lubricating pharmaceutical containers include:

Silicone Oils: Silicone oil usually refers to linear polysiloxane products that remain liquid at room temperature. Its repeating unit is alternating silicon and oxygen atoms, and there are two organic groups connected to each silicon atom. It is produced by hydrolysis and polycondensation of dichlorodimethylsilane and chlorotrimethylsilane. Among these, polydimethylsiloxane (PDMS) was the most widely accepted type of silicone oil used as a lubricant for pharmaceutical containers, particularly for internal surface of glass vials and syringes [EP Chapter 3.1.8. - Silicone

oil used as a lubricant]. Silicone oils are favoured for their chemical inertness, stability, low volatility, and ability to form a non-toxic, stable, and thin lubricating layer. Thanks to their high stability to heat and oxygen [137] they can withstand high-temperature sterilization processes, including autoclaving, without degrading or releasing harmful byproducts. However, silicone oils are generally used with strict limits on particle contamination, as they can potentially generate silicone droplets or particles in suspension, which is a concern for injectable drug products. For this reason, pharmaceutical manufacturers must validate the application process and ensure that particulate contamination remains within safe limits [EP Chapter 3.1.8. - Silicone oil used as a lubricant].

Oleic acid: has a long history as a lubricating coating for glass, typically applied through steam directly onto the glass surface, which allows for a significant degree of adsorption [50], [138],[139]. In the pharmaceutical sector, although it is considered a traditional method that is now outdated, its use is consolidated and is applied to specific bottles for specific end uses.

Polyethylene/polyethylene emulsions: are widely used in cold processing, especially in glass packaging for the food industry, for which there are several industrial formulations [140]. Despite this, in the pharmaceutical field it is often replaced by products such as macrogols stearates, which better meet the sterility requirements following thermal treatments such as the depyrogenation cycle.

Macrogol stearates: also known as polyethylene glycol (PEG) stearates, are widely accepted as excipients in pharmaceutical formulations due to their non-toxic and biodegradable properties. In the context of pharmaceutical packaging, particularly for glass containers, macrogol stearates are gaining attention as potential lubricants [EP 5.0 Macrogols]. One of their key advantages is their ability to undergo high-temperature processes, such as depyrogenation cycles, without leaving harmful residues. This makes them suitable for applications where cleanliness and the absence of contaminants are critical. During the depyrogenation process, which typically involves temperatures up to 300°C, the macrogol stearates are completely removed, ensuring that the glass container remains free of chemical residues that could compromise the purity or safety of the drug. Their acceptance in the European Pharmacopoeia (EP) and United States Pharmacopeia (USP) underscores their compliance with strict regulatory standards for pharmaceutical use.

Although their primary use has been as emulsifiers or solubilizers in drug formulations, their potential as external lubricants in pharmaceutical packaging is recognized due to their ability to reduce friction and prevent surface damage without compromising the sterility or integrity of the container. Another important feature relies in their water solubility making macrogols stearates valid alternative to traditional oil-based lubricants.

In recent years, non-silicone lubricants have been increasingly explored, especially in response to concerns about silicone-related particulate contamination [141]. Several alternative coating technologies have been developed, including plasma coatings and hybrid polymer coatings, which provide similar lubricating properties while minimizing the risk of interaction with sensitive drugs. Much has been done in the field of internal lubrication of glass containers, like syringes. Regarding the development of low-friction coatings for the external surface of vials, there are a few alternative studies to date, which are mainly the subject of patents. These patents concern in particular the formulation of polyimide-based coatings, fluoropolymer-based coatings, such as polytetrafluoroethylene (PTFE), functionalized polymers with amino groups and multilayer systems, incorporating materials such as silsesquioxane [patent US 11,737,951] [142]. These new coatings have been formulated not only to increase lubricity but also to increase thermal resistance to high temperature sterilization processes.

2.4 Experimental Techniques

2.4.1 Deposition Methods from Solutions

The following paragraphs contain a synthetic description of the main experimental techniques used to carry out this research activity. Each technique is presented through its basic operation principles, with a focus on the specific instrumentations used to obtain the results presented in the following chapters. Where necessary, the working conditions and experimental modalities chosen to address the samples peculiarities (i.e. organosilane coatings on glass samples) are discussed.

Dip-Coating

Dip coating is a straightforward, cost-effective, and high-quality deposition technique used in both industrial and laboratory settings. The process involves immersing a substrate into a solution containing the coating material, then withdrawing it to form a thin, uniform layer [143]. This technique is ideal for applying aqueous-based coatings, where the solute adheres to the substrate, and the solvent evaporates, leaving a dry film. The thickness and morphology of the resulting film depend on several parameters, including immersion time, withdrawal speed, number of coating cycles, solution concentration, density and viscosity, surface tension, substrate characteristics, and drying conditions.

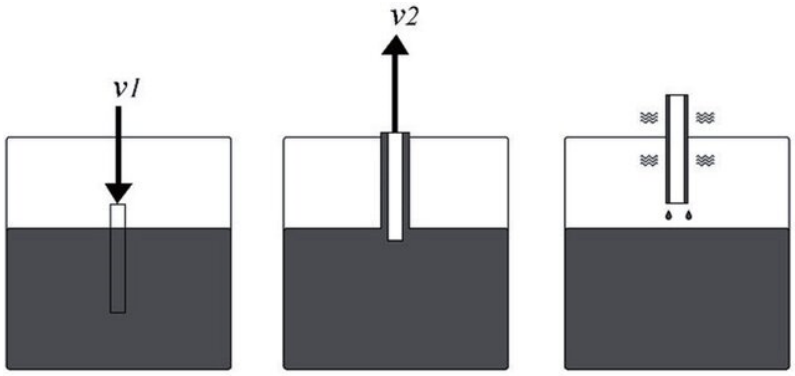

Figure 2.14 Schematic view of dip coating deposition in lab [143].

The dip-coating process consists of four main stages, as outlined below and shown in *Figure 2.14*:

i. Immersion: The substrate is fully immersed in the coating solution until completely covered by the liquid.
ii. Dwelling: The substrate remains submerged for a short interval to stabilize the liquid contact with the surface.
iii. Withdrawal: The substrate is gradually withdrawn from the solution, leaving a thin film of coating material on its surface. During this stage, entraining forces retain the solution on the substrate, while draining forces pull the liquid back into the bath. The balance between these forces determines the thickness of the wet film.
iv. Drying: The solvent evaporates from the deposited film, leaving a solid layer. At this stage, the film undergoes chemical or physical transformations to finalize its structure and properties.

In this study, soda-lime glass pieces and/or vials were coated by immersion in an aqueous organosilane solution at concentrations of 0.5%, 1%, and 2% by volume, using 50 mL beakers. The samples were suspended in the solution using tweezers to ensure complete immersion, with immersion times varying between 120 - 60 - 30 and 15 minutes. Following immersion, the samples underwent a drying (curing) phase in an oven at 150°C for 2 hours. Prior to deposition, the glass surfaces were prepared by ultrasonic cleaning in deionized water, acetone, and isopropanol to ensure surface cleanliness. An oxygen plasma treatment was then applied to activate the glass surface, as detailed in Chapter 2. In some cases, the samples were rinsed with deionized water after immersion in the silane solution to remove excess material before the curing phase (Chapter 3). The immersion method was also used for lubricant deposition as described in Chapter 3. This procedure allowed for controlled silane deposition, optimizing surface coverage and adhesion on the glass substrates.

Spray Coating

In recent years, spray coating has gained prominence as a low-cost, scalable technique for depositing solution-processed thin films on large areas. This method, illustrated in *Figure 2.15*, involves directing fine droplets of material onto a substrate using a carrier gas, allowing thin films to conform to the shape of the surface. Spray coating is contact-free, making it adaptable to various substrate materials and suitable for low-temperature applications [144].

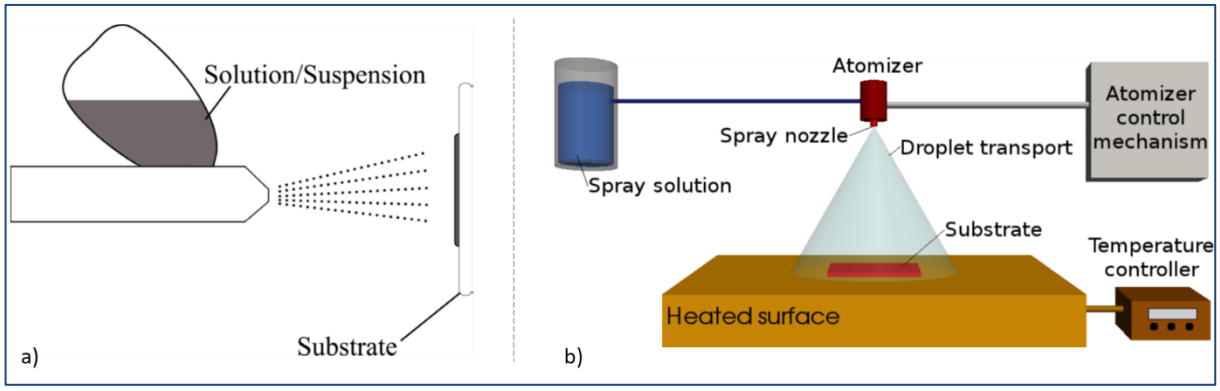

Figure 2.15 Schematic representation of the spray coating process using different tools. a) process with airbrush system; b) spray coating process with heated plate. Adapted from [143], [145].

The deposition process is influenced by complex fluid dynamics as droplets spread, splash, coalesce, and interaction with other droplets upon impact with the substrate (see *Fig. 2.16*). Factors such as surface roughness, permeability, and surface energy play significant roles in droplet behavior and wetting properties.

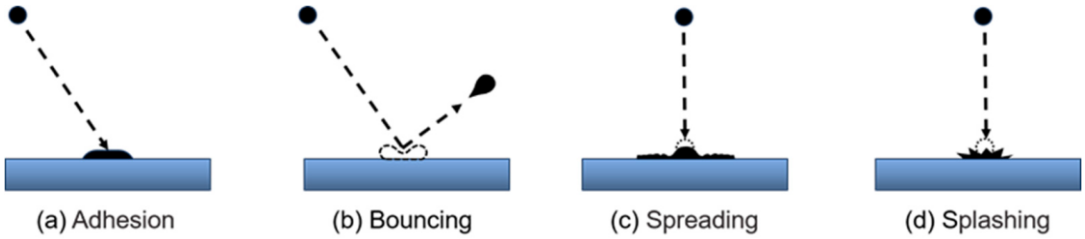

Figure 2.16 Impact modes of the droplets [146].

Atomization, or the breakdown of liquid into micron-sized droplets, is achieved by applying mechanical energy through a gas stream, which produces a spray pattern ideal for coating uniformity. The dynamics of atomization and droplet impact affect the morphological consistency of the resulting thin films. Key experimental parameters influencing film quality include [143]:

- Nozzle Tip Speed and Flow Rate: The speed of the nozzle, its height above the substrate, and the solution flow rate (FR) are critical in controlling the distribution and size of droplets impacting the substrate. These factors collectively determine the thickness and uniformity of the deposited layer.

- Number of Spray Cycles: Increasing the number of spray cycles improves surface coverage and enhances film thickness. Repeated cycles can smoothen the film by filling in any defects from earlier layers, though this effect is also temperature-dependent.

- Substrate Temperature: The substrate temperature affects film characteristics through its influence on droplet evaporation, viscosity, and spreading dynamics. Higher temperatures can lead to rapid solvent evaporation, limiting droplet spread. A balanced temperature range is ideal, providing sufficient time for droplet coalescence while supporting rapid solvent evaporation for a uniform film structure.

- Nozzle-to-Substrate Distance: The distance between the spray nozzle and the substrate is critical, as it depends on solution properties, droplet size, and substrate temperature. Adjusting this distance optimizes droplet impact and film coverage.

Two different spray deposition systems were used in this study: a FENGDA airbrush model BD-813 equipped with a HS-E550BLK spray booth, located at the CEITEC Institute in Brno, Czech Republic, and a ND-SP Precision Spray Coaters, model - ND-SP 11/4, at the FunGlass Institute in Trenčín, Slovakia, during two separate research periods abroad. A detailed analysis of the experimental procedures conducted with these systems is presented in Chapter 4, which deals

with the study of industrial scalability. The air-brush system used in the first case is operator-dependent, while the spray system in the second case is an automated system equipped with a heated plate, thus providing a closer simulation of the intended industrial deposition process.

2.4.2 Contact Angle Measurements

A key characteristic of a surface is its free energy, which can be evaluated by examining the shape of a liquid droplet on the surface. This shape provides, in effect, a measure of the wettability of the surface by a specific liquid. In fact, free energy and wettability are correlated: on surfaces with higher free energy, the saturation of surface bonds is favoured, resulting in increased wettability. The parameter of interest in these measurements is the contact angle θ that is the angle formed at the intersection of the liquid/gas interface and a solid surface (*Fig. 2.17*).

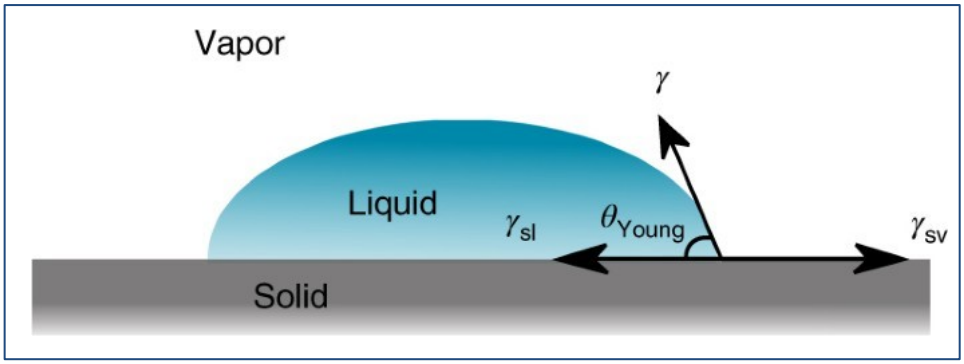

Figure 2.17 A drop of water on an ideal solid substrate. Young contact angle (ϑ_{Young}) is determined by a balance of the horizontal projection of the surface tension of the water along the solid surface ($\gamma \cos\vartheta_{Young}$) and interfacial tensions γ_{sv} and γ_{sl} [147].

A lower contact angle indicates better wettability, while a higher contact angle suggests poorer wettability. The contact angle reflects the degree of similarity between the interacting phases. Depending on the contact angle's value, three main cases (see *Fig. 2.18*) can be distinguished [148]:

- *Good wetting* occurs when $\theta < 90°$, indicating strong interaction between the liquid and the surface.

- *Poor wetting* is observed when θ>90°, meaning the liquid interacts weakly with the surface.
- *Absolute wetting* or *spreading* takes place when no equilibrium contact angle is formed, and the liquid spreads across the surface, forming a thin film.

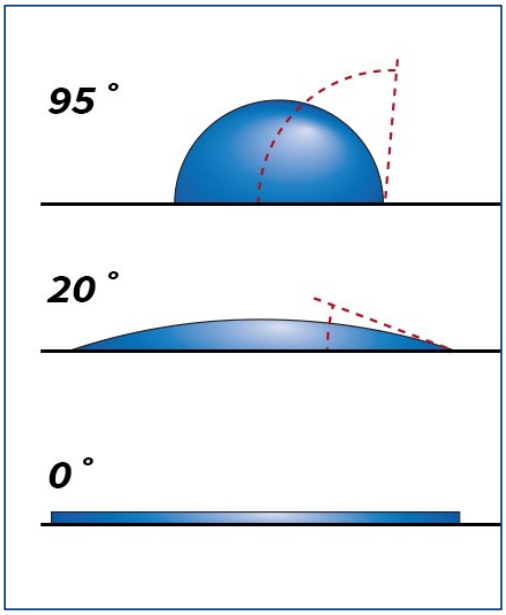

Figure 2.18 Different degree of wetting. Adapted from [149] .

The contact angle of water on solid surfaces is frequently used to assess surface hydrophilicity or hydrophobicity. On extremely hydrophilic surfaces, a water-drop spreads completely, while large water contact angles ($\theta > 90°$) indicate hydrophobicity.

The relationship between the contact angle and the thermodynamic properties of the phases involved is described by Young's equation (5):

$$\cos\theta_{Young} = \frac{\gamma_{SV} - \gamma_{SL}}{\gamma} \quad (5)$$

where γ_{SV}, γ_{SL} and γ are the interfacial energies of the solid/vapor, solid/liquid, and liquid/vapor interfaces, respectively.

One method for measuring the contact angle is the sessile drop method. This technique involves analysing the shape of a liquid drop resting on a solid surface. The profile of the drop is captured through imaging, and the contact angle is determined from the shape analysis. This method is widely used for evaluating surface wettability and interfacial interactions.

In this study, a See System E/S by Advex Instruments—a portable, computer-based instrument equipped with See System Software for Surface Energy Measurement—was employed to measure the contact angle. This system was used to assess the effectiveness of surface activation methods on glass substrates prior to coating deposition. Measurements were conducted following plasma pretreatment (as discussed in Chapter 2) and after chemical cleaning methods (detailed in Chapter 3). Additionally, as it will be shown in Chapter 3, this system was used to verify the successful deposition of the coating.

2.4.3 Surface Morphological Characterization

2.4.3.1 SEM

Scanning Electron Microscopy (SEM) is a high-resolution imaging technique that enables the detailed investigation of the surface of materials by scanning the sample with a focused beam of high-energy electrons, typically generated from an electron gun [150], (see *Figure 2.19*). The interaction between the electron beam and the atoms in the sample results in the emission of various signals, such as secondary electrons, back-scattered electrons, and characteristic X-rays, which are subsequently detected and used to produce detailed images and compositional information (see *Figure 2.20*).

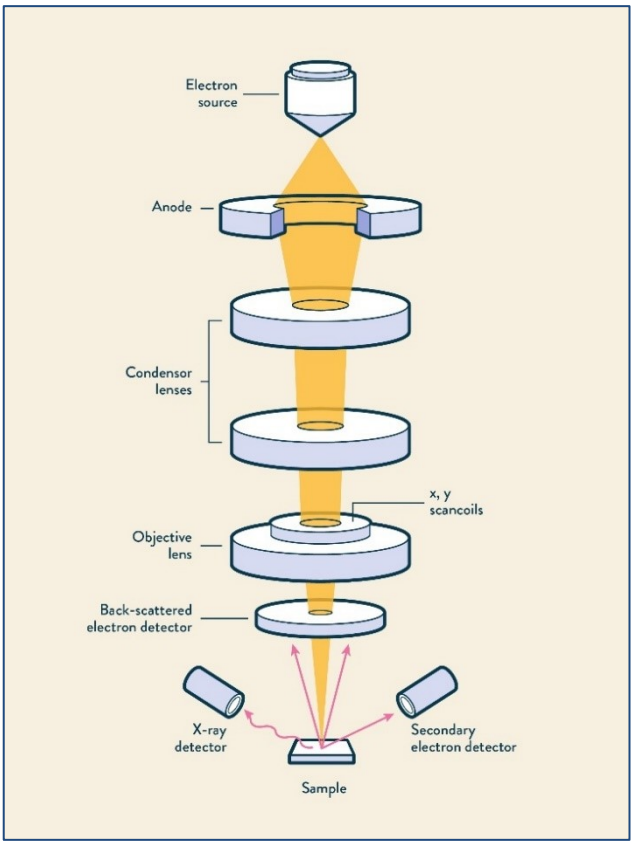

Figure 2.19 Scheme of Scanning Electron Microscope [151].

These interactions provide valuable insights into the surface topography, composition, and other properties of the sample, such as its electrical conductivity. Secondary electrons, with their lower energy and high topographic sensitivity, are the primary signal used for surface imaging, offering excellent spatial resolution. Meanwhile, back-scattered electrons provide contrast based on the atomic number, making them useful for identifying compositional differences. Additionally, the X-rays generated by electron bombardment can be analysed for elemental composition using techniques such as energy-dispersive X-ray spectroscopy (EDS), allowing for quantitative analysis of the sample elemental makeup.

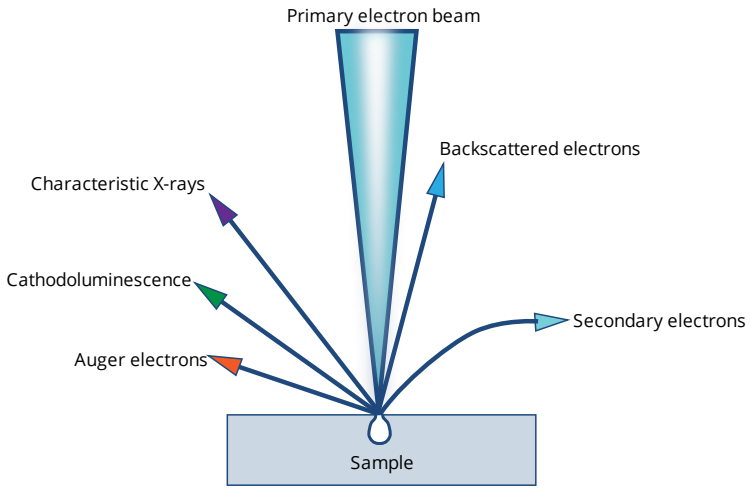

Figure 2.20 Electron-matter interactions [152].

To evaluate the homogeneity of surface features across the entire sample area, SEM analysis was conducted on selected uncoated glass samples using a Zeiss Auriga Compact system equipped with a field emission gun. To impart electrical conductivity to the surface, glass samples were metallized with a thin layer of gold. SEM imaging using secondary electrons confirmed key surface characteristics of the uncoated glass at the microstructural level. However, due to the thinness of the coatings applied in this study, these layers were not clearly visible in the SEM images, likely due to the additional gold coating required for conductivity. For morphological analysis at the nanometric level, where higher resolution and surface roughness evaluation were essential and could not be adequately captured by SEM, Atomic Force Microscopy (AFM) was employed. AFM allowed for a more detailed investigation of the thin coatings and provided a precise evaluation of the surface roughness, which could not be adequately captured by SEM.

2.4.3.2 AFM

Atomic Force Microscopy (AFM) is a type of scanning probe microscope introduced in 1986 by Binning, Quate, and Gerber [153], which provides surface morphology information with nanometric resolution. In essence, AFM operates by scanning a sharp tip attached to a cantilever

across the surface of the sample being analysed [154]. The tip establishes interactions with the atoms on the surface, allowing for the reconstruction of the surface profile and, consequently, the morphology of the scanned area. AFM utilizes relatively strong forces that act between the tip and the sample surface, which can range from Van der Waals and capillary forces to electrostatic or magnetic interactions. The tip, which has a curvature radius on the nanometer scale, is integrated into a cantilever (a small tip mounted on a flexible lever) that moves across the sample's surface. This tip is deflected by the interactions occurring between the atoms of the sample and those of the tip. The deflection is measured using a laser beam that is focused on the back of the cantilever. The reflected laser beam is then detected by a set of photodiodes, sensitive to two-dimensional positional changes (see *Fig. 2.21*).

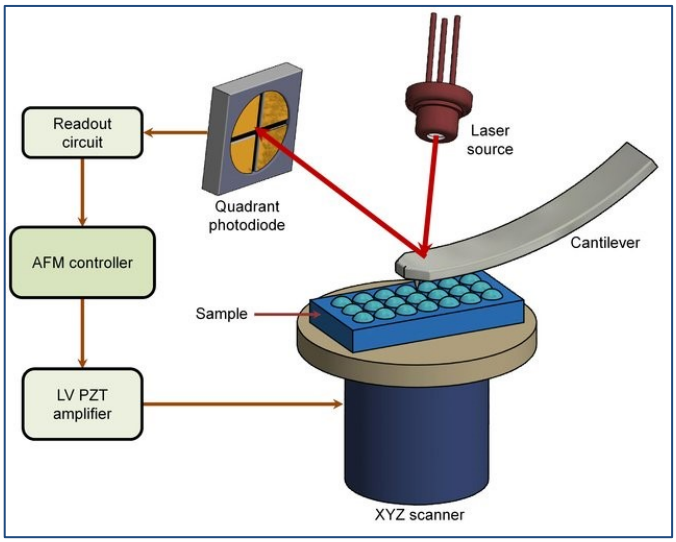

Figure 2.21 Schematic of an Atomic Force Microscope setup [155].

The forces between the tip and the sample atoms on the sample surface include both attractive and repulsive forces. The resulting deflection of the cantilever is a direct measure of the force acting between the tip and the sample surface. The variation of the force as a function of tip-sample distance is represented in *Figure 2.22*, illustrating the interaction regimes encountered during AFM measurements.

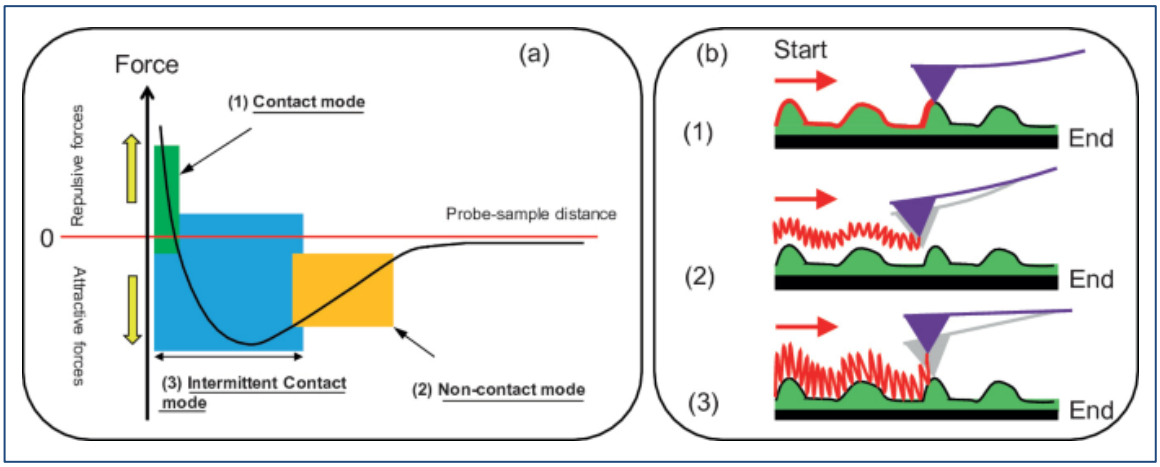

Figure 2.22 (a): Force applied on the tip by the surface as a function of the tip-sample distance. (b): different operative modes, contact-mode (1), non-contact mode (2) and tapping mode or intermittent contact mode (3) [156].

AFM can operate in several modes, each suited to different surface interactions and sample characteristics.

- In contact mode, the tip remains in constant contact with the surface, and the cantilever deflection is controlled by a feedback loop to maintain constant force, providing topographical information. However, this continuous contact can generate lateral shear forces, potentially damaging delicate samples by dragging atoms or molecules from the surface, thus altering both the topography and the imaging conditions.
- In tapping mode (or intermittent contact mode), the cantilever oscillates near its resonance frequency, and the tip touches the surface intermittently, maintaining a distance in the range of 1 to 100 nm. The interaction between the tip and sample dampens the oscillation amplitude, and a feedback system keeps this amplitude constant. Tapping mode reduces sample damage by minimizing contact time and prevents inelastic surface modifications, making it ideal for imaging delicate or loosely bound surfaces. It also provides high-resolution information on surface topography and roughness.
- Non-contact mode involves the tip hovering 5 to 15 nm above the surface, detecting long-range attractive forces such as van der Waals forces. This mode eliminates the risk of

sample damage but typically offers lower resolution due to the weaker interactions involved. It is useful for imaging soft or highly sensitive materials.

Each mode offers distinct benefits depending on the sample's sensitivity and the desired information, making AFM a versatile tool for nanoscale surface characterization.

For the surface topographic analysis of glass samples, Atomic Force Microscopy (AFM) was conducted in tapping mode using a Dimension 3100 scanning probe microscope equipped with a Nanoscope IVa controller (Bruker). Three types of AFM tips were employed: OTESPA-R3 from Bruker, and PPP-NCR-10 (Tapping mode) and PPP-NCSTR-10 (Soft Tapping mode) from Nanosensors, with spring constants of 2 N/m, 10-58 N/m, and 1.2 - 29 N/m, respectively. For the characterization of coated glass samples, soft-tapping tips were specifically chosen to minimize the tip-sample interaction on organic coatings, despite the operation being in tapping mode. This approach was critical to preserving the integrity of the organic layers while ensuring high-resolution imaging.

2.4.4 Surface Chemical Characterization

The surface characterization of glass substrates coated with organosilanes was carried out by two widely employed techniques for this purpose which are Fourier-transform infrared spectroscopy (FT-IR) and X-ray photoelectron spectroscopy (XPS). Both methods provide complementary information, allowing for a comprehensive analysis of the chemical bonds, functional groups, and surface elements.

2.4.4.1 FT-IR

Fourier Transform Infrared Spectroscopy (FT-IR) [157] is a highly sensitive technique used for analyzing molecular vibrations and is widely employed in the characterization of organic-inorganic coatings. Introduced in the 1980s [158], FT-IR involves the interaction of electromagnetic

radiation in the infrared (IR) region with matter, providing information on molecular composition through the absorption of specific photon frequencies. When a material is exposed to IR radiation (in the 4000-200 cm^{-1} wavelength region), its molecules absorb energy at specific wavelengths, resulting in changes of their dipole moments. Some radiation is transmitted, while the rest is absorbed, causing transitions from the molecular ground state to excited vibrational states. The resulting spectrum captures these absorption events, producing a molecular fingerprint unique to the sample, with peaks corresponding to the vibration frequencies of atomic bonds.

Each vibrational transition corresponds to an energy absorption at a specific frequency, determined by the bond strength and atomic masses involved. The wave number ν, directly proportional to the vibration frequency, can be expressed as:

$$\nu = \frac{1}{2\,\pi\,c}\sqrt{\frac{k}{\mu}} \tag{6}$$

where c is the speed of light, k is the bond force constant, and μ is the reduced mass of the involved atoms (Eq. 6).

The magnitude of the absorption peaks depends on the probability of energy transitions and on the changes in dipole moments during molecular vibrations, but it is also influenced by several other factors. For this reason the FTIR technique is mostly used to obtain qualitative data, though reliable quantitative analysis is possible but not trivial to achieve.

FT-IR spectrometers utilize an interferometer, which allows the scanning of all frequencies of IR radiation emitted by the source. This is achieved by using a movable mirror, which creates a difference in optical path length, resulting in constructive or destructive interference with the beam reflected by a fixed mirror. The resulting interferogram represents intensity in the time domain (see *Fig. 2.23*). The Fourier transform is then applied to convert this into an IR spectrum, which shows intensity (transmittance) as a function of frequency.

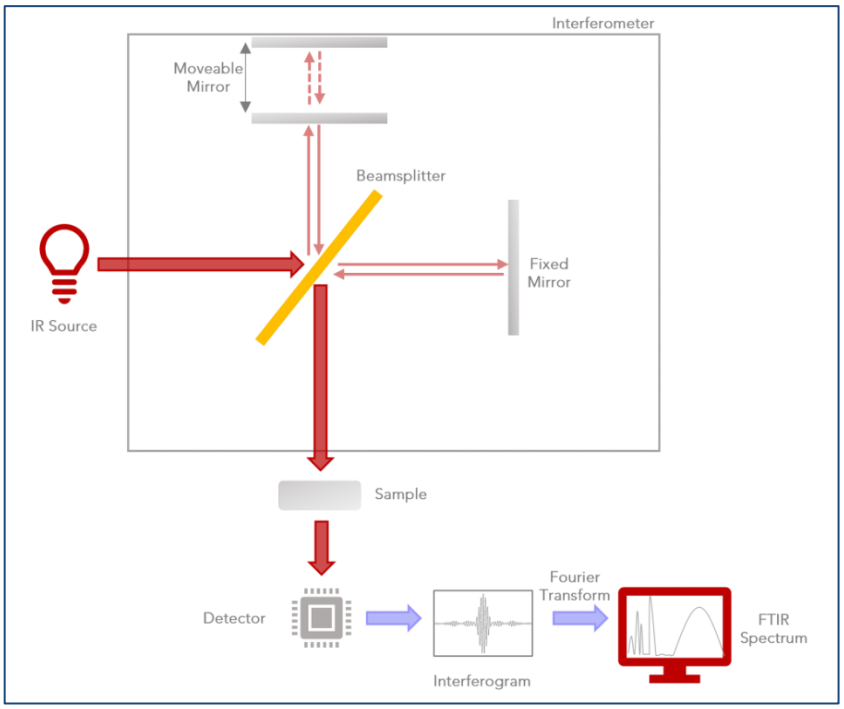

Figure 2.23 FT-IR spectroscopy setup [159].

The IR spectrum typically displays wave numbers on the x-axis and the percentage of transmitted radiation on the y-axis. It is divided into three key regions:

- Functional group region (3800–1300 cm^{-1}): Contains bands due to stretching and deformation of functional groups.
- Fingerprint region (1300–650 cm^{-1}): Features bands unique to individual molecules, resulting from the collective vibrations of the molecular skeleton.
- Far IR region (650–200 cm^{-1}): Contains bands associated with the stretching of heavy atoms, deformations in groups without hydrogen, and skeletal vibrations.

In this study, the attenuated total reflectance (ATR) mode [160] was employed for analysing coated glass samples and studying the hydrolysis time in solution for a particular type of organosilane (section 3.2 of Chapter 3). ATR measures the total reflection that occurs at the interface between the sample and an internal reflection element (IRE), typically made of an inorganic crystal (see *Fig. 2.24*). Infrared rays penetrate the sample at this interface as evanescent

electromagnetic waves. The penetration depth d of these waves is defined by the following equation (7):

$$d = \frac{\lambda}{2\pi n_1 sin^2\theta - {n_2}^2} \quad (7)$$

where λ is the wavelength of the incident radiation, θ is the angle of incidence, n_1 is the refractive index of the IRE, and n_2 is the refractive index of the sample.

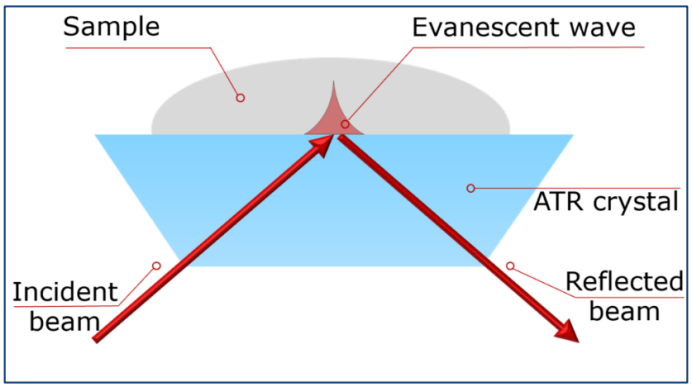

Figure 2.24 Schematic representation of the Attenuated Total Reflectance principle [159].

The penetration depth of ATR typically ranges from a few hundred nanometers to approximately 1 micron. As a result, the signal often represents both the interface and the near-surface layer of the material.

In this study, two FT-IR instruments operating in ATR mode were employed: a Thermo Scientific Nicolet 5PCFT-IR-ATR (diamond) spectrometer in the 4000-400 cm-1 interval, from the Department of Chemistry at the University of Parma, and The Agilent Cary 630 FTIR spectrometer with ATR sampling module, from IMEM-CNR in Parma. Specifically, the first instrument was utilized to characterize samples coated with organosilane films, while the second was used to investigate the hydrolysis time of organosilane in solution. A detailed account of these analyses is provided in Chapter 3.

2.4.4.2 XPS

XPS (X-ray photoelectron spectroscopy), on the other hand, is a highly surface-sensitive technique that provides quantitative and chemical state information about the elements present on the surface.

X-ray Photoelectron Spectroscopy (XPS), also referred to as Electron Spectroscopy for Chemical Analysis (ESCA), is a surface analysis technique based on the photoelectric effect [161]. When a material is irradiated with X-rays, core-level electrons can be ejected from the material with a certain kinetic energy (E_K), which is then measured by the spectrometer (see *Fig. 2.25*). Knowing the energy of the incident X-rays (hv, where h is the Planck's constant (h = 6, 62608 · 10−34 J·s) and ν is the frequency of the X-rays), the binding energy (E_b) of the electrons can be calculated using the equation (8):

$$hv = E_k + E_b + \phi \quad (8)$$

where ϕ represents the work function, the energy required to free the electron from the material.

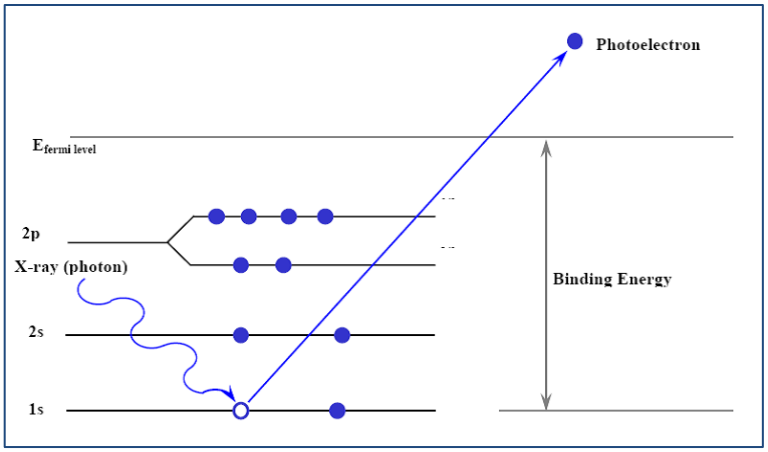

Figure 2.25 Principle of X-ray Photoelectron Spectroscopy [162].

To ensure accurate measurements and avoid contamination of the sample or interference of X-rays and electrons with gas molecules, XPS measurements are performed in ultra-high vacuum (UHV) conditions, typically maintaining pressures between 10^{-6} and 10^{-8} Pa. In XPS experiments, X-rays are usually generated using aluminum (Al) or magnesium (Mg) anodes, producing

characteristic Kα radiation with energies of 1486.6 eV and 1253.6 eV, respectively. To ensure X-rays of a specific wavelength, a monochromator can be positioned between the X-ray source and the sample. The emitted electrons are then directed into an electrostatic hemispherical analyser, which consists of two hemispherical electrodes with applied voltages V_1 and V_2 (see *Fig. 2.26*). Electrons are repelled by V_2 and attracted by V_1, and by adjusting these voltages, electrons with different kinetic energies are able to reach the detector. An electron multiplier is typically used as the detector to enhance the signal from the ejected electrons.

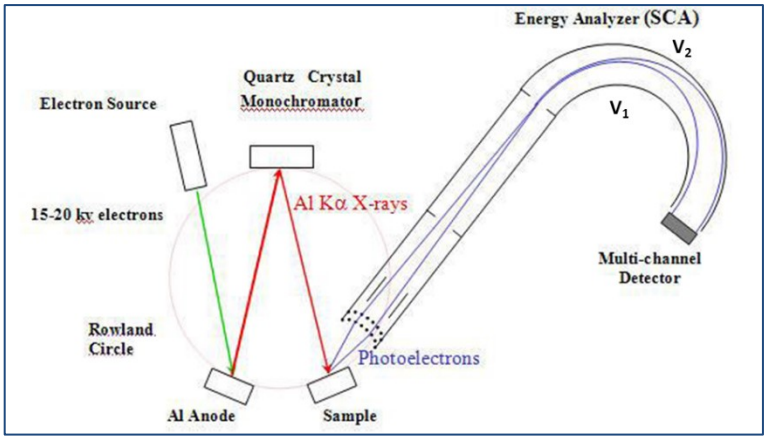

Figure 2.26 Schematic setup of X-ray Photoelectron Spectroscopy. Adapted from [162].

X-ray Photoelectron Spectroscopy (XPS) is highly sensitive to the outermost surface layers of a material. The majority of the detected signal originates from electrons emitted just a few nanometers below the surface. This is due to scattering processes that occur as the electrons travel through the solid, with only near-surface electrons having sufficient energy to escape into the vacuum. The depth of information gathered is greatest when the detector is positioned perpendicular to the surface. As the take-off angle, which is the angle between the surface normal and the analyser, decreases, the depth of information also reduces.

XPS allows for the identification of elements based on the unique binding energies of their core-level electrons. Every element in the periodic table, except hydrogen and helium, produces at least one characteristic signal in the spectrum. In addition to elemental identification, XPS provides insights into the oxidation state and chemical environment of the atoms. Generally,

atoms with higher electron densities experience a lower effective Coulomb potential, resulting in lower observed binding energies. The variation in binding energy due to differences in the chemical environment surrounding the atoms is known as the chemical shift.

The surface composition of the coated glass samples prepared by dipping (paragraph 3.1) was investigated by a hemispherical analyser model 10-360 and a monochromatic X-ray source model 10–610 by Physical Electronics. The instrument is hosted in an ultra-high vacuum (UHV) chamber with base pressure lower than $5x10^{-8}$ mbar and a load-lock system for fast sample entry. XPS spectra were acquired using monochromatic AlKα photons of energy hv = 1486.6 eV; photoemitted electrons were collected from a spot of approximately 100 µm diameter. Due to the insulating nature of the samples, an electron gun was used for charge neutralization during the measurement. The binding energies (Eb) were calibrated by setting the maximum of the C 1s line to 285.0 eV, that is suitable for adventitious carbon. All regions were fitted with an appropriate number of Voigt functions.

The XPS analysis on coated samples by spray system (paragraph 4.2) was performed using the Thermo Scientific™ Nexsa G2 X-Ray Photoelectron Spectrometer, an advanced surface analysis system. The Nexsa G2 model features a monochromated, microfocused Al K-Alpha X-ray source with an adjustable spot size ranging from 10 to 400 µm, in 5 µm increments. The analyser is a 180° double-focusing hemispherical analyzer equipped with a 128-channel detector, ensuring high precision in spectral acquisition. The vacuum system consists of two turbo molecular pumps, supported by an automated titanium sublimation pump and a backing pump, to maintain the ultra-high vacuum required for XPS measurements. Depth profiling capabilities are provided by the EX06 monatomic ion source, allowing for detailed compositional analysis at varying depths within the sample.

2.4.5 Mechanical Characterization

2.4.5.1 Scratch Analysis

The scratch test is a widely used technique for evaluating the adhesion and mechanical integrity of coatings on various substrates. Initially developed in the 1950s [163] the scratch test works by

moving an indenter across the surface of a specimen under a controlled load. It can work in two mode, with a progressive load or constant load, creating a scratch that reveals information about the coating's resistance to mechanical stress and its adhesion to the substrate. By the 1980s, the scratch test was automated with advances that allowed for precise control [164], [165]. Modern scratch test equipment often integrates optical microscopy with motorized stages, allowing immediate visualization and correlation between load and observed failures and thus capable of precise control and monitoring. The test is often performed using a diamond indenter, typically shaped to a Rockwell C profile and a variety of radii, which allows for constant and repeatable contact with the surface (see *Fig. 2.27*).

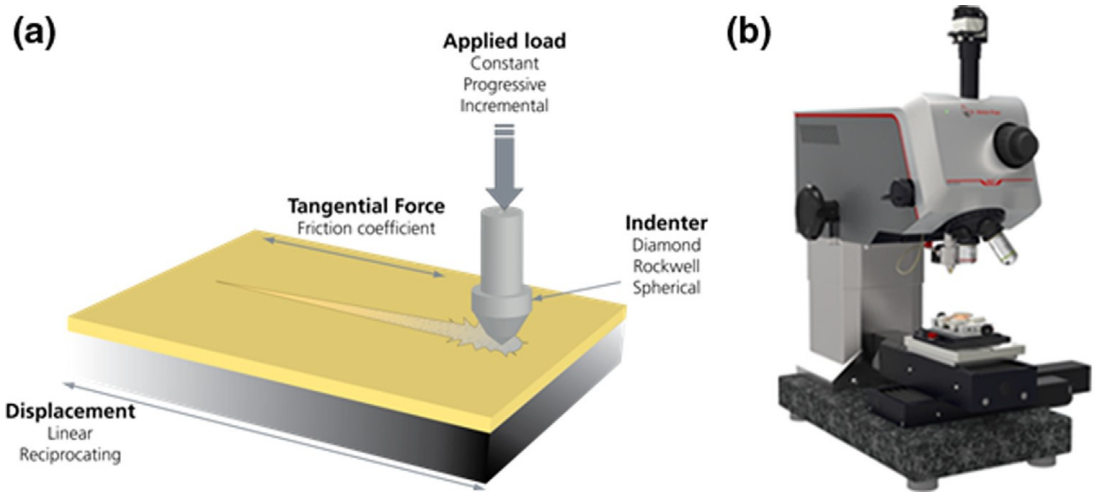

Figure 2.27 Operational principle of the scratch test (a) and example of a commercial scratch tester (b) showing the video optical microscope mounted next to the diamond indenter, as well as the XY translation stage that synchronizes the exact position between the two [166].

The loads required to induce failures, known as critical loads Lc, are measured and analysed as indicators of coating performance, providing a qualitative measure of coating adhesion and durability. This progression of increasing stress provides a comprehensive view of how the coating responds to mechanical loads of varying magnitudes, which is critical for applications where coatings must withstand significant wear. To capture and analyse the coating response during scratching, the equipment records multiple signals [166]:

- F_N: Applied normal load

- P_D: Penetration depth
- AE: Acoustic emission signal
- F_T: Tangential force (or lateral force) signal
- μ: Friction coefficient (usually a direct recalculation of the ratio of F_T/F_N).

The coefficient of friction, μ, can signal critical failure events, particularly when friction changes accompany transitions from one material layer (e.g., coating) to another (e.g., substrate). AE signals, which arise from elastic waves during cracking or coating failure, require precise synchronization with the indenter position for accurate interpretation. Friction force (F_T) and penetration depth (P_D) further aid in identifying coating or substrate damage, although P_D interpretation can be challenging, especially for samples with irregular surfaces or unknown coating thicknesses. This technique is particularly valuable for testing the resilience of coatings under realistic loading conditions and provides a comprehensive characterization of coating performance, although there are still challenges in interpreting data from non-flat or transparent substrates such as curved glass with transparent coatings. On curved surfaces, maintaining uniform penetration contact is difficult, which can reduce reproducibility and accuracy. Transparent coatings pose additional challenges for optical analysis, as cracks or delaminations within the coating or at the interface may be indistinct, making it difficult to identify the source of the failure and critical loads. Modern panoramic imaging and motorized XYZ stages partially address these limitations by allowing precise tracking and high-resolution imaging of the entire scratch path. Using sequential imaging and focal stacking, clear, in-focus images of the scratch track are obtained, facilitating advanced analysis and allowing post-test adjustments to identify the point of failure based on the recorded data.

In this study, we used two types of instrumentation. In the Chapter 4 scratch images of coated soda-lime glass samples were analysed to assign critical loads to various types of surface damage, with the aim of evaluating whether the presence of coatings conferred a protective effect on the glass substrate by shifting the critical load Lc to higher values. For this purpose, a scratch tester (CSM Instruments Revetest RST2, Anton Paar Group AG, Austria), equipped with a Rockwell type “C” diamond indenter with a radius of 200 µm, was used. Scratch tests were performed in a linear progressive mode, starting with an initial load of 0.3 N and increasing to a final load of 10 N at a

loading rate of 1.46 N/min. This configuration allowed a controlled and gradual application of stress on the surface, facilitating the observation of progressive coating failure events and the determination of critical load values associated with specific types of damage. For scratch analysis, images captured by the instrument's integrated optical microscope were examined in panoramic mode, allowing a complete overview of the scratch track and damage progression. Subsequent high-resolution imaging was performed using a laser confocal microscope (Olympus LEXT OLS5000 3D) to obtain a detailed view of the damage signs.

In chapter 3 we used a scratch tester that can operate in multipass mode, scratching the sample back and forth a certain number of times. This instrument simulates the wear that is obtained with the ball-on-flat tribometer that we will discuss in the next section. In particular we worked with a Nano Scratch Tester (NST3) from Anton Paar, equipped with a High Load cantilever with maximum normal force up to 1 N. The system is suited to the analysis of thin films and coatings (with thickness lower than 1000 nm) and, thanks to a real-time feedback on the normal force actuator, measurements can be performed also on complex surface geometries, like uneven or curved samples. For this reason, the system is particularly suited to the characterization of the surfaces of industrial glass vials. In particular, to gain insight into the frictional properties of the surfaces, we combined the use of a friction module, essential for recording the tangential force, to the multipass functionality of the NST3, that allows the realization and controlled repetition of scratches (hereafter called “passes”) at constant normal load. We used a Zr_2O_3 sphere with a 3 mm radius counterpart, normal load of 800 mN, speed of 1 mm/min, mark length of 0.2 mm along the walls of the vial, accommodating the vial in a lying position. This kind of measurement allows to evaluate the coefficient of friction along the scratch and its evolution as a function of the number of passes, as it will be shown in Chapter 3.

2.4.5.2 Tribological Analysis

‘Tribometry is recognised as the comprehensive experimental approach within tribology, which employs specific instruments called ‘tribometers’ to measure friction and wear on various materials. The term ‘tribometer’ is derived from ‘tribos’, meaning friction, and ‘meter’, meaning measurement, to denote its role in quantifying friction forces and wear rates. Evaluations of these

forces and rates in different configurations follow standardised protocols [167]. Key measurements, such as the coefficient of friction (COF), are determined by factors such as type of movement, applied load, speed, test duration and controlled environmental parameters such as humidity and temperature. These controlled settings allow for a realistic representation of operating conditions, ensuring accurate calculation of COF [168] and wear track diameter, essential indicators of contact conditions. Tribological tests generally involve the sliding or rolling of a guided body against a static counter-body, classified according to the geometry of the contact. Friction, as a force opposing movement, causes energy and power losses [169]. This force is influenced by factors such as surface finish, material composition, dimensional tolerances, operating temperature, material hardness and type of lubrication, solid or liquid. During tribometer tests, the normal load (Fn) is applied through a sensor, while the tangential friction force (Ft) is captured by a separate sensor. The motor rotates the substrate against a ball, creating a sliding contact, where friction acts as a resistance between two surfaces, opposing movement or displacement. The coefficient of friction (COF or μ) is defined as:

$$\mu = Ft / Fn \quad (9)$$

where μ is dimensionless and *Ft* is independent of the contact area (Eq. 9).

This coefficient depends on the object's weight, dynamic forces in motion, surface finish, and material type [170]. Experimental tests are generally classified by contact geometry, leading to varied tribometer configurations. In this work, the ball-on-disk and linear ball-on-plate tribometer configurations were used.

Ball-on-disk setup

The pin-on-disc tribometer, shown in the *Figure 2.28*, is designed to evaluate friction and wear characteristics by allowing pins of different shapes, whether spherical, pointed or flat, to interact with a rotating disc. The disc holder fixes discs of various sizes and shapes, while the pin maintains a stable contact point on the disc surface. Typically, this configuration includes a motor-driven spindle and mandrel to rotate the disc, a lever arm to hold the pin in place, and mechanisms to apply a controlled load by forcing the pin against the rotating disc (see *Fig. 2.28*). In other

configurations, the pin rotates around the centre of the stationary disc. In both cases, a circular wear track is produced that results in several passes over the same area [171].

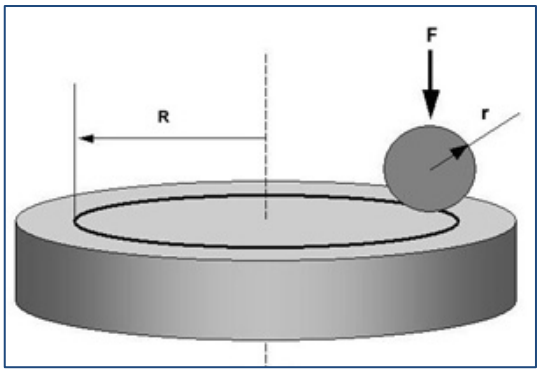

Figure 2.28 Typical ball-on-disk setup, where F is the normal force applied on the ball, r is the ball radius, and R is the radius of the wear track [172].

Under operation, the desired normal load is applied to the pin of the tribometer, while the speed is controlled via the stage. The arm of the tribometer measures the tangential friction force and transmits the data to a controller via integrated sensors. The controller processes this information, displaying the friction coefficient over time on a computer interface.

The test parameters are:

- Load: Force in Newtons applied at the wear contact point.
- Speed: Relative sliding speed between contacting surfaces, measured in meters per second.
- Distance: Total sliding distance accumulated over the test, in meters.
- Temperature: Temperature at the contact area, either on one or both specimens, near the wear interface.
- Atmosphere: Environmental conditions surrounding the contact point, such as laboratory air, controlled humidity, inert gas (e.g., argon), or a lubricant film.

Ball-on-flat setup

The ball-on-flat tribometer configuration involves: a flat test specimen and a spherical counterface, herein referred to as the ‘ball’, sliding on the flat surface in a linear, alternating

motion under controlled conditions. As illustrated in *Fig. 2.29*, the alternating ball-on-flat test configuration places the ball with the spherical tip in rigid contact, moving back and forth on the flat specimen. An alternative configuration, in which the flat specimen moves while the ball remains stationary, can also be used [173]. A mechanism is included that applies a constant normal load to the contact area between the ball and the flat surfaces. As the contact oscillates, the tangential force is continuously recorded, allowing the calculation of the coefficient of friction.

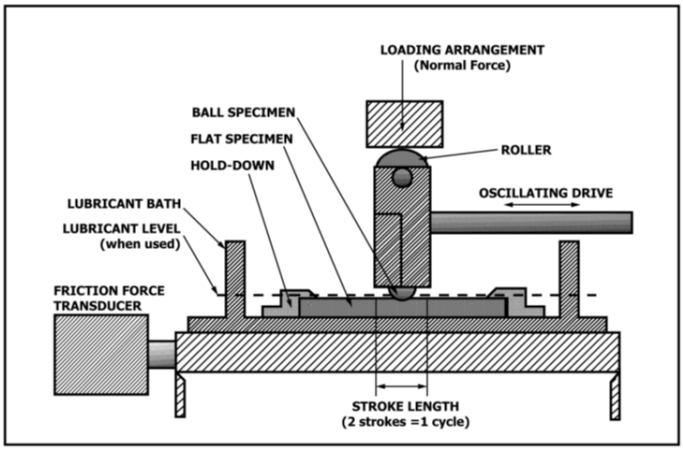

Figure 2.29 Scheme of ball-on-flat friction test setup [173].

The test records friction forces, providing indications of changes in contact conditions or fluctuations in the kinetic friction coefficient over time. Due to the alternating nature of the movement, both sliding velocity and direction vary during the test, preventing constant velocity conditions. The pattern of velocity variation depends on the specific mechanism used to guide the ball or flat specimen in its oscillatory motion. Other parameters include normal load, stroke length, frequency and type of oscillation, test temperature, presence of lubricant (if any), test duration and surrounding atmosphere (with controlled humidity levels, if necessary).

Tribological tests were conducted using two types of instrumentation. A CSEM high-temperature tribometer (Alpnach, Switzerland) in a ball-on-disk configuration was utilized at the STEMS-CNR Institute in Torino to perform mechanical characterization on coated glass samples prepared by

the dip-coating method (Chapter 2). Additionally, a Bruker TriboLab UMT device in a ball-on-flat configuration, located at the Department of Engineering Technologies and Materials at Alexander Dubček University in Trenčín, was employed to characterize coated glass samples prepared via the spray-coating method (Chapter 3.2).

2.4.5.3 Tilt -Table

The Tilt Table apparatus is designed to evaluate the sliding angle, providing an indirect measure of the friction coefficient of coated glass containers. In this apparatus, three containers are arranged in a pyramidal configuration on the table surface. When the test starts, an electric motor gradually tilts the table, increasing the angle of inclination. The two lower containers are held in place, remaining stationary for the duration of the test. When the tilt angle reaches a point sufficient to overcome the friction forces involved, the upper container begins to slide, coming into contact with a stop bar. At this point the motor stops and the table stabilised to prevent further unintended movements that could lead to inaccurate readings. The measured angle is then called the “sliding” angle.

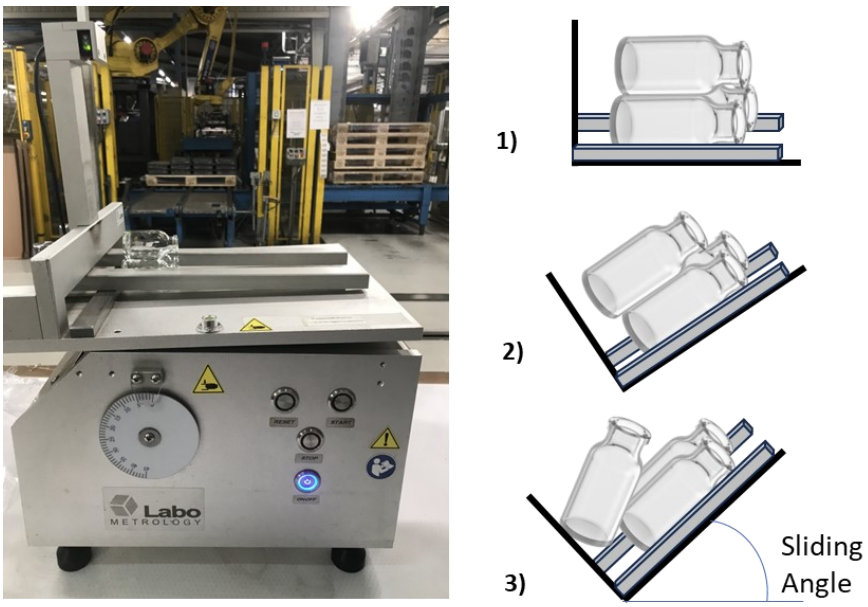

Figure 2.30 On the left: Tilt-Table instrument from Bormioli Pharma S.p.A. plant in Bergantino (Italy); on the right: a schematic representation of the mechanism of sliding angle evaluation.

The sliding angle tests were conducted using Agr Tilt-Table instrumentation *(see Fig. 2.30*), at the Bormioli Pharma S.p.A. plant in Bergantino on coated glass vials (Chapter 3).

3. Experimental Dipping Deposition

This Chapter is divided into two main sections (3.1 - 3.2), each addressing a different approach to organosilane-based coatings deposited via immersion. The first section focuses on the deposition of an aminosilane used as a primer to anchor the lubricant onto the glass surface, while the second section explores the deposition of a different type of organosilane, tested as a single-component coating to evaluate its potential lubricating effect on the glass. These two strategies represent distinct approaches to the development of anti-friction coatings for pharmaceutical glass vials. Each section is systematically organized, beginning with the description of the materials and methods used in the experiments, followed by surface preparation and deposition procedures, and concluding with the presentation and discussion of the results obtained. For both the aminosilane primer and the single-component silane coating, morphological and chemical characterizations were performed on the coated glass surfaces and the results were related to the deposition parameters. In particular, for the study of the aminosilane as a primer, deposition parameters such as post-deposition step, concentration and immersion time were explored in detail. Following chemical and morphological analysis, mechanical characterizations were conducted to assess the performance of the coatings in terms of their friction-reducing properties. In the case of the aminosilane-primer, mechanical tests were performed after the application of the lubricant on top of the primer, allowing for an evaluation of its effectiveness in anchoring the lubricant on the glass surface. Conversely, for the single-component organosilane coating, mechanical tests were conducted directly on the glass coated solely with the silane to determine whether this coating alone could provide sufficient lubrication without the need for an additional lubricant layer. This dual approach enables a comprehensive comparison of the two coating strategies, providing valuable insights into their potential for industrial application in the pharmaceutical packaging sector.

As presented below, not all the materials investigated in this study were subjected to the same series of analyses, either in terms of chemical characterization or mechanical testing. This decision was guided by a combination of scientific priorities and practical considerations. The specific research objectives played a pivotal role in shaping the analytical approach for each material.

The work conducted on the aminosilane primer was significantly more extensive compared to that on the single-component coating. This was primarily due to its role as a primer, which necessitated a more thorough investigation of its chemical and physical properties. In contrast, for the single-component material, the research emphasis was placed on exploring its potential lubricating effects, which required a different methodological approach. Furthermore, the availability of this material occurred during the final stages of my doctoral research, which inherently constrained the scope of its analysis. Consequently, the study on the single-component coating will be further developed as part of the continuation of my research.

This approach reflects the balance between the scientific goals of the study and the practical constraints encountered during the research process. It also allowed for a more focused and manageable set of analyses, tailored to the specific characteristics and research objectives associated with each material.

3.1 Aminopropylsilsesquioxane Primer

3.1.1 Materials and Methods

Substrates: All the substrates used to carry on this activity consist of soda-lime-silicate (SLS) glass produced by Bormioli Pharma S.p.A. accurately chosen from Type II and Type III glass vials (*the differences between Type II and Type III are discussed in detail in Section 1.1.1, page 8*) without the external standard coating usually provided by the industry. In particular:

- SLS glass pieces sourced from 500 mL vials were used for surface characterization of the glass coated with primer;
- SLS vial bottoms from 20 mL vials were employed for tribological testing in ball-on disk mode;
- whole 20 mL SLS vials were used for tribological testing in multipass mode and mechanical measurements with the tilt-table method.

Chemicals: Waterborne Aminopropylsilsesquioxane (*Figure 3.1*), a commercial product purchased from Gelest - Mitsubishi Chemical Group, was used as the silane primer in aqueous solution. As a lubricant, a macrogol stearate - a mixture of mono- and di-esters of stearic and/or palmitic acid with macrogol (*Figure 3.2*), was employed in aqueous solution. The commercial name of the lubricant is omitted for reasons of confidentiality.

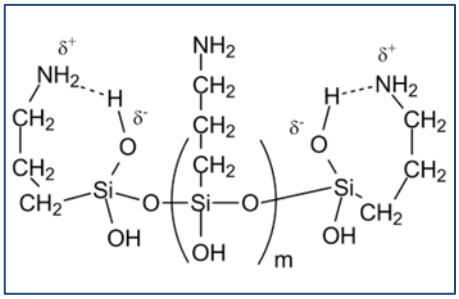

Figure 3.1 Aminopropylsilsesquioxane in aqueous solution, Gelest[114].

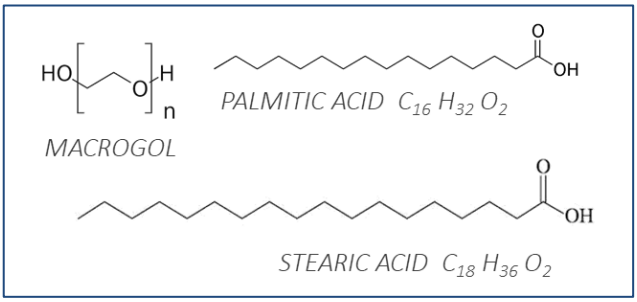

Figure 3.2 Mixture of macrogol stearate components used as a lubricant.

3.1.1.1 Surface Preparation

These substrates underwent chemical cleaning through sonication in deionized water, isopropanol, acetone and isopropanol in sequence. Each step lasted 2 minutes and all processes were conducted at room temperature; the final step consisted in air-drying. After cleaning and immediately prior to immersion in the silane solution, the samples were treated with oxygen plasma for 5 minutes at a power of 40 W using a plasma cleaner (Femto, Diener electronic, Germany) to expose hydroxyl (OH) groups on the glass surface (see paragraph 2.2.3).

3.1.1.2 Primer Deposition

The silane coatings were deposited as follows: clean and activated glass samples were immersed in an aqueous solution of aminopropylsilsesquioxane at a concentration *C*, stirred gently for a duration *t*, and subsequently either left unrinsed or rinsed in deionized water for 10 minutes under stirring. Then all samples were cured at 150°C for 120 min in a non-ventilated oven. After curing, the samples, once cooled, were stored in a desiccator for no longer than 2 weeks. Within this time the samples were characterized, beyond this period, if necessary, new samples were prepared with the same deposition parameters. Taking advantage of the assessed reproducibility of the process, this procedure allowed us to account for undesired aging and weathering effects on the coating properties. *Table 1* provides a comprehensive summary of the parameters used in this study. In addition to the treated samples, reference glass samples that did not undergo the silane coating deposition were also analysed for comparison.

Table 1. Representative samples of primer-coated glass and parameters used for deposition. C is in volumetric concentrations.

Sample	C (%)	Dipping t (min)	Rinsing
Sample1	1	120	no
Sample2	1	120	yes
Sample3	0.5	120	yes
Sample4	0.5	60	yes
Sample5	0.5	30	yes
Sample6	0.5	15	yes

3.1.1.3 Primer-Lubricant Coating Deposition

A second set of samples was prepared using same deposition parameters of *Table 2*, for the primer application. Immediately after the primer-polymerization phase, we kept the samples at 120°C and immersed them in a 0.1% aqueous lubricant solution for 30 seconds, and then dried them in air. In this way we simulated the industrial application procedure that involves spraying

the lubricant on the vials when these have a temperature between 120 and 80°C, but with dipping method.

Table 2. Representative samples of primer/lubricant coated glass and parameters used for deposition, analysed by mechanical techniques. Ref. is uncoated glass sample as a reference. C is in volumetric concentrations.

Sample	C (%) - Primer	Dipping t (min)	Rinsing	Lubricant
Ref.				
SLS + Lubri				yes
Sample 3 + Lubri	0.5	120	yes	yes
Sample4 + Lubri	0.5	60	yes	yes
Sample5 + Lubri	0.5	30	yes	yes
Sample6 + Lubri	0.5	15	yes	yes

3.1.2 Results and Discussion

3.1.2.1 Surface Activation Evaluation

As mentioned in section 2.2.3, the activation of glass surface results in an increased surface wettability. The effective activation of sample surfaces was assessed by measuring the contact angle, which was significantly reduced ($\theta < 5°$) following plasma treatment, compared to the contact angle measured on glass subjected only to chemical cleaning ($\theta = 72{,}6°$), as shown in *Figure 3.3*. This reduction in contact angle indicates a substantial improvement in surface hydrophilicity after plasma treatment.

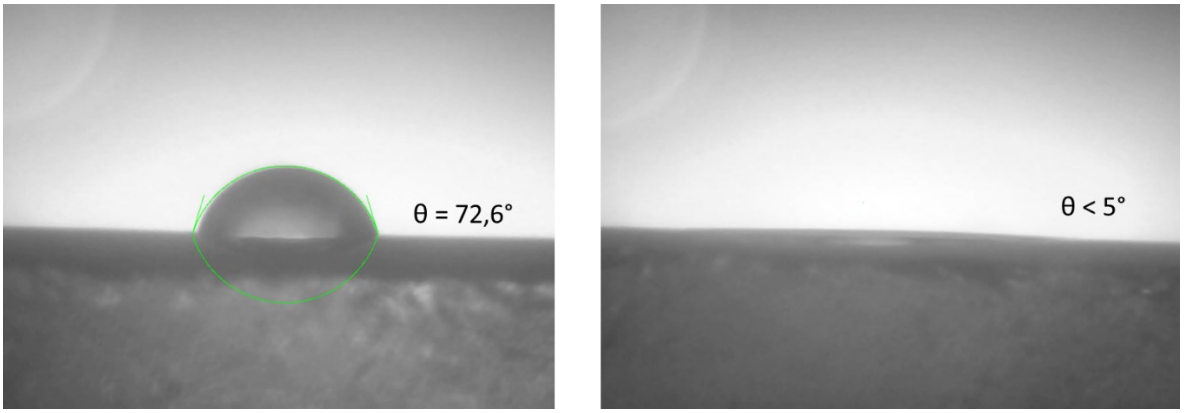

Figure 3.3 Images of contact angle measurement on SLS glass after chemical cleaning on the left and after plasma treatment on the right. The angle is captured by LB-ADSA method with ImageJ software.

The same chemical cleaning and surface activation procedure was applied to the vials and vial bottoms used for mechanical characterization.

3.1.2.2 Surface Characterization

In this section, we present the results of the morphological and chemical characterization of curved glass samples coated with aminosilane - primer, applied using different deposition parameters (see *Table 1*). A relevant part of the activity involved the morphological characterisation of the uncoated glass. The surface morphology of glass samples from industrial vials is often affected by the presence of uncontrolled micrometric defects attributed to the ageing process during storage [174] or, in the case of Type II vials, to uncontrolled contamination during internal treatments [175]. This latter effect, in particular, is caused by a leakage of harsh gaseous compounds from the vial opening during internal treatment procedure and may cause the presence of voids non-homogeneously distributed on the vial surface, with a larger density close to the vial shoulder and upper body. The results of AFM/SEM analysis of a large number of uncoated samples derived by different vials confirmed the presence of this peculiar morphology; in *Fig. 3.4* we show both a surface without defects and a surface with a large number of defects

consisting in voids with depths a few nm and widths ranging from tens to hundreds of nm (*Fig. 3.4*).

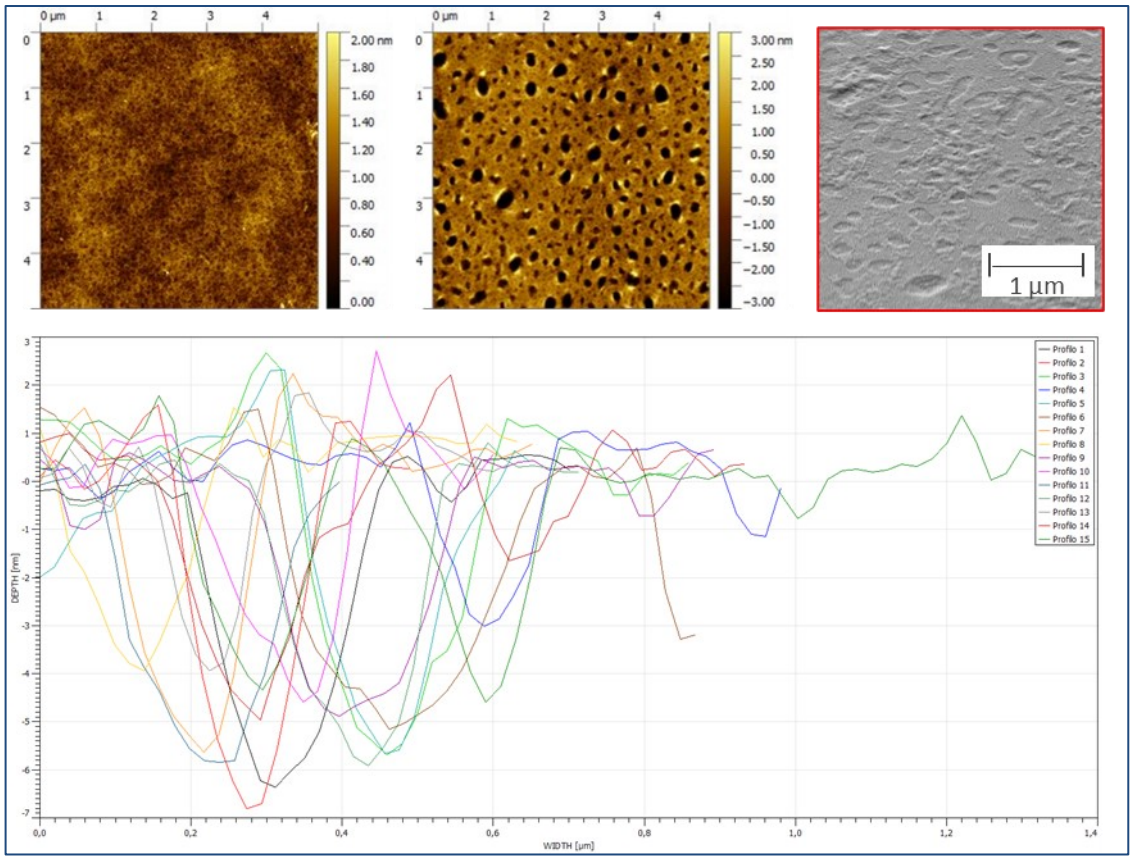

Figure 3.4 AFM/SEM images of uncoated glass samples derived by different vials of same Type and size (Type II, 500ml). Top: from left to right, AFM image of uncoated glass without defects, AFM image of uncoated glass with voids, SEM images captured with 45° tilt-angle of uncoated glass with voids. Bottom: Depth voids-profiles of the second AFM image on the top.

This analysis was necessary in order to understand how to correctly evaluate the morphology of the coatings and to differentiate it from that of the underlying glass substrate. In addition, in order to support our evaluations on AFM analysis of coated surfaces, as it will be discussed in detail in the following sections, the presence of the coating has been consistently confirmed through chemical analysis of the surface, including FT-IR spectroscopy and, most conclusively, XPS spectroscopy.

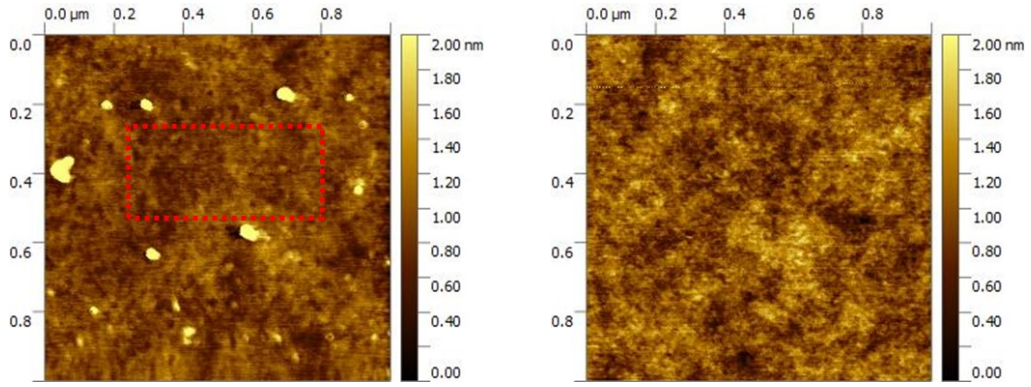

Figure 3.5 AFM images (left) of clean uncoated glass and (right) of Sample 1, glass coated with 1% aminosilane for 2 hours.

Figure 3.5 shows the AFM images of an uncoated glass sample and of Sample 1 (coated with aminosilane 1% for 2h) a change in morphology and an increase in roughness can be observed in the case of the coated sample. In the latter case, the R_q (root mean square roughness) was 0.25 nm compared to 0.16 nm for the uncoated glass. R_q values are calculated over the entire image area or over smaller areas (as shown in *Fig. 3.5* with the area dashed in red) if voids, defects or contaminants are present as in this case for the uncoated glass sample.

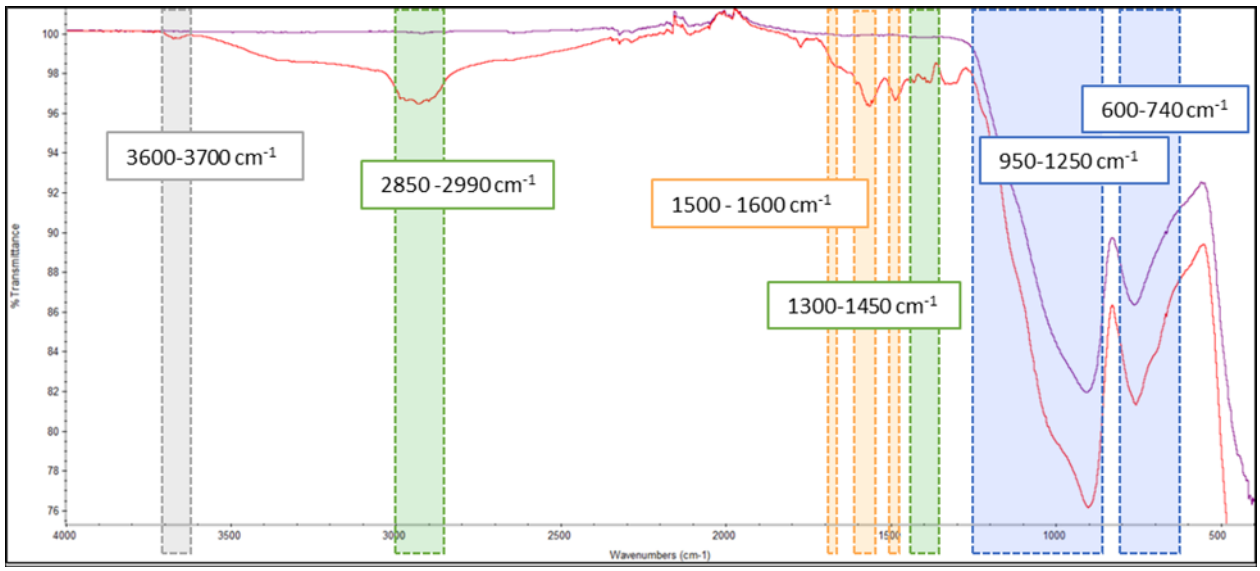

Figure 3.6 FT-IR spectra of uncoated glass in violet and coated glass (Sample 1) in red.

Analysing the surface of both coated (Sample1) and uncoated glass through FT-IR spectroscopy, several characteristic peaks were identified in each sample. For both the coated and uncoated glass (red spectrum and violet spectrum respectively in *Fig. 3.6*), two key regions are evident: the 600-740 cm^{-1} range, which corresponds to the Si-O bending mode [176] associated with the glass substrate, and the 950-1250 cm^{-1} range, which includes the Si-O-X modes [89], [118]. The Si-O-X region encompasses the Si-O-Si peaks, typically found around 1045 cm^{-1}, which are associated to siloxane groups. These peaks can originate from three sources: (i) the glass surface, (ii) silane molecules condensed onto the glass, and (iii) self-condensed silane molecules. As a result, it was concluded that the peaks in the range below 1250 cm^{-1}, don't allow to clearly distinguish the contributions of the glass substrate from those arising from the silane coating. To obtain this result, we focus the attention on the peaks that are present only in the FTIR spectrum of the coated glass and are absent in the uncoated sample. Specifically, new peaks appear in the 1500-1600 cm^{-1} range, associated with amino groups, and in the 2850-2990 cm^{-1} range, corresponding to alkyl chains from the silane coating. Notably, a peak at approximately 1568 cm^{-1} is observed, which is attributed to the NH_2 scissor vibration, confirming the presence of NH_2 terminal groups. Additionally, a peak at 1490 cm^{-1}, likely related to the symmetric deformation of $-NH_3^+$, and a small peak at around 1610 cm^{-1}, associated with the asymmetric deformation mode of $-NH_3^+$ [89], were identified. In the region between 2850 and 2960 cm^{-1}, peaks corresponding to the C-H stretching of propyl groups, originating from the alkyl chains in the silane molecules, are observed.

Other less intense bands appear exclusively in the spectrum of the coated glass. One is located between 3600 and 3700 cm^{-1}, which could correspond to O-H stretching (likely due to adsorbed water). The N-H stretching mode from amine groups typically appears around 3300 cm^{-1}, though it is generally very weak, particularly in the case of very thin coatings, due to its small dipole moment [89]. Additionally, a minor band between 1300 and 1450 cm^{-1}, probably related to the CH_2 and $Si-CH_2$ bending modes [177], [178] from the propyl chain backbone was detected.

These results confirm the presence of the silane coating on the glass surface, as indicated by the appearance of peaks corresponding to amino and alkyl functional groups. The characteristic peaks of the amino groups, in particular, validate the successful attachment of the aminosilane onto the

glass surface, while the alkyl chain signals further corroborate the presence of the coating. Summarizing the results of these characterizations, we showed that aminosilane coated glass samples are characterized by a rougher surface with respect to an uncoated one and that the functional groups of the aminosilane coating give rise to FTIR peaks clearly distinguishable from those of the glass surface. Starting from this evidence, we show in the following the characterization results obtained by varying the coating deposition parameters.

The Effect of Rinsing

We investigated the effect of rinsing in deionized water immediately after immersion and before curing, by comparing rinsed (Sample2) and unrinsed coated surfaces (Sample1).

As mentioned at the beginning of this section, AFM measurements of glass vial samples are often complicated by the presence of substrate defects. As shown in *Figure 3.7*, Sample 2 presents a distribution of voids of considerable depth as compared to the roughness of the coating; we attribute these defective morphologies to the underlying glass surface. As can be seen in *Fig. 3.7*, it was possible to measure the roughness in the areas between the voids (dashed in red), and it was comparable to that observed in the unrinsed coated glass samples (R_q = 0.25 nm). We note here that the voids are not completely covered by the silane coating, this suggests that the thickness of the coating should be limited to a few nm, an evaluation that will be supported also by the results of further analyses shown in the following.

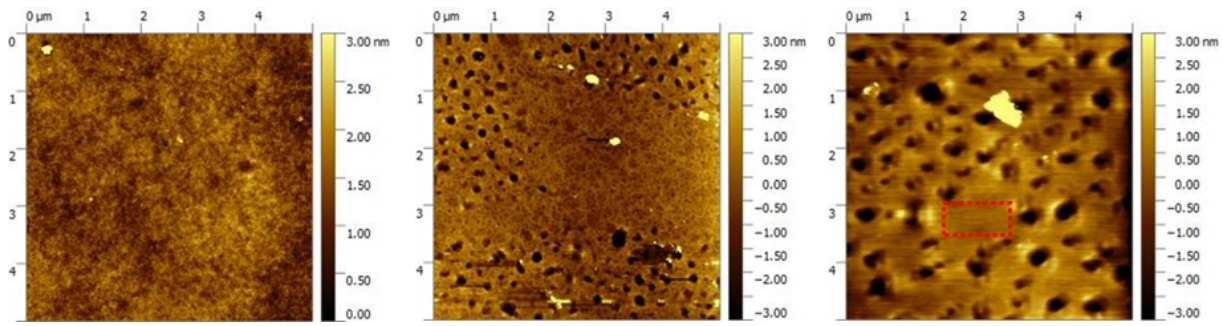

Figure 3.7 AFM images of unrinsed coated glasses (Sample 1), first on the left, and of rinsed coated glasses (Sample 2) at center and right.

Comparing the spectra of Sample 1 (unrinsed, red in *Fig. 3.8*) and Sample 2 (rinsed, pink in *Fig. 3.8*) with that of the uncoated glass (violet in *Fig. 3.8*), it is evident that the N-H bending band in the 1500-1600 cm^{-1} region disappears in the rinsed coated glass.

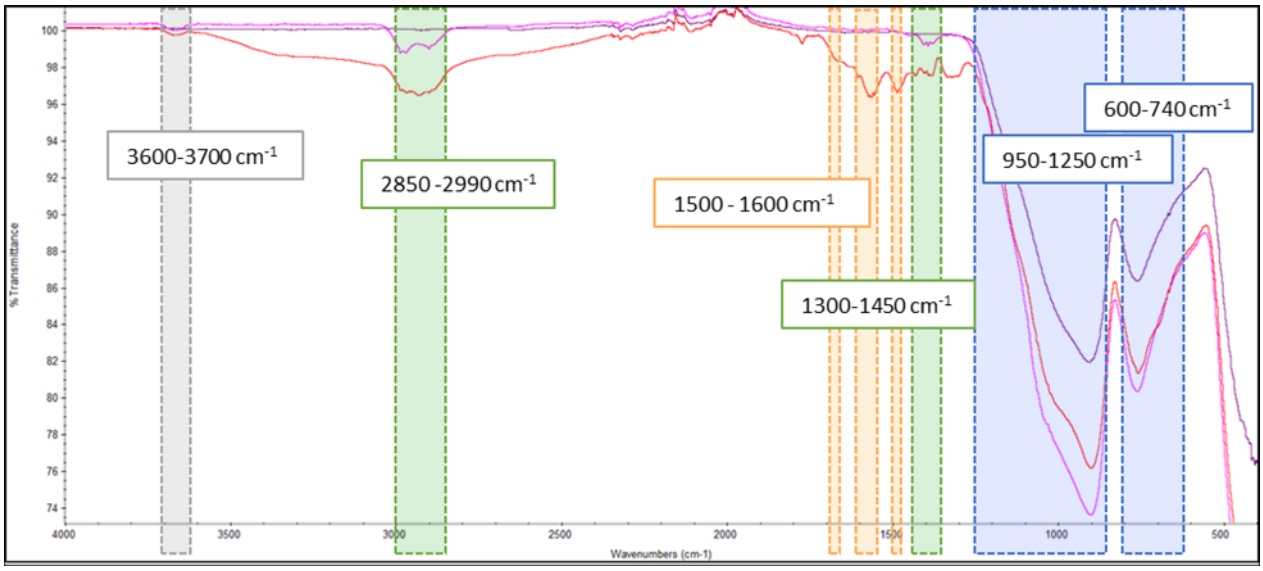

Figure 3.8 FT-IR spectra of uncoated glass in violet, unrinsed coated glass (Sample 1) in red, and rinsed coated glass (Sample2) in pink.

However, the band corresponding to the propyl chain, along with the two low-intensity bands between 3600-3700 cm^{-1} (O-H water adsorbed) and 1350-1450 cm^{-1} (CH_2/ Si-CH_2 bending modes), remain visible, as observed in Sample 1. The presence of the coating is confirmed by the peaks related to the alkyl groups, which are absent in the spectrum of the uncoated glass. The amino groups, on the other hand, may be present in quantities too low to be detected by the instrument, unlike the C-H groups from the alkyl chains. This discrepancy is likely due to the fact that the C-H groups are approximately three times more abundant than NH_2 groups in aminosilane molecules. These results suggest that rinsing in water, a post-treatment typically employed to remove physisorbed molecules prior to the curing step [94], [179], reduces the amount of coating molecules adsorbed on the glass surface. The disappearance of the N-H modes after rinsing indicates a partial removal of amino-functional silane molecules, while the persistence of the alkyl

peaks confirms that some coating remains on the glass substrate. A similar trend was evident in the XPS results.

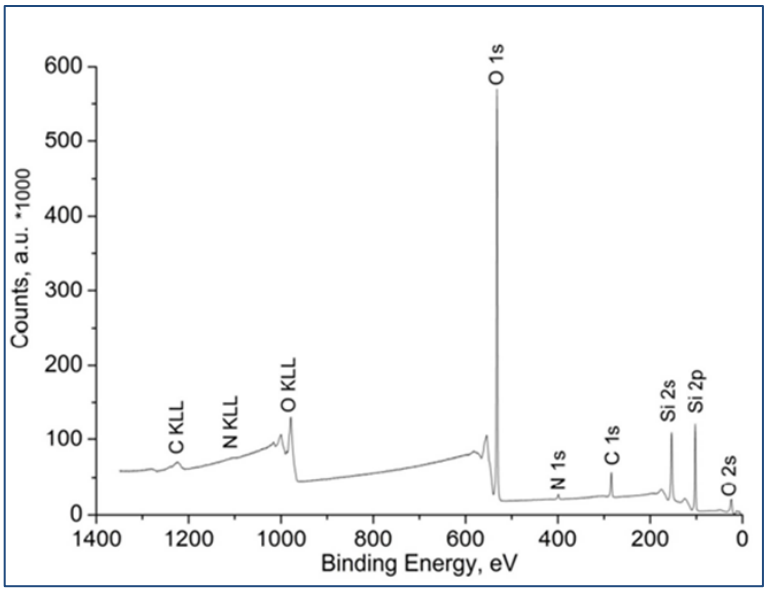

Figure 3.9 Typical XPS survey spectrum of APS molecules adsorbed on silicon substrate [180].

Typical XPS survey spectrum, for aminosilane-coated glass surfaces, shows characteristic peaks for nitrogen (N), oxygen (O), carbon (C), and silicon (Si), with the nitrogen and carbon peaks attributed to the aminosilane molecules deposited on the surface and the silicon and oxygen peaks originating mainly from the underlying glass substrate (as shown in the *Figure 3.9* of a reference spectrum for aminopropylsilane – APS, on silicon substrate).

High-resolution XPS spectra in the C 1s and N 1s binding energy regions provide additional information on the chemical composition of the surface.

The C 1s spectrum typically shows three distinct peaks related to different contributions: one at 285.0 eV, corresponding to C−C and C−H bonds, another at 286.0 eV representing C−N bonds, and a peak at 289.0 eV, which can be assigned to the O−C=O groups. The N 1s spectrum generally shows two peaks: one at 399.5 eV, which indicates free amino groups ($-NH_2$), and another at 401.5 eV, which represents protonated amino groups ($-NH_3^+$). In the analysis of XPS spectra, special attention is paid to the C−N, $-NH_2$ and $-NH_3^+$ peaks, since these peaks can only be

attributed to the coating and therefore their presence allows us to monitor changes in the chemical state of the aminosilane molecules adsorbed on the glass surface.

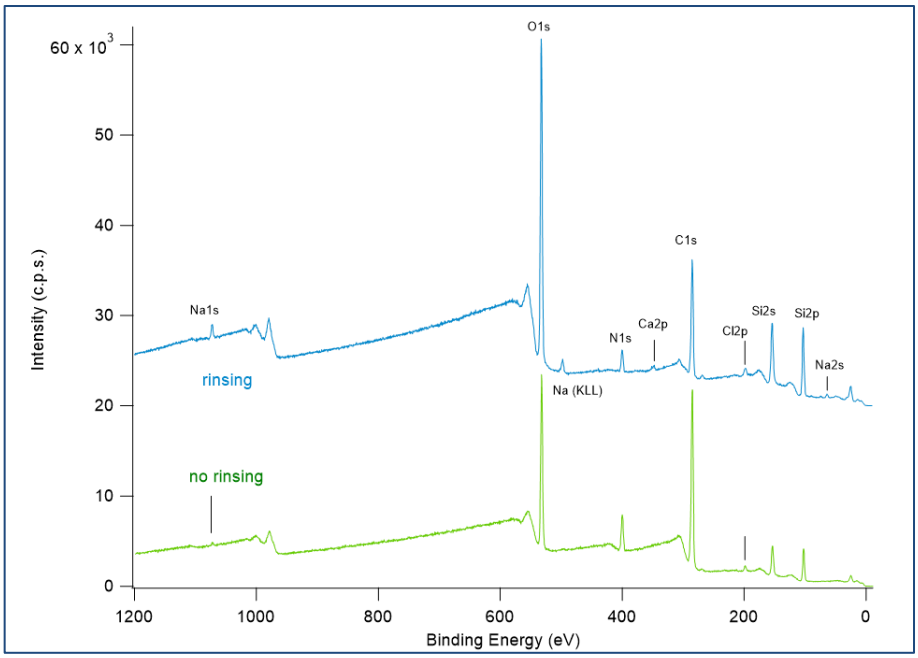

Figure 3.10 XPS survey spectra of unrinsed coated glass (Sample1) in green, and rinsed coated glass (Sample 2) in blue.

By analysing the peak intensities of the survey XPS spectra for Sample 1 (green in *Fig. 3.10*) and Sample 2 (blue in *Fig. 3.10*), it becomes evident that the O 1s and Si 2p components are anticorrelated with the C 1s and N 1s components. Specifically, in Sample 2—which differs from Sample 1 due to the addition of the rinsing step—the O 1s and Si 2p signals increase, while the C 1s and N 1s signals decrease.

Sodium (Na in *Fig. 3.10*), aluminium and magnesium (Al2p – 74-75.5 eV and Mg2s – 88-90 eV in *Fig. 3.11*), appear in the spectrum of Sample 2 but are not evident in Sample 1. These elements are the typical lattice modifiers of soda-lime-silica glass, so we attribute these signals to the glass substrate; as a reference, a typical XPS spectrum of soda-lime glass is reported in *Figure 3.12* in which the signals relating to the lattice modifiers of this glass, such as sodium, aluminium, magnesium and calcium are clearly visible.

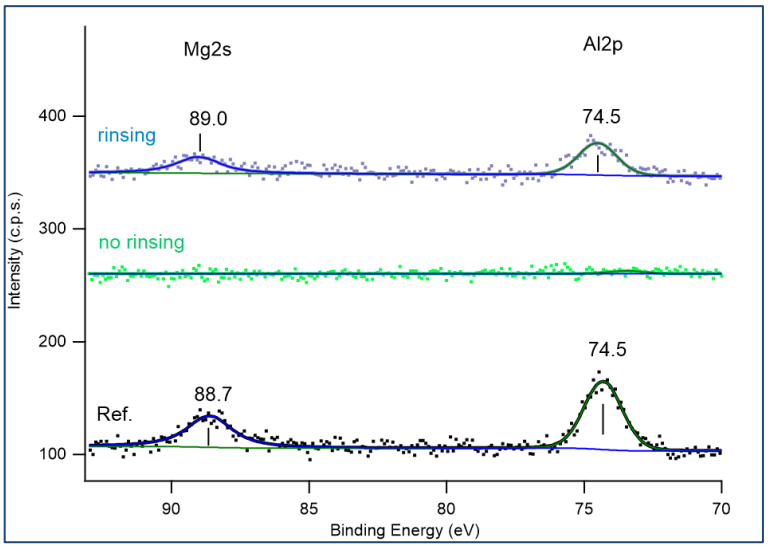

Figure 3.11 XPS spectra of Al and Mg contents in uncoated glass in black, unrinsed coated glass (Sample1) in green, and rinsed coated glass (Sample 2) in blue, from bottom to top respectively.

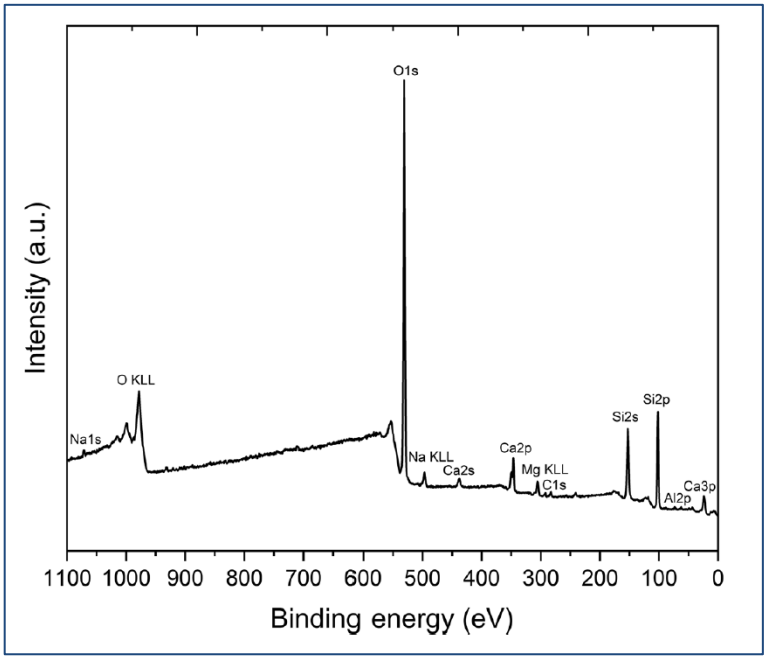

Figure 3.12 Representative survey spectrum of the surface of soda–lime–silica (SLS) glass [181].

As we already mentioned, while the O 1s and Si 2p peak intensities increase in Sample 2, the nitrogen and carbon signals are reduced as compared to Sample 1 (*Figure 3.13)*. Notably, the nitrogen spectrum for Sample 2 shows a significant decrease in the protonated amino component

around 399 eV. Similarly, in the carbon spectrum, the component around 286 eV, corresponding to the C−N bond, is also reduced.

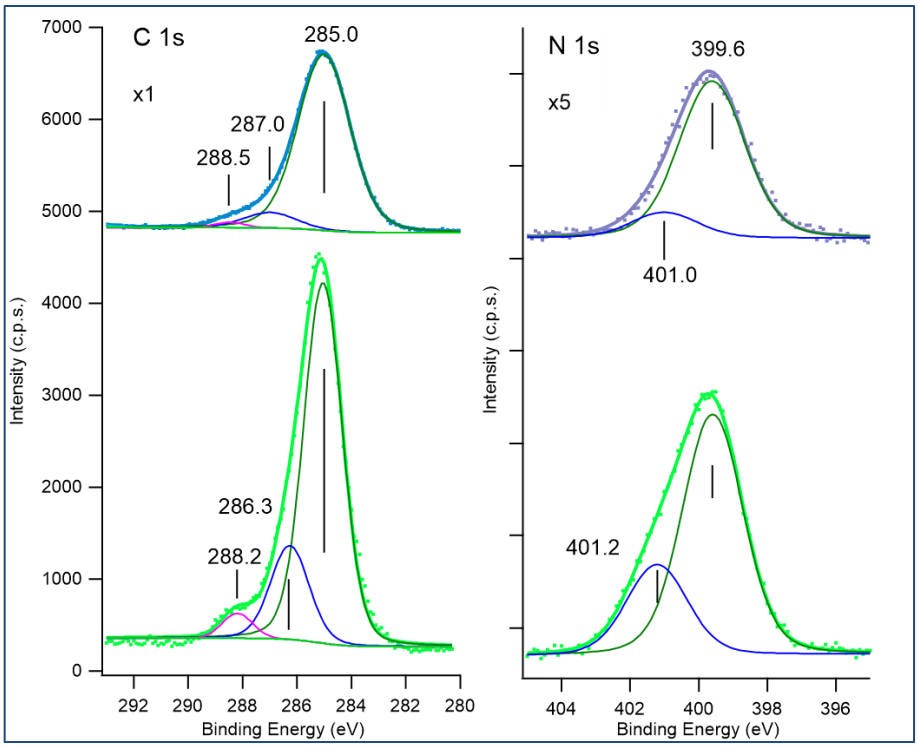

Figure 3.13 C 1s (left) and N1s (right) spectra of unrinsed coated glass (Sample1) in green, and rinsed coated glass (Sample 2) in blue.

The decrease in the intensity of nitrogen and carbon signals indicates that fewer molecules remain on the surface after rinsing. At the same concentration, pre-polymerization rinsing with water plays a crucial role in determining the structure of the siloxane network and the molecular orientation of the aminosilane on the substrate. Protonated amines can arise from two possible mechanisms: (i) in the internal layers, the amino group can interact with the silanol groups present on the glass surface, as reported by several studies [179]. However, other research suggests that the initially adsorbed layers are typically denser and more tightly packed and are therefore rich in free amines, which are not involved in intermolecular hydrogen bonding; (ii) cyclic structures with an internal hydrogen-bonded ring (*Fig. 2.9*), tend to form in the weakly bonded layers of the "grid-like" siloxane network [120], as shown in *Figure 3.14*.

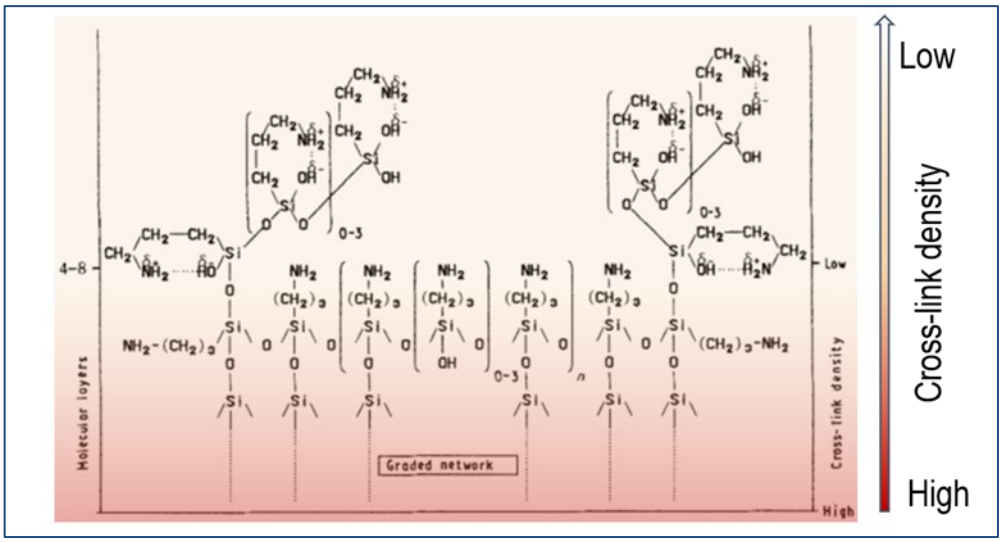

Figure 3.14 Model of three-dimensional poly(aminosilane) possible structure of chemical-bonded and weakly-bonded layers in the siloxane network; the cross-linking density tends to decrease with increasing stratification, as shown in the figure by the arrow and the gradient from red (high-density) to yellow (low-density. Adapted from [120].

Physisorbed layers, in addition, typically exhibit a high percentage of free amine groups [117]. Thus, in the case of long-term deposition with relatively high organosilane concentration, it is possible that the higher percentage of these cyclic structures is caused by a lower degree of condensation between the molecules of the outermost physisorbed layers, and that this is eliminated by rinsing.

Summarising the results, we conclude that the rinsing step doesn't significantly affect the roughness of the coated surface, but it is effective in eliminating the outermost layers of the coating, presumably composed by physisorbed molecules; thanks to this process, rinsed coated surfaces expose a larger ratio of free-to-protonated amino groups as compared to unrinsed coated surfaces.

The Effect of Aminosilane Concentration

Another parameter investigated was the silane concentration, with a comparison made between samples coated with 1% (Sample 2, *Fig. 3.15* same as *Fig. 3.7*-right, reported here to favour the comparison) and those coated with 0.5% (Sample 3, *Fig.3.16*) silane solution.

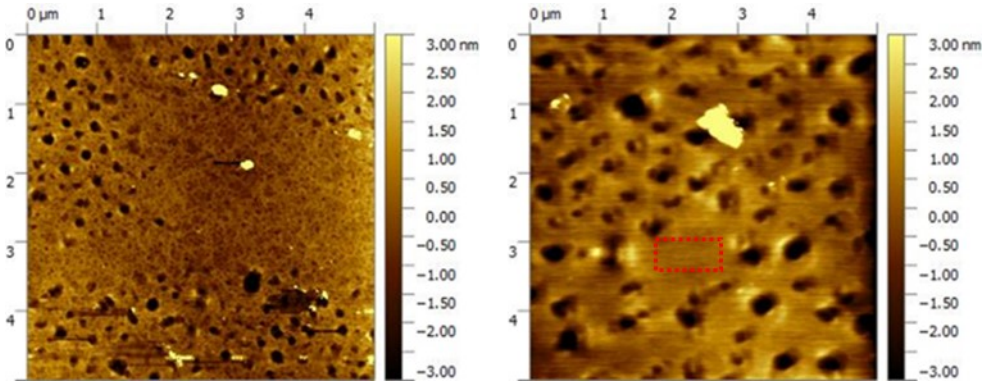

Figure 3.15 AFM images of glass coated with 1% of aminosilane (Sample 2) obtained on different pieces of glass vials.

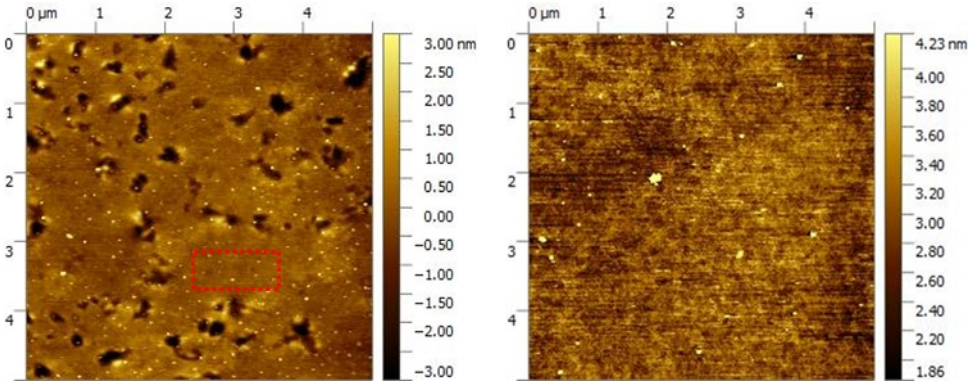

Figure 3.16 AFM images of glass coated with 0.5% of aminosilane (Sample 3) obtained on different pieces of glass vials.

The AFM images of Sample 3 revealed the presence of voids in some instances, while in others, voids were absent (*Fig.3.16*); on both images of *Fig 3.16*, the surface roughness, R_q = 0.29 nm, was found to be comparable. This roughness value is also similar to that of the sample coated with 1% silane (R_q = 0.29 nm), though it shows a slight increase in comparison to the latter.

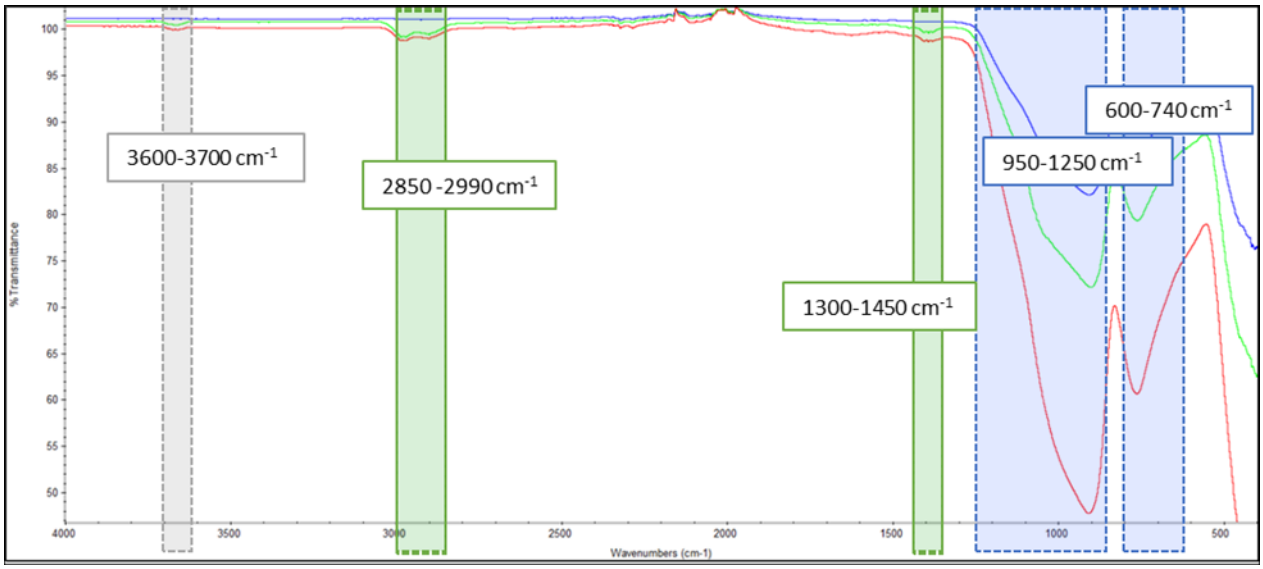

Figure 3.17 FT-IR spectra of uncoated glass (blue), and of glass coated with 1% aminosilane (green), and with 0.5% aminosilane (red).

FT-IR spectra of Sample 2 (1%) and Sample 3 (0.5%) show similar bands and peaks, as shown in *Figure 3.17*. In both Samples, the peaks associated with the alkyl chains (2850-2990 cm^{-1}) of the silane molecules are clearly present and confirmed the presence of the coating. However, the peaks corresponding to the amino groups are not detectable in either sample, probably due to the sensitivity limitations of the instrument, as mentioned above for Sample 2. For more detailed considerations, XPS analysis proved to be very useful.

XPS analysis of Sample 3 (lower concentration) revealed a significant decrease in the signals from the glass substrate, particularly for Na (*Fig. 3.18*), Al, and Mg (see *Fig. 3.19*), as compared to Sample 2.

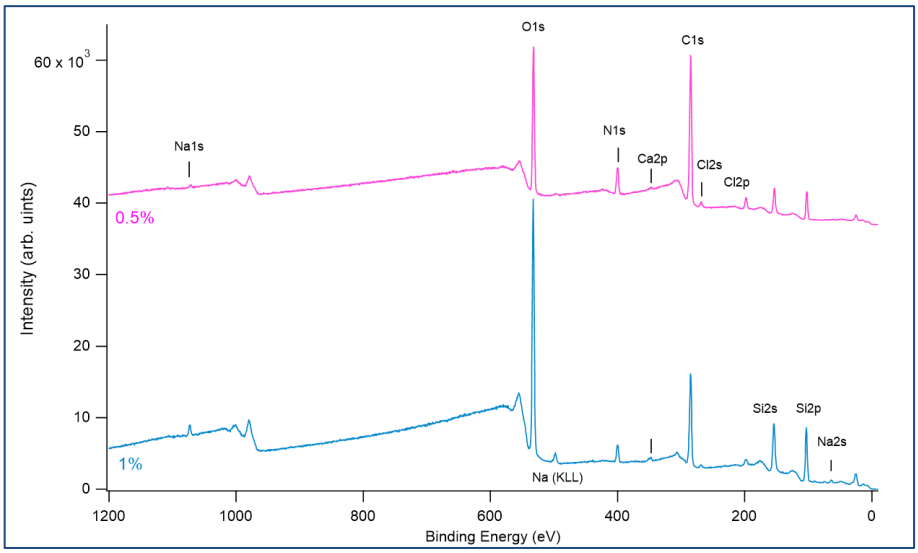

Figure 3.18 XPS survey spectra of 1% coated glass (Sample2) in blue, and 0.5% coated glass (Sample 3) in pink.

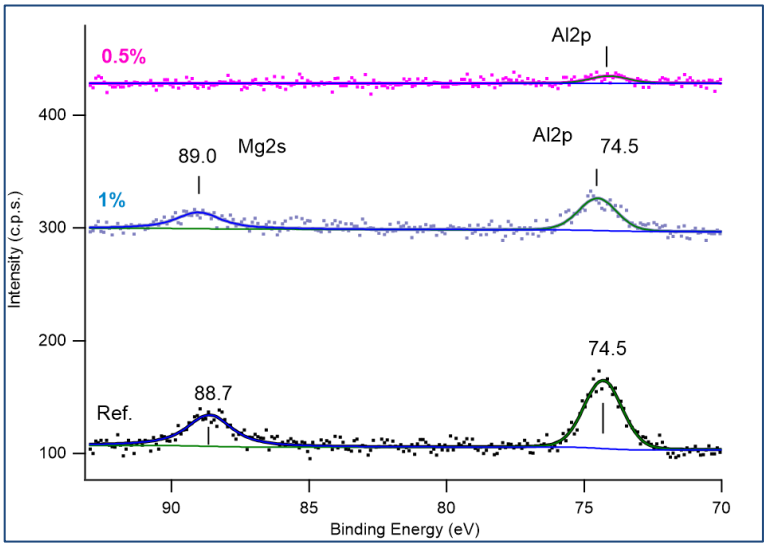

Figure 3.19 XPS spectra of Al and Mg contents in uncoated glass in black, 1% coated glass (Sample2) in blue, and 0.5% coated glass (Sample 3) in pink, from bottom to top respectively.

In contrast, the nitrogen and carbon signals increased (see *Fig. 3.20*). The carbon spectrum of sample 3 showed an increase in the C-N content at 286 eV, together with other components that are difficult to distinguish from adventitious carbon. The nitrogen spectrum of Sample 3 showed a dominant peak at 399 eV corresponding to free amines, as well as an increase in the peak related to protonated amines.

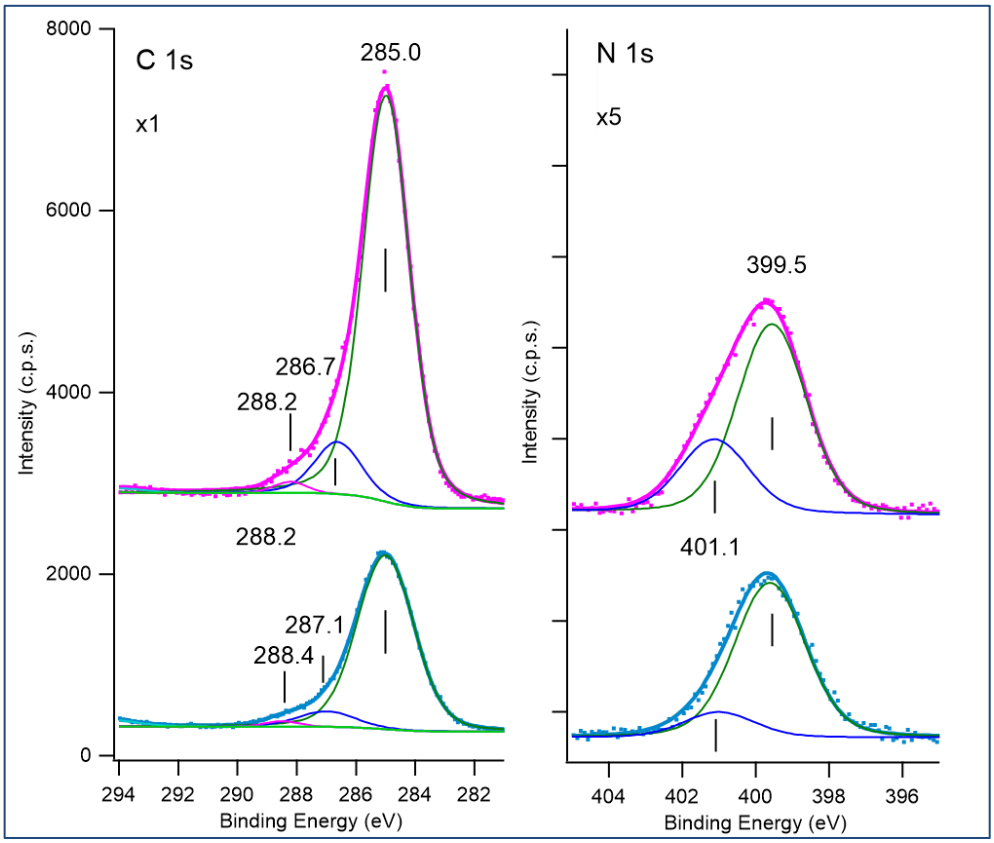

Figure 3.20 C 1s (left) and N1s (right) spectra of 1% coated glass (Sample2) in blue, and 0.5% coated glass (Sample 3) in pink.

The molecular sizes of silanol oligomers formed in solution vary depending on the concentration, which in turn affects their adsorption to the hydroxyl groups on the glass substrate [119]. In a lower concentration solution, there are likely fewer large oligomers, allowing for better surface coverage. Additionally, the larger presence of zwitterionic species on the sample coated with the lower concentration may be explained by the fact that smaller molecular species are more prone to form cyclic structures in the outermost layers of the siloxane film, due to reduced steric hindrance. An important finding is that, at a lower silane concentration, the glass surface is more thoroughly covered, while the number of free amino groups remains predominant.

XPS analysis is particularly useful in investigating the surface chemistry of coated glass compared to FT-IR, which is less sensitive, especially when dealing with very thin coatings. Therefore, it was

decided to analyse the samples coated with a 0.5% concentration and shorter immersion times directly using XPS spectroscopy.

The Effect of Dipping Time

AFM measurements for samples treated with 0.5% silane and different times, 120 minutes (Sample 3) – 60 minutes (Sample 4) - 30 minutes (Sample 5) - 15 minutes (Sample 6) and final rinsing step, revealed a consistent trend of roughness reduction on the nanometric scale, ranging from 0.29 nm for Sample 3 to 0.19 nm for Sample 6 (*Figure 3.21)*. This reduction in roughness can be attributed not only to a decrease in the thickness of the silane film but also to the formation of denser and more well-organized layers.

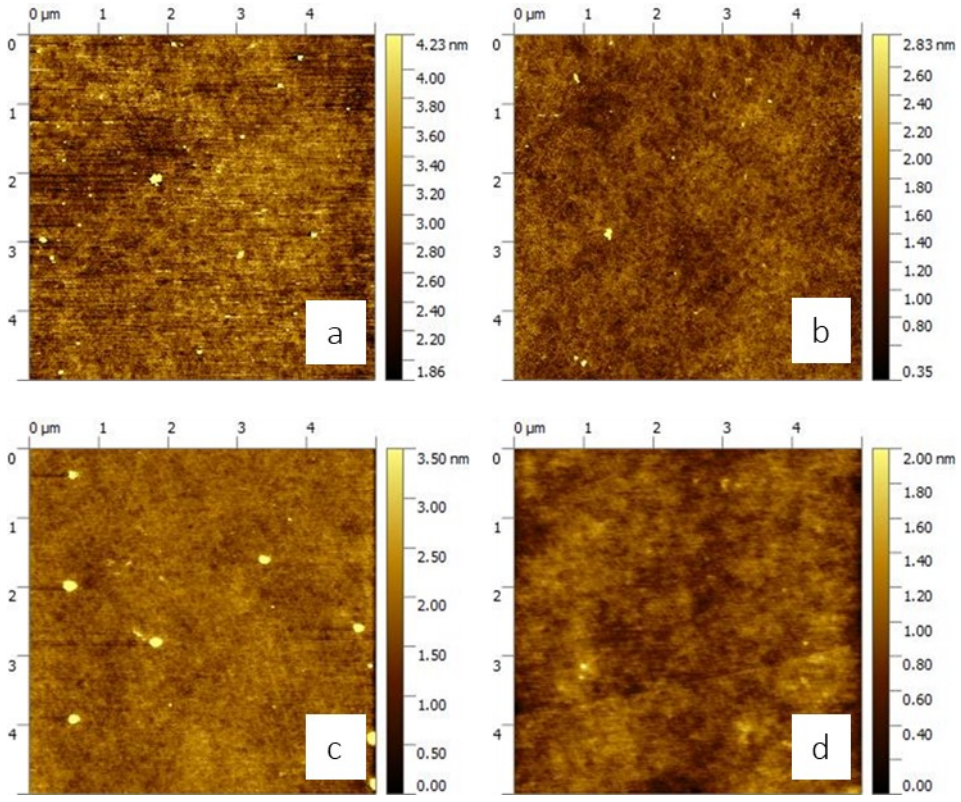

Figure 3.21 AFM images of 0.5% coated glass for 2 hours (a), 1 hour (b), 30 minutes (c) and 15 minutes (d). Rq (a) = 0,29 nm; (b) = 0,22 nm; (c) = 0,24 nm and (d) = 0,19 nm.

With an immersion time of 5 minutes the coated samples exhibited higher roughness compared to samples with longer immersion times. In this case, the increased roughness could be linked to the molecular organization of the layers rather than to the coating thickness, suggesting that during the initial phase of molecule adsorption, the resulting layers are less compact. Additionally, the surface morphology of this sample appears significantly different, as illustrated in *Fig. 3.22*, further indicating that 5 minutes as immersion times may lead to less organized and more irregular coating structures.

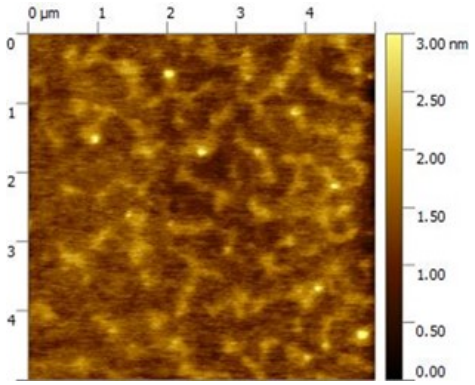

Figure 3.22 AFM image of 0.5% coated glass for 5 minutes, Rq = 0,28 nm.

Results obtained suggest that immersion time plays a key role in controlling the morphology and organization of the silane coating [89].

XPS analyses of Samples treated with different immersion time, showed that the signals coming from the glass substrate, almost completely covered in the case of the 2h time, become detectable for progressively shorter times (as shown in the full spectra *Fig. 3.23*).

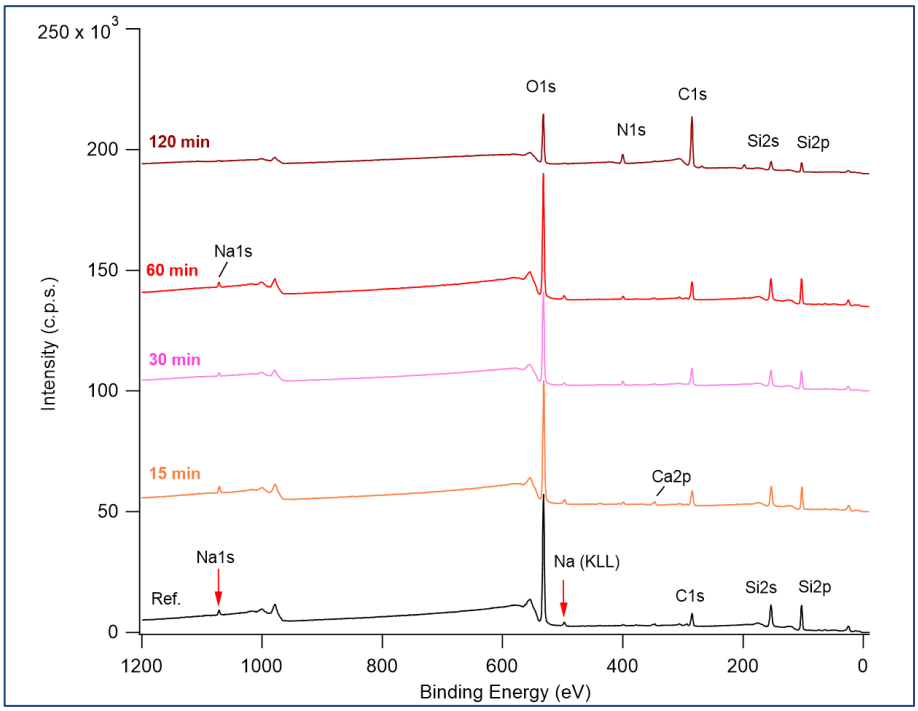

Figure 3.23 XPS survey spectra of uncoated glass in black, and 0.5% coated glass for 2h (Sample3), 1h (Sample 4) , 30 min (Sample 5) and 15 min (Sample 6, from bottom to top respectively.

The carbon and nitrogen spectra revealed an increase in the intensity of the corresponding peaks with increasing immersion time, compared to the uncoated glass reference spectrum. Specifically, the peak at 286.6 eV, attributed to the C−N bond, showed a consistent increase, with the exception of the 1-hour immersion, where a slight decrease in intensity was observed as compared to the 30-minute immersion (see C 1s spectrum in *Fig. 3.24*). Similarly, the N 1s spectrum exhibited a gradual increase in nitrogen content as the deposition time increased. In particular, at the longest immersion time, the zwitterionic component of the protonated amines became evident, with an emerging peak at 401.1 eV, in addition to the enhancement of the peak at 399 eV of the unprotonated amines (see N 1s spectrum in *Fig. 3.24*).

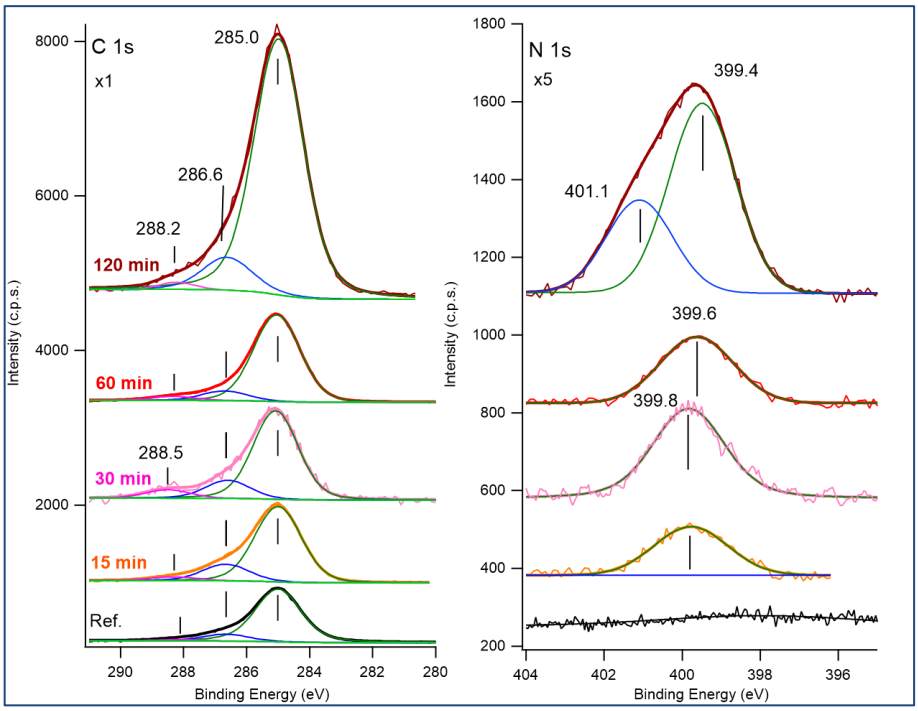

Figure 3.24 C 1s (left) and N 1s (right) spectra of uncoated glass in black, and 0.5% coated glass for 2h (Sample3) , 1h (Sample 4) , 30 min (Sample 5) and 15 min (Sample 6, from bottom to up respectively.

Between 15 and 30 minutes, a slight increase in carbon and nitrogen content is observed, suggesting the formation of initial high-density layers during this early phase of adsorption. This could be attributed to a predominant horizontal polymerization component, with only a small fraction of the physisorbed molecules being effectively removed during the rinsing process. For these immersion times, the absence of protonated amines may be due to the fact that in denser layers, the molecular chain ends are too short to enable sufficient internal hydrogen bonding, preventing the formation of zwitterionic species at this stage [120]. As immersion time increases, vertical polymerization becomes more significant, leading to an increase in both the weakly-bound and physisorbed layers. At 120 minutes, there is a notable increase in the carbon and nitrogen signal, as well as in the protonated amine component. The growth of the intermediate weakly-bound layer and physisorbed molecules, probably not completely removed, thereby increased the overall carbon and nitrogen content. Since this intermediate layer is less dense than the layer closest to the substrate, it is likely to be characterized by a larger zwitterionic component, with protonated amino groups. In particular, within the three-dimensional network,

these cyclic structures are more likely to form at the ends of the polymer network, which are free to adopt the most stable hydrogen-bonded configurations. In contrast, in the rest of the polymer network, free NH_2 groups are likely to remain oriented perpendicular to the glass surface [120]. Additional physisorbed molecules accumulate on top of this intermediate layer, although some are partially removed during the rinsing process.

It is evident that, for all immersion times, the predominant nitrogen peak is the one at 399 eV, corresponding to free NH_2 groups. This suggests that, at least in the most superficial layers of the coating, the amino groups are oriented outward, making them available for anchoring the lubricant [117]. The use of a silane primer is expected to result in a strong adhesive bond between the silanized glass and the organic layer, largely due to the network structure formed by multiple molecular layers in the interphase region. This interphase, chemically adsorbed onto the inorganic substrate, extends into the polymer matrix, while the polymer matrix also penetrates into the chemically adsorbed silane layer [100]. This interaction leads to the formation of a complex network structure, as discussed in Chapter 2.

Comparing these data with the results of the AFM analysis, both the increase in roughness observed between 15-30 minutes and 120 minutes and the increase in carbon and nitrogen content, suggest an increased adsorption of molecules over time. In particular, in the 120 minutes case, the increase in roughness can also be attributed to a more layered and less dense network in the outermost layer. For the 60 minutes immersion, the decrease in roughness could be due to a tighter packing of the deposited layers compared to shorter immersion times. However, this does not completely explain the observed decrease in carbon and nitrogen content for 60 minutes immersion, suggesting that other factors may have contributed to the reduction in elemental composition.

3.1.2.3 Mechanical Tests

Tribological Tests – Ball-on-disk

Tribological tests were conducted to investigate the effect of surface treatments on the friction coefficient (COF). For these tests, a specific set of parameters was chosen, corresponding to Sample2 in Table 1, with an additional dipping step in a lubricant solution, as outlined in the Experimental section.

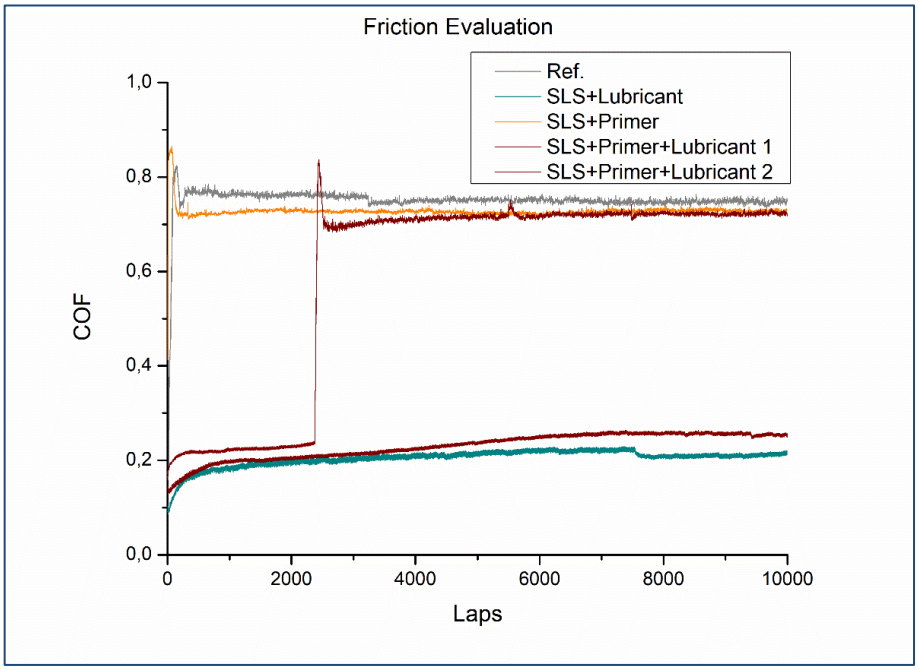

Figure 3.25 Representative curves of the COF evolution as a function of the number of Laps (10000). In grey the uncoated Ref. glass sample; in orange the coated sample with only Primer; in red the coated samples with primer and lubricant; and in blue the coated sample with only lubricant.

The results in *Figure 3.25* showed that both untreated and silane-treated glass exhibited a rapid increase in the COF. For the untreated specimen, the COF stabilized at 0.7, while the glass coated with silane reached a COF of 0.72, indicating that the silane primer alone had no significant influence on the friction coefficient. For the sample treated with a lubricant, a significant reduction in the COF was observed, with the friction coefficient starting at 0.08 and quickly stabilizing at 0.2. This is consistent with the behavior reported in tribological studies where

lubricants form a protective layer that significantly reduces friction by preventing direct contact between the surfaces [182]. In fact, at the end of the test, no visible wear trace was observed, suggesting that the lubricant provided substantial wear protection. In some studies this is true especially when the lubricant is applied to surfaces treated with primers/additives [183], [184], [185]. Samples treated with both the silane primer and the lubricant initially showed a COF of approximately 0.21 (*Figure 3.26, close up of Fig. 3.25 for 2000 laps*).

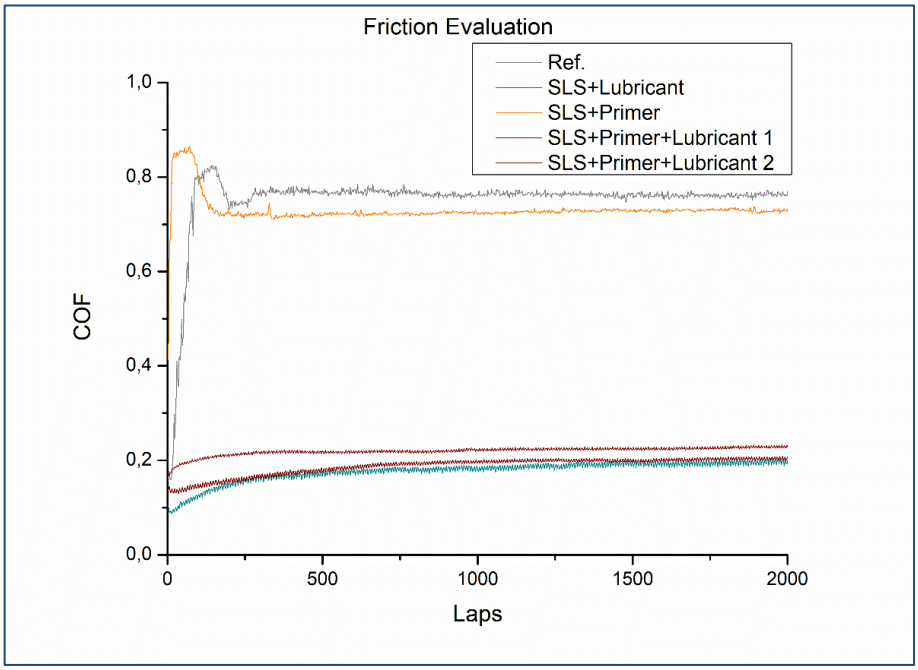

Figure 3.26 Representative curves of the COF evolution as a function of the number of Laps (2000). In grey the uncoated Ref. glass sample; in orange the coated sample with only Primer; in red the coated samples with primer and lubricant; and in blue the coated sample with only lubricant.

However, after about 2000 laps, in some cases the COF remained very low, in others it rapidly increased to 0.7 (comparison of SLS+Primer+Lubricant 1 and SLS+Primer+Lubricant 2 in *Fig. 3.25*). The sudden increase in COF indicates a premature detachment of the lubricant layer under high tribological stresses, a behavior that has been reported in other studies involving surface coatings and primers. In several studies, the interaction between the silane and the substrate can improve the bond strength, but does not necessarily result in a lower coefficient of friction [186], [187]. These studies have shown that the application of silane often results in similar COF values

compared to untreated surfaces under certain test conditions. In this study the tribological behavior of the primer was found to be not always repeatable, this could also be due to the fact that for this instrumental setup (ball-on-disk) it was necessary to deposit the coating on the bottoms of the bottles which was not always homogeneous due to the concave shape of the sample. Up to 2000 laps however the primer maintains a low surface friction, and it should be noted that the in-line friction to which the vials are subject is presumably lower than that simulated with the instrumentation under examination.

Scratch Analysis in Multipass Mode

Representative measurements of the COF values obtained operating the Nano Scratch Tester in multipass mode are shown in *Fig. 3.27* as functions of the number of passes for the samples of *Table 2*, consisting of whole 20 mL SLS glass vials with different coatings.

The uncoated glass reference sample displayed a rapid increase in the coefficient of friction (COF), rising from 0.4 to approximately 0.8 within less than 20 passes, which confirms the high surface friction of bare glass vials. In contrast, the sample coated only with lubricant exhibited an initial COF of 0.2, and only after almost 400 passes it increased towards larger values. These results proof that this kind of measurement is sensitive to the properties of the surface (glass vs lubricant) and is also able to explore the resistance of the coating against the increase of the number of passes, evidenced through the transition from low to high COF values in the lubricated surface.

When a 0.5% primer layer, applied by dipping as described in Section 3.1.1.3, is interposed in between glass and lubricant, COF behaviors clearly showed a dependence on the primer immersion time (see *Table 2*). In all cases, COF values tend to increase as the number of passes increases, but the presence of the silane primer with lubricant pins the COF to low values (0.2-0.3) for a certain number of passes before it increases to larger values. In particular, Sample 6, with a primer immersion time of 15 minutes, showed an COF value of approximately 0.25 until 24-26 passes then it gradually rose to achieve a value of 0.9 after 50 passes. Sample 5, immersed for 30 minutes, showed at COF in the 0.2-0.3 range for a number of passes as high as 138-140, then progressively increased to a value of about 0.9 after 174 passes. For Sample 4, with a 60-

minute immersion, the stabilization at a COF value in the 0.2-0.3 range lasted for 58-60 passes, rising steadily to stabilize at 0.9 after 74 passes. Sample 3, with a 120-minute primer immersion time, had an initial COF of 0.1 which increased rapidly to 0.4, and stabilized at approximately 0.7 after 150 passes.

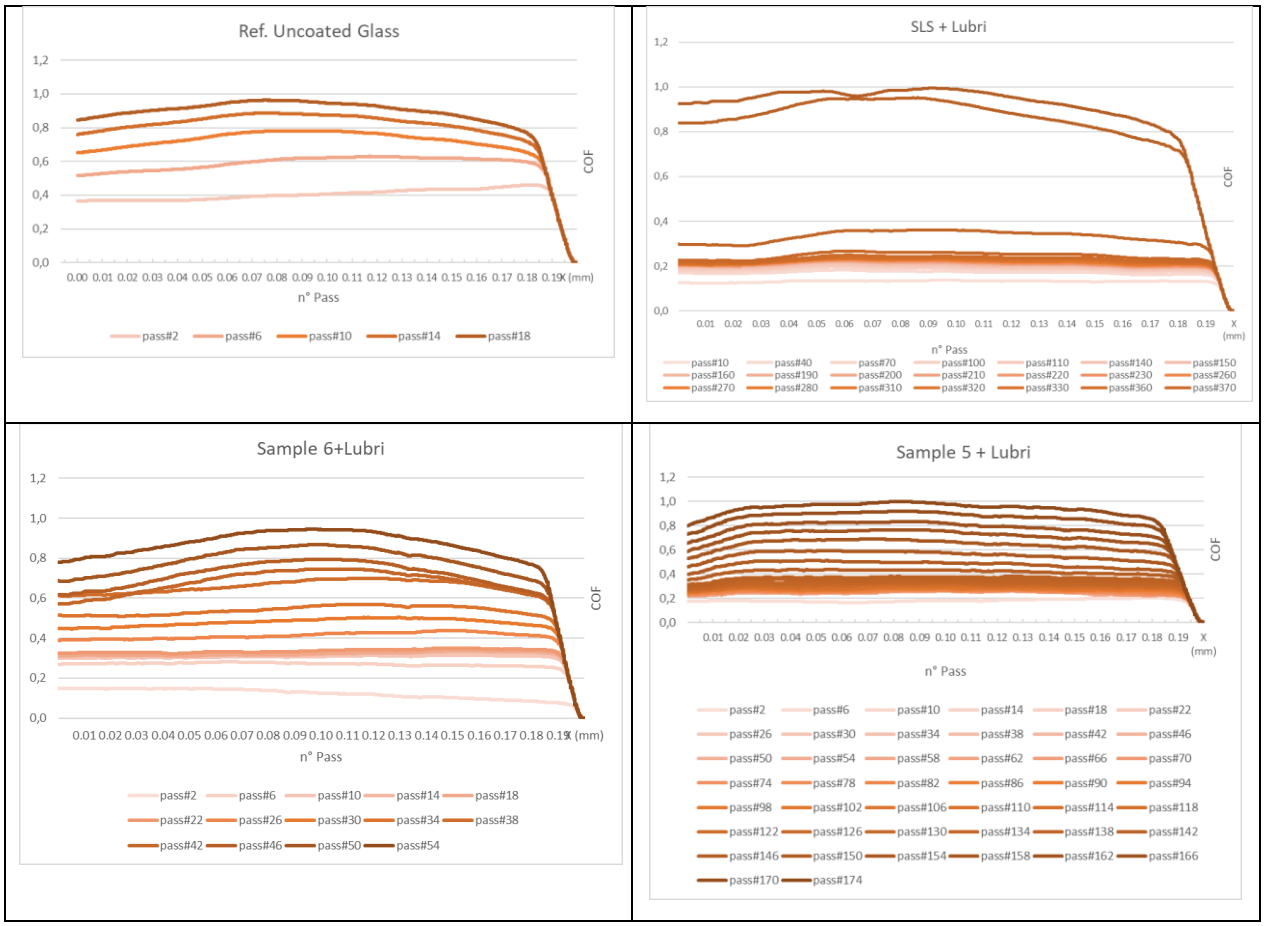

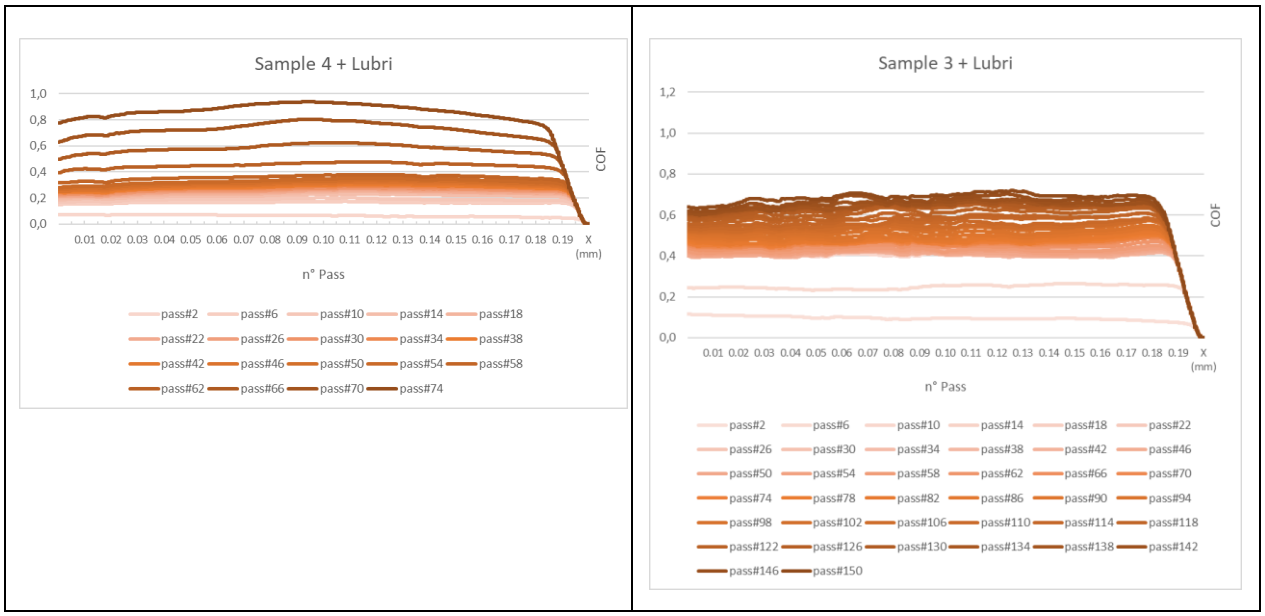

Figure 3.27 Representative evaluation of friction as a function of the number of passes. As shown, from top left to bottom right, reference uncoated glass sample, sample coated with lubricant only (SLS+Lubri), sample 6 + Lubri (15 min immersion time), sample 5 + Lubri (30 min immersion time), sample 4 + Lubri (60 min immersion time), and sample 3 + Lubri (120 min immersion time).

The results indicate that dipping time has a notable impact on the adhesion-promoting effect of the lubricant. Specifically, the number of passes required before the lubricant's effect diminishes (i.e. the COF approaches that of bare glass) substantially increases with longer dipping times in the 15 to 30 minutes range, then decreases for 60 minutes immersion time and finally shows a different behavior for the structure with 120 minutes silane dipping time. We note here that these findings show a strong similarity with XPS observations reported in the previous section, where we concluded that deposition times < 60 minutes allowed to obtain denser and closely packed silane layers with a predominance of free amino groups on the surface, while for deposition times ≥ 60 minutes the silane deposits start showing a more layered and less dense structure characterized by weakly-bound, physisorbed layers with longer zwitterionic components, with a measurable fraction of protonated amino groups in the 120 minutes structure.

By combining XPS and multipass results, we conclude that the functionality of the silane primer strongly depends on the structure of the siloxane-network interface (maximized in the 30-minute and 120-minute structures). The loss of anchorage at 60 minutes does not allow to highlight a trend as a function of time, further investigations will be required to clarify this aspect. In fact,

the adhesion promotion by silanes could be related both to chemical bonds of amine functionals groups present than to the formation of an interpenetrating network between primer and polymer thanks to the graduated stratification of the siloxane network.

Interestingly, the behavior of the lubricant without a primer presents inconsistencies compared to observations from production lines. This discrepancy may be due to the dip-coating method, which might result in a relatively thick lubricant layer that does not chemically bond to the surface but instead spreads during measurement, thereby maintaining a lower COF over a prolonged period.

The primer's effectiveness will be further explored in the following chapter, where results from spray deposition, a method more closely aligned with industrial practices, will be discussed.

Tilt – Table Tests

In parallel with the tribological study of the coated surfaces, industrial in situ tests were conducted as part of standard quality control procedures to evaluate the sliding angle using tilt-table instrumentation available at Bormioli Pharma facilities. This test is routinely employed in the industry to assess the frictional properties of the vial surface, with an acceptable maximum sliding angle set at 30° (red dashed line *in Fig. 3.28*). If the sliding angle exceeds this threshold, adjustments to the lubricant application process are typically implemented to enhance performance. For this study, 20 mL vials were tested in groups of three for each coating type. Sliding angle measurements were obtained by positioning three bottles on the tilt table and rotating the top-positioned sample for each measurement to ensure consistency. In this case, it was possible to use a glass vial with SnO_2-primer taken from the industrial plant and subsequently immersed in the aqueous lubricant solution using the same procedure as for the other samples, as explained in Section 3.1.1.3.

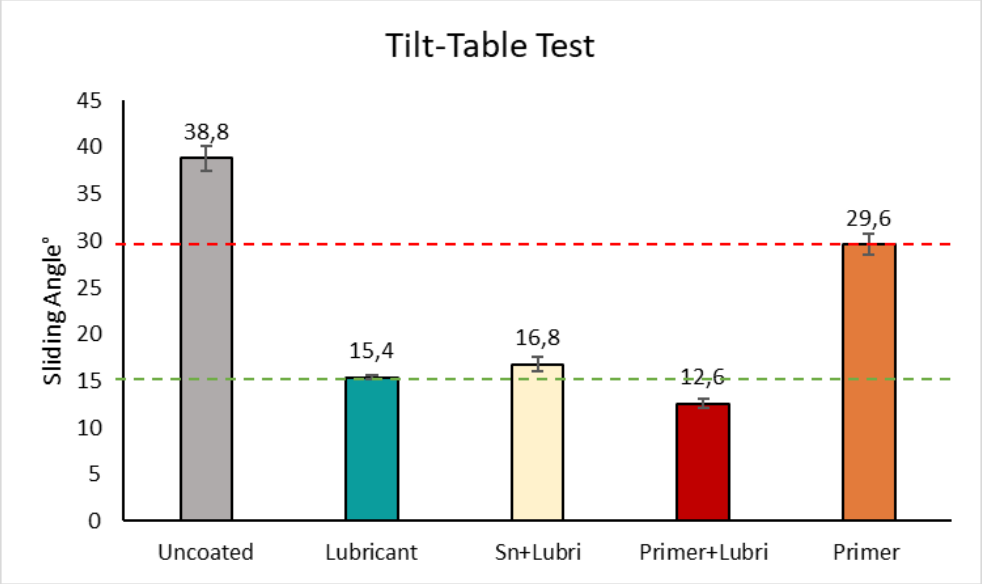

Figure 3.28 Plot of sliding angle (°) values showed are mean ± SE (Standard Error). The histogram is the vale of the average obtained from 5 measurements made for each sample. In grey the reference uncoated vial (Uncoated); in blue the coated vial with only lubricant (Lubricant); in yellow the coated vial with standard primer (SnO_2) and lubricant (Sn+Lubri); in red the coated vial with silane primer and lubricant (Primer+Lubri) and in orange the coated vial with only silane--primer (Primer).

The results showed in *Figure 3.28* demonstrate that uncoated glass exhibits a sliding angle exceeding 30°, indicating a high degree of friction between the bottle surfaces. In contrast, glass coated with the standard lubricant shows a sliding angle of approximately 15° (green dashed line in *Fig. 3.28*), which aligns with good sliding performance according to quality control standards. Notably, the sliding angle for glass coated with the silane primer is even lower than that obtained with the conventional tin-based primer, demonstrating improved performance. As expected, however, the silane primer alone does not achieve high sliding values.

3.2 Single– Component Coating

3.2.1 Materials and Methods

Substrates: Soda-lime-silicate (SLS) glass pieces sourced from 500 mL vials produced by Bormioli Pharma S.p.A. were used for surface characterization of the glass coated. Whole 20 mL SLS vials were used for mechanical measurements with the tilt-table method.

Chemicals: 2-[(acetoxy(polyethyleneoxy) propyl] triethoxysilane (*Fig. 3.29*) a commercial product purchased from Gelest - Mitsubishi Chemical Group, was used in aqueous solution at the concentration of 2%.

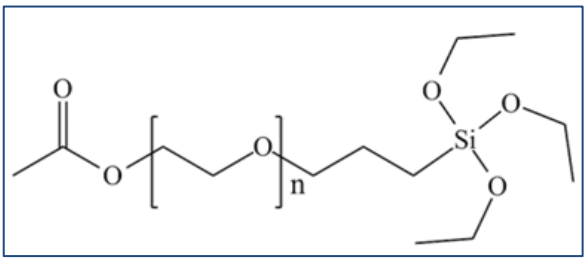

Figure 3.29 2-[(acetoxy(polyethyleneoxy) propyl] triethoxysilane, Gelest[114].

3.2.1.1 Surface Preparation

The glass samples were prepared by cutting the vials into pieces approximately 1 cm x 1 cm in size. These pieces underwent chemical cleaning through sonication in deionized water, isopropanol, acetone and isopropanol. Immediately prior to immersion in the silane solution, the samples were treated with oxygen plasma for 5 minutes at a power of 8 W using a plasma cleaner (Femto, Diener electronic, Germany) to expose hydroxyl (OH) groups on the glass surface. The increase in surface wettability was assessed by measuring the contact angle.

The same chemical cleaning and surface activation procedure was applied to the vials used for mechanical characterization.

3.2.1.2 Coating Deposition

The silane aqueous solution at 2% in volume, was stirred for 15 minutes prior to immersing the sample. This period allows for the hydrolysis of the alkoxy groups, as studied through IR spectroscopy in solution, which will be discussed in Section 3.2.2.1. After the 15-minute stirring period, the glass sample was immersed in the solution and kept under gentle agitation for 60 minutes. Finally, the sample was subjected to curing at 150°C for 120 minutes.

3.2.2 Results and Discussion

3.2.2.1 Hydrolysis Study in solution

The 2-[acetoxy (polyethylenoxy) propyl] triethoxysilane, referred to as SIA, contains a long functional side chain with repeated ether linkages and a carbonyl group as the organic portion, as well as three -$SiOCH_2CH_3$ groups that must undergo hydrolysis to form -SiOH groups, which then condense with -SiOH groups on the substrate surface. The hydrolysis of silanes follows the reaction pathway shown in Eq. (10), where Et represents an ethyl group.

$$\text{—Si(OEt)}_3 + H_2O \longleftrightarrow \text{—Si(OH)}_3 + 3\ EtOH \qquad (10)$$

We investigated the hydrolysis time for a 2% SIA solution in water. The natural pH of the solution was 4.5, which is sufficiently acidic to promote the hydrolysis process, making the addition of catalysts unnecessary. The study was conducted using FT-IR spectroscopy in solution by taking a droplet of the solution at increasing reaction times (t=0 – 5min – 15min – 30min – 1h – 2h) (see *Fig. 3.30*) and monitoring the growth of the band at 1045 cm^{-1}, which is characteristic of the ethanol released [75] in the reaction described by Eq. (10).

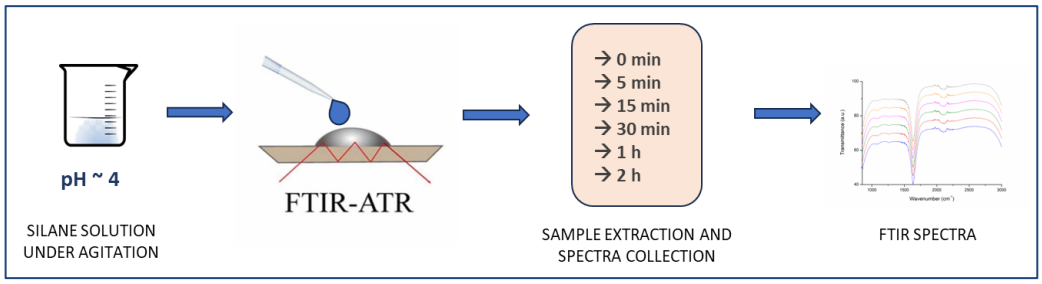

Figure 3.30 Schematic view of the IR analysis conducted in solution, adapted from [188].

The peak corresponding to the release of ethanol begins to appear as early as 5 minutes into the reaction and shows no significant increase beyond 15 minutes, as demonstrated in *Figure 3.31* of the collected FT-IR spectra. Based on these observations, 15 minutes was selected as the optimal hydrolysis time before immersing the glass samples in the silane solution.

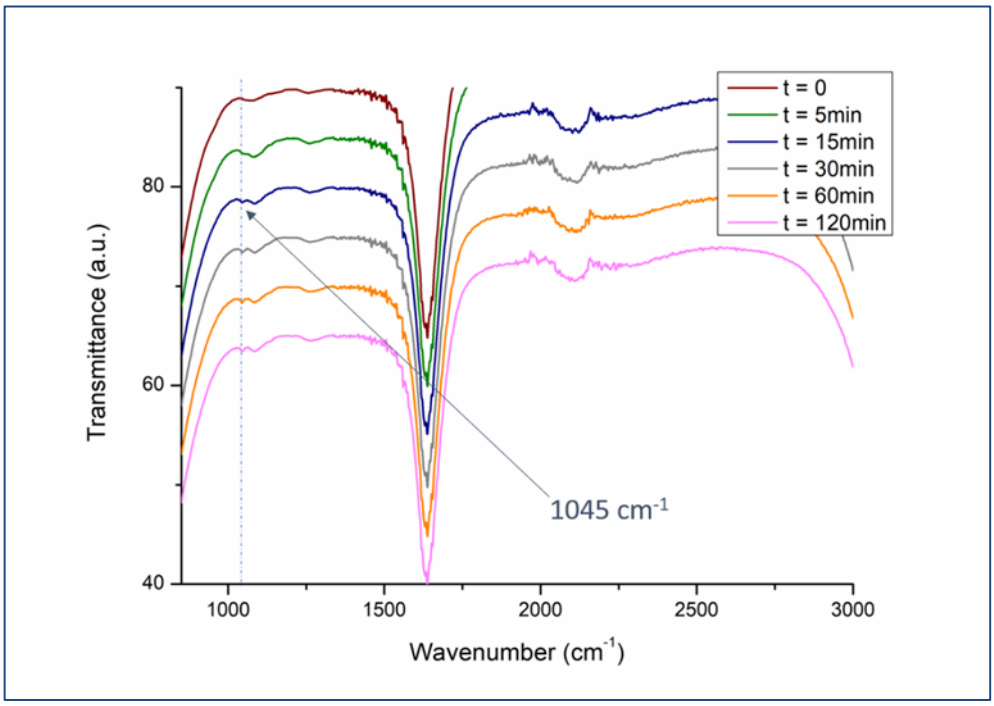

Figure 3.31 FT-IR spectra of SIA aqueous solution from different reaction times. The peak at 1045 cm^{-1} is related to ethanol release for hydrolysis time evaluation.

3.2.2.2 Surface Characterization

The SIA-coated samples were analysed using AFM microscopy and FT-IR spectroscopy. AFM analysis confirmed the presence of the coating through changes in morphology and an increase in roughness, with R_q = 0.33 nm compared to the uncoated glass (R_q = 0.16 nm). The AFM images showed good surface coverage, as illustrated in the *Figure 3.32*.

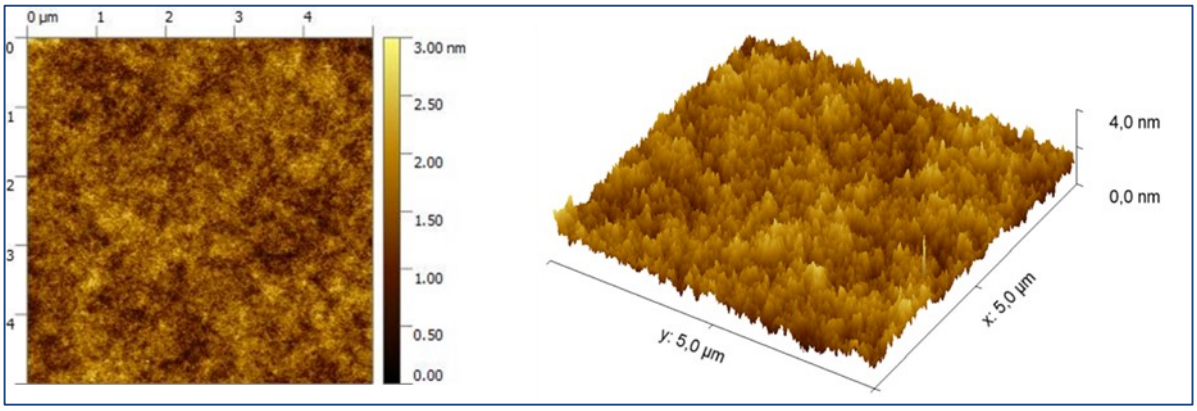

Figure 3.32 AFM images of coated glass with 2% of SIA. R_q = 0,33 nm.

FT-IR analysis further confirmed the presence of the coating, with the appearance of peaks in the 2850-2960 cm^{-1} region, corresponding to the C-H stretching of the alkyl chains, and a peak around 1736 cm^{-1}, attributed to the carbonyl (C=O) groups (see *Fig. 3.33*) of the organic portion of SIA molecules. The peak typically associated with the C-O group, located around 1136 cm^{-1}, is likely obscured by the strong band in the 950-1250 cm^{-1} region, corresponding to Si-O-X bonds.

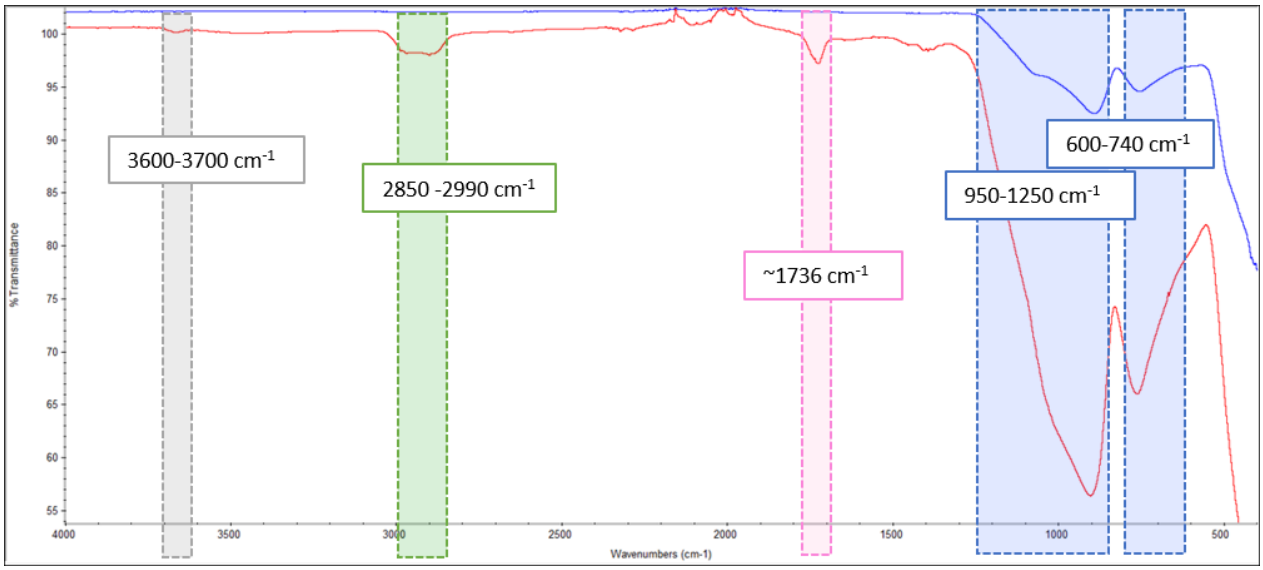

Figure 3.33 FT-IR spectra of coated glass sample with 2% of SIA (in red) compared with the spectra of uncoated glass (in blue).

3.2.2.3 Mechanical Tests

Tilt-Table Tests

The 20 mL glass vials coated with SIA underwent quality control assessment using the Tilt-Table instrumentation available at the Bormioli Pharma facility. As shown in *Figure 3.34*, the sliding angle measurements for SIA-coated vials were higher than those of vials coated with the standard lubricant; however, they remained within the threshold of industrial acceptability. This indicates that the SIA coating meets the minimum sliding performance required in production, despite not reaching the lower friction levels associated with standard lubricant.

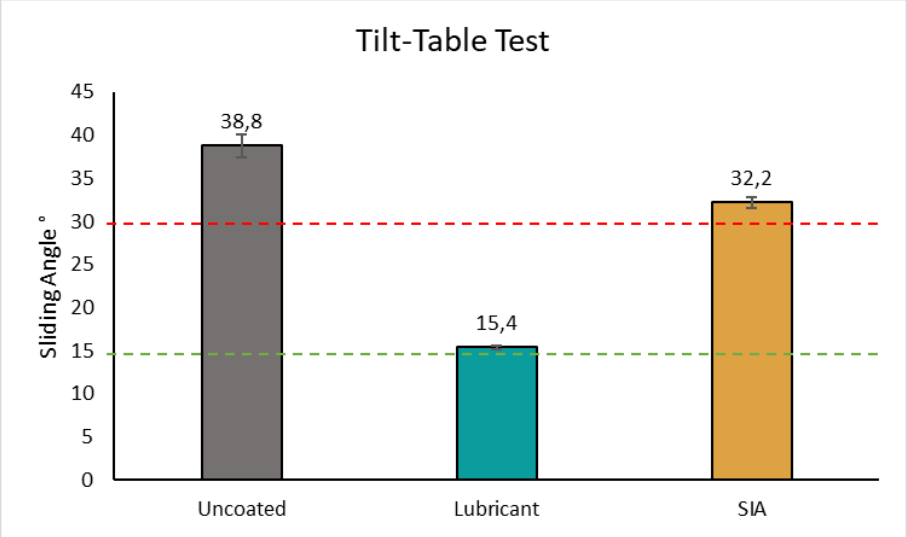

Figure 3.34 Plot of sliding angle (°) values showed are mean ± SE (Standard Error). The histogram is the value of the average obtained from 5 measurements made for each sample. In grey the reference uncoated vial (Uncoated); in blue the coated vial with only lubricant (Lubricant); in orange the coated vial with SIA (SIA). The red dashed line at 30° = threshold of industrial acceptability; the green dashed line at 15° = good value in industrial control quality.

The potential to utilize a single-molecule in aqueous solution that forms a covalent bond with the glass surface while also providing lubrication offers significant industrial advantages, particularly in terms of process simplification and reduced material use. Consequently, further investigation into the spray deposition of this solution was undertaken, as detailed in Chapter 4, to assess its scalability and performance in an industrial setting. This approach aims to evaluate whether SIA is able to provide adequate surface protection and lubrication through a simplified and single-step coating process.

4. Experimental Studies for Industrial Scalability

This chapter is divided into two main sections (4.1 - 4.2), each addressing studies on organosilane-based coatings deposited using spray systems. Section 4.1 focuses on the aminosilane primer and single-component coatings deposited via an airbrush system, including comprehensive characterization. In this section, various methods for chemical activation of the glass surface were explored to facilitate the silanization process, and the effectiveness of these methods was evaluated through contact angle measurements, which also served to confirm the presence of the coating. Following deposition, scratch tests were conducted on the lubricated coating samples to assess their resistance to surface damage under controlled parameters.

Section 4.2 investigates the performance of the aminosilane primer coating, applied with and without lubricant, using an automatized spray system. The presence of the primer coating was verified through XPS analysis, and the mechanical performance of the coated samples was evaluated through tribological testing in a ball-on-flat configuration. The primary objective of this experimental work was to evaluate the industrial scalability of these coatings by testing the spray deposition method, the intended approach for industrial application. In this context, a primer-lubricant mixture was introduced to enable a one-step spray application, simplifying the process for potential large-scale implementation.

As presented in the results of these sections, the airbrush and spray deposition studies were conducted on samples with different coatings, and the corresponding characterizations were also distinct. These investigations took place during separate research stays at different international research centers. As a result, it was not possible to perform the same types of chemical, physical, and mechanical characterizations due to practical constraints related to equipment availability and time. It was preferred to analyse the samples shortly after their preparation, using the instrumentation available on site, to preserve their properties and ensure reliable results. Specifically, in the study involving the spray system, it was not feasible to test the SIA, as the instrument's heating plate could not reach the curing temperature required for the material. For this reason, this set of analyses was performed exclusively on the aminosilane primer in combination with the lubricant.

This distinction underscores the necessity of adapting the experimental work to the conditions and resources available during these research periods, while ensuring that the objectives of each study were effectively achieved.

4.1 Air-Brush Deposition

4.1.1 Materials and Methods

Substrates: Soda-lime-silicate (SLS) glass pieces sourced from 500 mL vials produced by Bormioli Pharma S.p.A.

Chemicals:

Amino propyl silsesquioxane (*Figure 3.1*), a commercial product purchased from Gelest - Mitsubishi Chemical Group, was used as the silane primer in aqueous solution. As a lubricant, a macrogol stearate - a mixture of mono- and di-esters of stearic and/or palmitic acid with macrogol (*Figure 3.2*), was employed in aqueous solution. The commercial name of the lubricant is omitted for confidentiality reasons. 2-[(acetoxy(polyethyleneoxy) propyl] triethoxysilane (*Fig. 3.29*) a commercial product purchased from Gelest - Mitsubishi Chemical Group, was used in aqueous solution at the concentration of 2%, as a single-component coating.

4.1.1.1 Surface Preparation

The glass samples were prepared by cutting the vials into pieces approximately 2 cm x 2 cm in size. Three different chemical cleaning methods were tested and compared to a standard cleaning procedure, with surface activation effectiveness assessed through contact angle measurements.

Method-1: The sample was immersed in a 1:1 solution of methanol (MeOH) and hydrochloric acid (HCl) for 30 minutes. Following this, the sample was rinsed with deionized (DI) water and dried under a nitrogen (N_2) stream. Subsequently, the sample was immersed in concentrated sulfuric acid (H_2SO_4) for 30 minutes, followed by a second rinse with DI water and drying under N_2.

Method-2: The sample was immersed in a 1 M sodium hydroxide (NaOH) solution for 20 minutes. After the incubation period, the sample was rinsed with deionized water and dried under a nitrogen (N_2) stream.

Method-3: The sample was immersed in a 9% aqueous hydrofluoric acid (HF) solution for varying durations (20 s, 60 s, 240 s, 720 s). After immersion, the sample was rinsed in an ultrasonic bath for 4 minutes and then dried under a nitrogen (N_2) stream.

Method-0 (Reference Method): The sample was subjected to sonication in deionized water for 2 minutes, followed by sonication in isopropanol for 2 minutes, acetone for 2 minutes, and isopropanol for an additional 2 minutes. The sample was then dried under a nitrogen (N_2) stream. These methods were employed to evaluate the surface activation efficiency through contact angle measurements.

4.1.1.2 Coatings Deposition

The coatings were deposited as follows. The glass substrates were placed on the airbrush platform and secured in place with an adhesive to prevent movement during the deposition process. The airbrush gun was positioned at an angle of approximately 60° to the sample surface, with the air compressor pressure set at 2.0 kg/m². The coating was applied to the 2 cm² sample area, over which approximately 1 mL of precursor solution was evenly distributed at room temperature. The air-brush gun was moved slowly back and forth for four passes, maintaining a constant distance of approximately 20 cm between the glass substrate and the airbrush gun (see *Figure 4.1*).

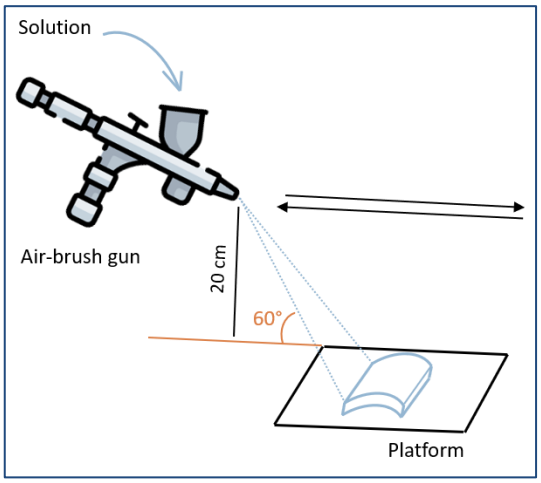

Figure 4.1 Schematical set-up of the air-brush deposition.

Table 3 provides a detailed summary of the sample preparation using different coating solutions. For comparison, a sample coated solely with the lubricant was prepared by depositing the lubricant on a heated glass substrate according to the current industrial process. The SIA aqueous solution was prepared and stirred for 15 minutes before being sprayed onto the surface, to allow hydrolysis as studied in section 3.2.2.1. In addition, a solution containing a mixture of aminosilane-primer and lubricant (Primer/Lubri in *Tab. 3*) was prepared to explore the feasibility of a one-step application. As a reference, uncoated glass samples were also analysed.

Table 3. Parameters used to deposit coatings by air-brush.

Sample	Pre-treatment	Silane	Curing	Lubricant
SIA	HF 9% for 720s	SIA 2% in water	150°C for 30 min	no
Primer	HF 9% for 720s	Aminosilane 0.5% in water	150°C for 30 min	no
Primer+Lubri	HF 9% for 720s	Aminosilane 0.5% in water	150°C for 30 min	yes
Primer/Lubri	120°C for 2h	Aminosilane 0.5%/Lubricant 0.1% in water		
Lubri	120°C for 2h	Lubricant 0.1% in aqueous solution		yes
Ref.	Cleaned	Uncoated		

4.1.2 Results and Discussion

4.1.2.1 Contact Angle Measurements

The effectiveness of the chemical methods tested for the activation of glass surfaces was evaluated through contact angle measurements. This was measured by placing a 2.0 µL drop of deionized water on the surface using a pipette. The image of the droplet was captured within a few seconds of placing it on the surface. The measurement was obtained by software circle interpolation for the angle determination as showed in *Fig. 4.2*. As a reference, glass samples cleaned with Method-0, a routine chemical cleaning process for removing contaminants (previously described in the Materials and Methods section), were used. In *Table 4* the results obtained.

Among all tested methods, Method-3, involving immersion in hydrofluoric acid for 720 seconds, proved to be the most effective. With this pretreatment, the contact angle was reduced from approximately θ = 60° for the glass cleaned with Method-0 to less than 6° (see *Fig. 4.2*). The measurement was repeated after three days, and the contact angle remained unchanged, indicating the stability of the surface treatment. Consequently, this method was selected for the pretreatment of samples prior to the deposition of coatings via the air-brush technique.

Table 4. Evaluation of the contact angle on glass substrate treated with different chemical cleaning methods for surface activation.

Method	Acquisition Time	Contact Angle θ
M - 0	t = 0	59.8°
M - 1	t = 0	36.8°
M - 2	t = 0	21.2°
M – 3 (20s)	t = 0	19.7°
M – 3 (720s)	t = 0	5.8°

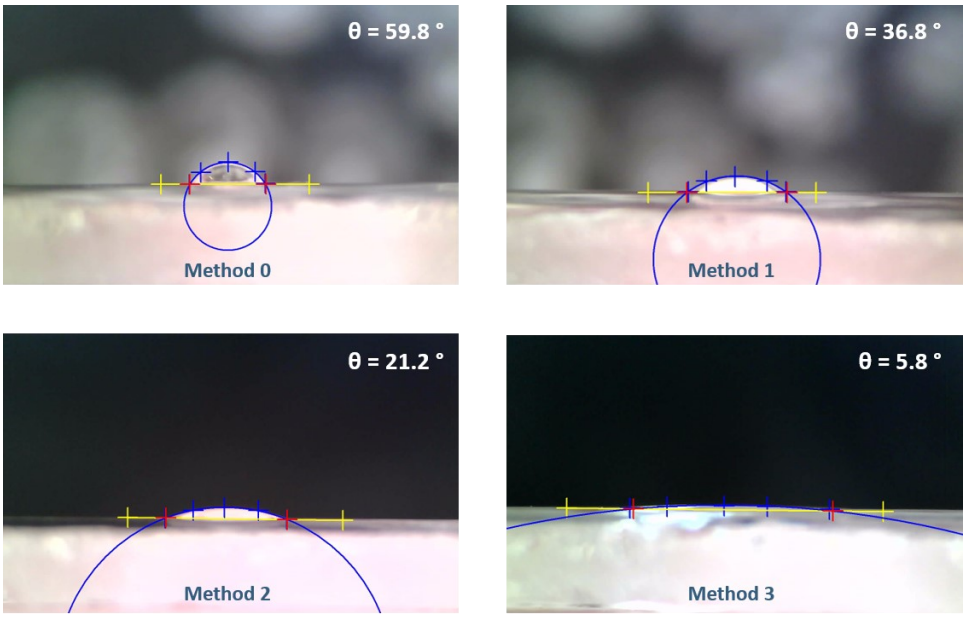

Figure 4.2 Images of droplet captured with contact angle measured on glass substrate after different activation methods; the image of Method-3 refers to the surface immersed for 720s.

The contact angle was measured, also, on the glass surface after coating deposition using an air-brush system. *Figure 4.3* shows images of water droplets on the different samples, highlighting the captured contact angles. The results confirm the presence of the coating, evidenced by changes in surface wettability. The application of an aminosilane primer, whether applied sequentially (Primer + Lubri) or mixed with the coating (Primer/Lubri), resulted in a contact angle indicative of hydrophilicity comparable to that achieved with the lubricant alone. When the primer was applied independently, the contact angle was approximately 40°, aligning with values reported in the literature [125].

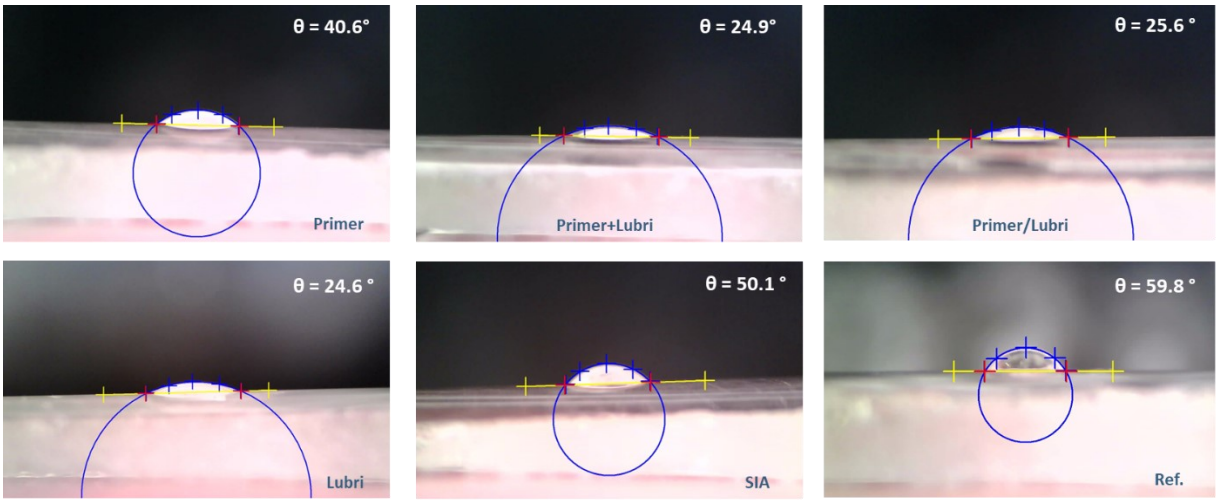

Figure 4.3 Images of droplets captured with contact angle measured on different glass samples.

For the SIA coating, the measured contact angle was around 50°, indicating an increase in hydrophilicity compared to uncoated glass, as expected for this type of molecule. This shift suggests that the SIA coating effectively enhances the glass surface affinity for water, consistent with the intended surface characteristics of this molecule type. These variations in contact angle reflect the distinct interactions between each coating formulation and the glass surface, providing insight into the effectiveness of the coatings in altering surface wettability.

4.1.2.2 Mechanical Tests

Scratch Analysis

The coated samples were subjected to scratch tests to evaluate surface damage following the application of a progressive load on the glass surface. The initial load applied was 0.3 N, while the final load reached 10 N, over a scratch length of 8 mm. For each sample, three measurements were taken: one at the center of the substrate, and the other two immediately to the left and right of the central measurement, with an approximate distance of 3 mm between them (as schematically shown in *Fig. 4.6*). A panoramic view of the scratch mark was captured immediately after the load was applied, as provided by the light microscope. These images were analysed to

assess the nature and extent of the damage, with Critical Loads (Lcs) being assigned to specific damage indicators.

The uncoated reference glass exhibited all the typical damage defects of soda-lime glass, as confirmed by the literature and shown in *Figure 4.4*. Three distinct regimes are commonly observed:

i) The first is a micro-ductile regime, associated with a permanent groove and the potential formation of lateral cracks beneath the surface, underneath the plastic track;

ii) The second, known as the micro-cracking regime, is characterized by significant damage from median cracks propagating deeply into the material, lateral cracks occurring beneath the indenter at a depth corresponding to the so-called plastic zone limit, radial cracks, and chipping originating from the intersection of lateral cracks;

iii) The third regime is a micro-abrasive regime, resulting in a significant amount of debris, with occasional small lateral cracks along the scratch track [189].

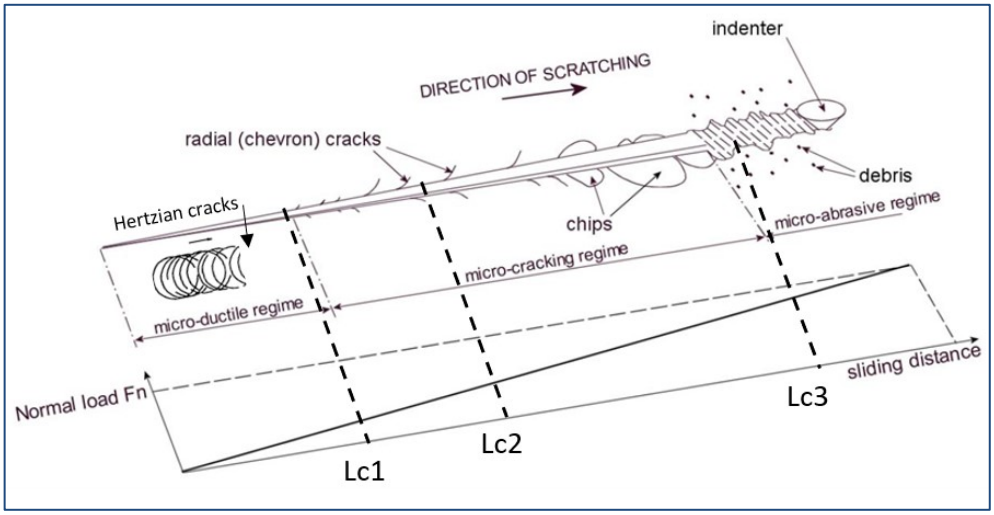

Figure 4.4 An example of typical signs of damage that occur on SLS glass after a scratch and the assignment of critical loads corresponding to some of these. Adapted from [190].

For the surface damage analysis, critical loads corresponding to each typical defect were identified and compared across the different samples. The first defects to appear are almost always Hertzian cracks, as defined by ASTM C1624-05 Standard; these initially form as small ring

cracks and progressively begin to interconnect. Subsequently, radial cracks, or so-called Chevron cracks, appear, oriented outward from the scratch. The interaction between these radial cracks and lateral cracks eventually leads to chipping, where smaller glass fragments break off in the immediate vicinity of the scratch [189], [190], [191]. Following this, fractures leading to the breakage of the glass occur, typically at higher loads. In some cases, subsurface lateral cracking phenomena appear either before or after the appearance of radial cracks and may be related to the cohesion of the surface layers. In this study, three critical loads (Lc) were identified: Lc1, corresponding to interconnected Hertzian cracks; Lc2, associated with radial cracks; and Lc3, indicating the onset of fractures. This latter critical load (Lc3) was assessed as the initiation point of crack propagation, where the reflection on the glass surface appeared as a halo, visible both internally and externally to the scratch.

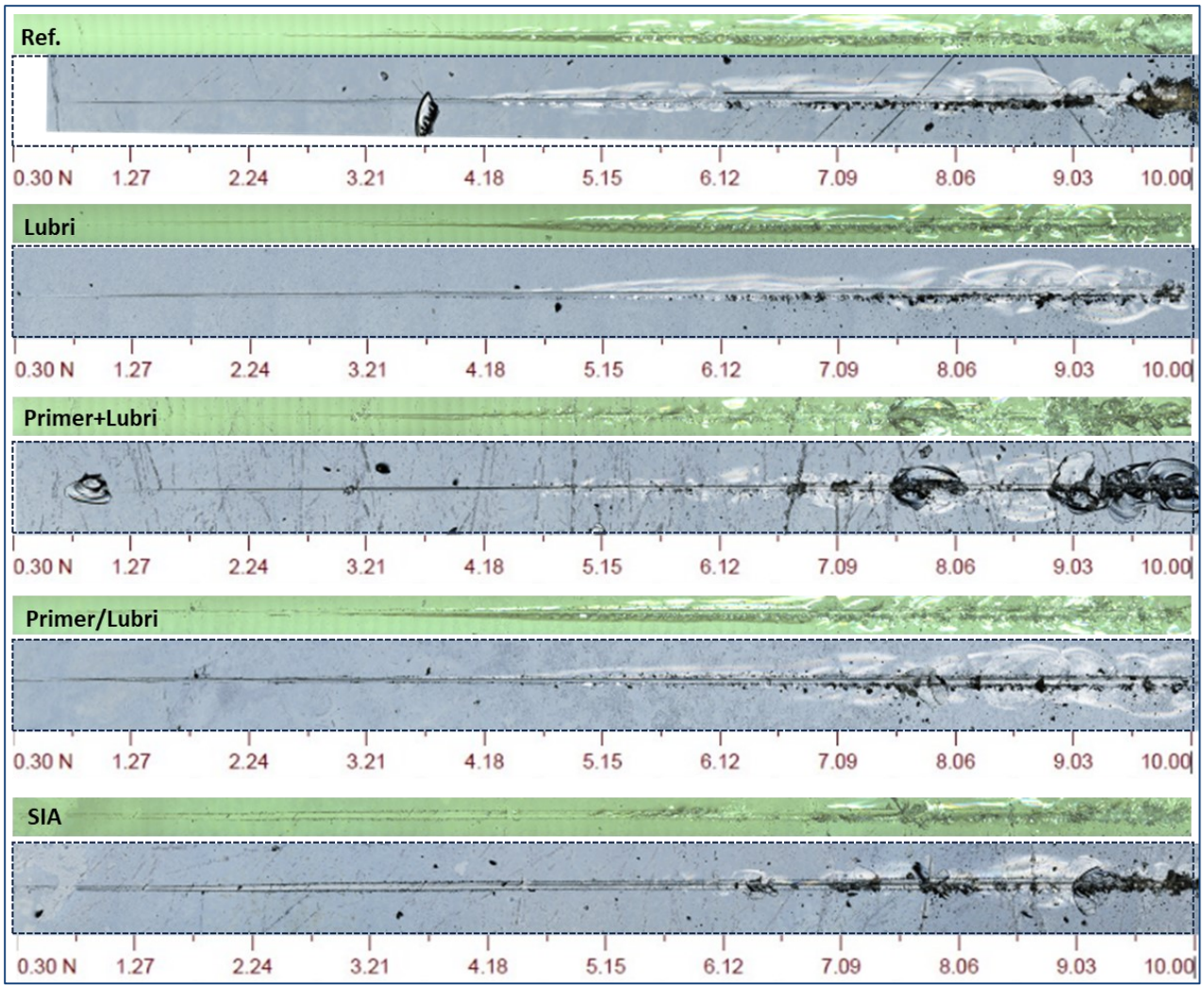

Figure 4.5 Images of scratches made on glass samples, from top to bottom: Reference sample, Lubri, Primer and Lubri, Primer/Lubri mix and SIA coated samples. For each sample, the panoramic image of the scratch (top in green) through the optical microscope integrated in the scratcher and the confocal image (bottom in black and white) acquired after several hours are shown.

The defect analysis was conducted based on microscopic observation of images captured immediately after scratching, using the light microscope objectives connected to scratch tester for initial imaging and subsequently observed with a confocal microscope, as shown in *Figure 4.5*. Confocal microscopy was particularly used for the assessment of Lc3; however, the general assignment of critical loads relied on scratch images that provided an instant capture of surface damage. Indeed, as documented in the literature [192], a reorganization of the scratch pattern may occur after several hours.

For each sample and each of the three scratch tests performed, the values of Lc1, Lc2, and Lc3 were assigned, as reported in the *Table 5*.

Table 5. Damage assessment by assigning critical loads, Lc1 – Lc2 – Lc3, to the different damage marks on each scratch track per Sample.

Figure 4.6 Schematic view of the 3 scratches applied on the same sample spaced approximately 3 mm apart, approximately.

Sample	Scratch n°	Lc1 (N)	Lc2 (N)	Lc3 (N)
Ref.	1	2,5	4,18	4,66
Ref.	2	1,7	2,7	4,3
Ref.	3	3,3	5	7
Lubri	1	2,9	5,15	5,6
Lubri	2	1,75	3,2	5,2
Lubri	3	6	no	7,5
Primer+Lubri	1	3,2	4,3	6,12
Primer+Lubri	2	1,8	2,6	5
Primer+Lubri	3	3	4,8	6,5
Primer/Lubri	1	2,7	4,7	7
Primer/Lubri	2	2	3	5,6
Primer/Lubri	3	4,5	6,15	7
SIA	1	5	5,6	7,3
SIA	2	3	4	5,6
SIA	3	4,5	5,3	6,6

Not all scratch tests on the same sample showed reproducibility; in particular, the *scratch3-Ref*. and *scratch3-Lubri* tests were excluded from the calculation of the mean value, as they differed significantly from the first two tests and never reached the breaking point. In this case, it is assumed that the curvature of the sample prevented an optimal approach between the indenter tip and the sample surface, thus affecting the reliability of the results obtained.

Figures 4.7 - 4.11 show pictures illustrating the occurrence of various types of damage for scratch 1 of each sample.

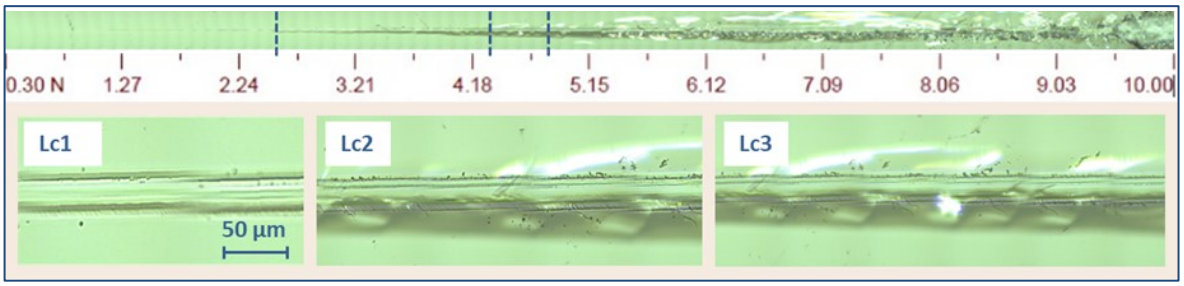

Figure 4.7. Panoramic view images of the scratch mark for the Reference sample and the assigned critical loads with dashed line (above), and enlargements of the points relating to the three critical loads (below), Lc1, Lc2 and Lc3 from left to right.

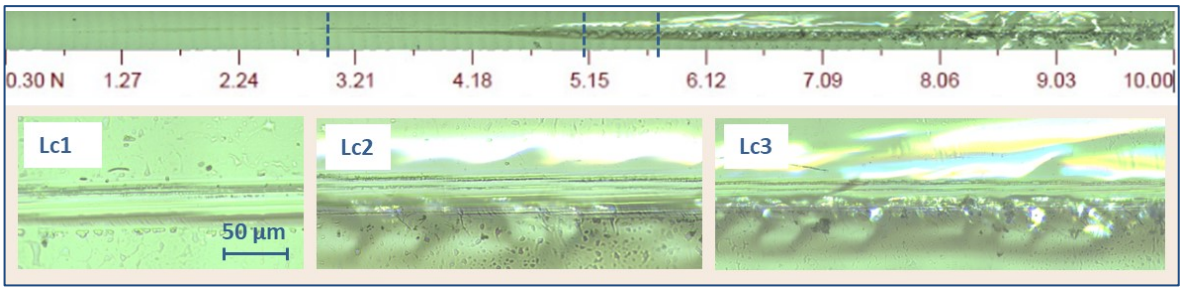

Figure 4.8 Lubri

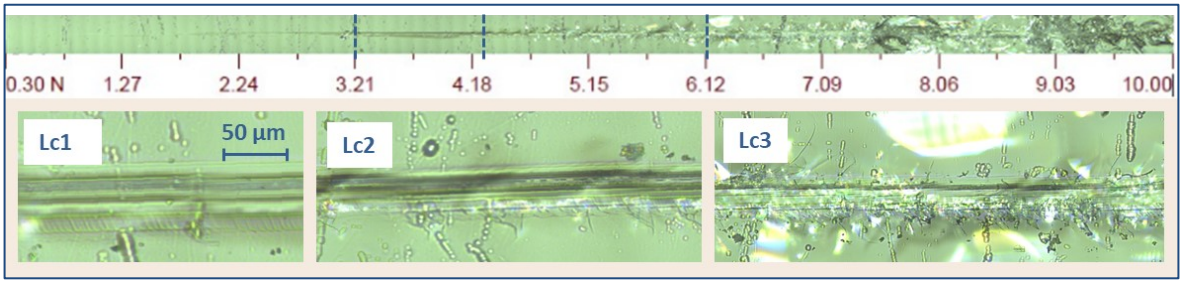

Figure 4.9 Primer+Lubri

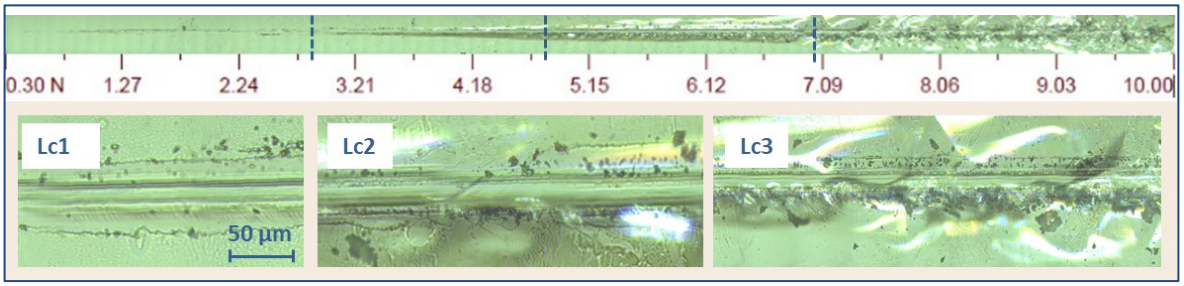

Figure 4.10 Primer/Lubri

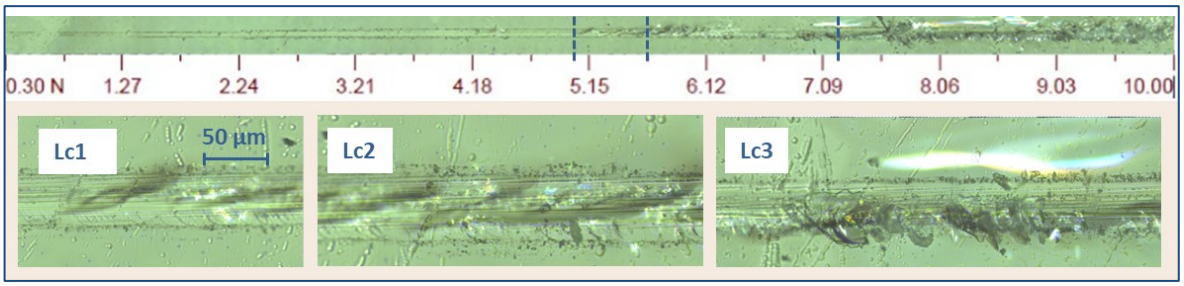

Figure 4.11 SIA

In general, it was observed that the presence of a surface lubricant coating resulted in the occurrence of damage at higher loads than uncoated glass (see *Figure 4.12*). This was particularly evident for Lc3, especially in the samples coated with a primer-lubricant mixture and with SIA, as shown in *Figure 4.12*, where this trend for the different types of surface damage is highlighted.

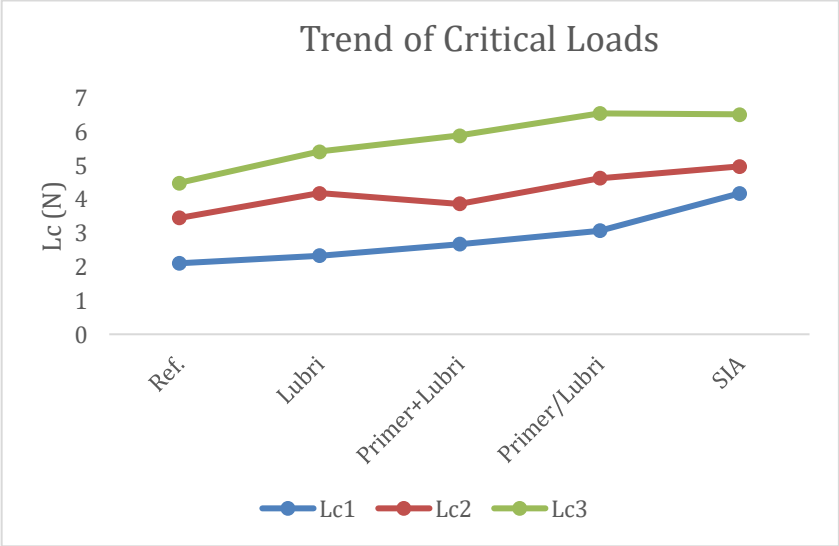

Figure 4.12 Trend Graph showing the average values for each sample of the critical loads, Lc1 - Lc2 - Lc3. These values are reported in Table 6 with standard deviations associated.

Table 6. Mean value and standard deviation of critical loads, Lc1 – Lc2 – Lc3, for the different Samples.

Samples	Lc1	Dev.st.	Lc2	Dev.st.	Lc3	Dev.st.
Ref.	2,1	0,57	3,4	1,17	4,5	1,47
Lubri	2,3	0,81	4,2	1,38	5,4	1,23
Primer+Lubri	2,7	0,76	3,9	1,15	5,9	0,78
Primer/Lubri	3,1	1,29	4,6	1,58	6,5	0,81
SIA	4,2	1,04	5,0	0,85	6,5	0,85

Based on the obtained results, we can state that in the presence of coatings, there is a protective effect on the glass surface when subjected to increasing loads. This is especially promising in the case of using the primer mixed with the lubricant and a coating with a single silane component, with industrial advantages over the process currently used in the factory.

4.2 Spray Deposition

4.2.1 Materials and Methods

Substrates: Soda-lime-silicate (SLS) glass pieces sourced from 500 mL vials produced by Bormioli Pharma S.p.A. The glass samples were prepared by cutting the vials into pieces approximately 2 cm x 2 cm in size.

Chemicals:

Amino propyl silsesquioxane (*Figure 3.1*), a commercial product purchased from Gelest - Mitsubishi Chemical Group, was used as the silane primer in aqueous solution. As a lubricant, a macrogol stearate - a mixture of mono- and di-esters of stearic and/or palmitic acid with macrogol (*Figure 3.2*), was employed in aqueous solution. The commercial name of the lubricant is omitted for confidentiality reasons.

4.2.1.1 Coatings Deposition

The coatings were deposited using an automatic spraying system under controlled conditions as showed in *Figure 4.13*. The glass substrates were placed on a heated platform, with the temperature maintained between 80°C and 120°C to facilitate uniform deposition. The spray gun was aligned perpendicularly (90°) to the substrate surface and operated at an air pressure of 0.6 bar. A flow rate of 20 ml/h was used to apply the solution to a target area of 2 cm^2 on each

substrate. To ensure uniform coverage, the spray gun moved back and forth over the substrate at a speed of 300 mm/min for a total of three passes, maintaining a fixed distance of 40 mm between the nozzle and the substrate. This configuration allowed the formation of a uniform and transparent layer on the glass surface, contributing to the reproducible deposition of the coating.

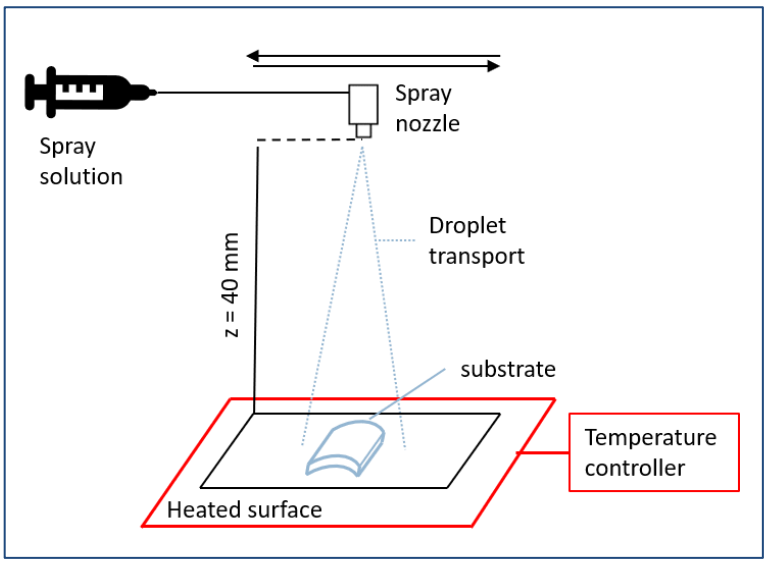

Figure 4.13 Schematic view of the spray deposition setup.

In this study, surface activation was intentionally omitted to replicate the industrial coating process, relying instead on heating the spray system platform to facilitate solvent evaporation, act as a curing step and promote condensation of organosilanes on the glass surface. Sample preparation consisted solely of a chemical cleaning procedure with sonication in deionised water, acetone and isopropanol to ensure a clean surface prior to coating.

Table 7 summarises the sample preparation steps using different coating solutions. For comparison, a sample was prepared by applying only the lubricant, which was deposited on a heated glass substrate following the established industrial protocol. In addition, a solution combining aminosilane primer and lubricant was tested to assess the feasibility of a one-step deposition process. Uncoated glass samples were included as a reference to evaluate the effect of coatings on surface properties.

Table 7. Description of samples prepared by spray system.

Sample	Pre-treatment	Silane	Lubricant
Primer+Lubri		Aminosilane 0.5% in water	yes
Primer/Lubri		Aminosilane 0.5%/Lubricant 0.1% in water	
Lubri		Lubricant 0.1% in aqueous solution	yes
Ref.		Uncoated	

4.2.2 Results and Discussion

4.2.2.1 XPS Analysis

XPS analysis was conducted to confirm the presence of the primer coating. To this purpose, we acquired and compared the survey spectra of the uncoated reference glass sample with those of the primer-coated glass. As shown in *Figure 4.15* the coated glass sample has distinct carbon and nitrogen peaks associated with the presence of aminosilane, which are absent in the investigation spectra of the uncoated sample (*Fig. 4.14*). Furthermore, in the spectra of the coated glass sample, some substrate elements, such as sodium (Na) and calcium (Ca), are still detectable, probably due to the deposition of a thin film. The results obtained on the flat slides (*Fig. 4.14 – 4.15* -right) are comparable to those obtained on the vial pieces (*Fig. 4.14 – 4.15*-left), and confirm the deposition on curved surfaces.

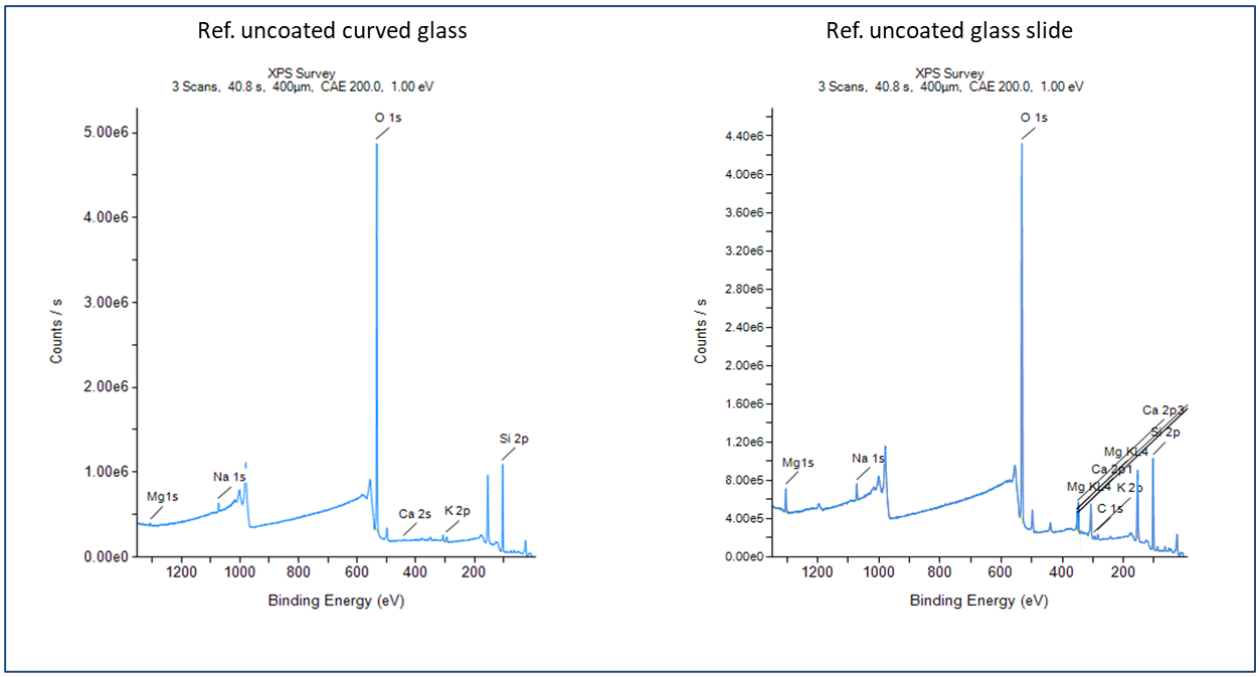

Figure 4.14 XPS survey spectra of Reference uncoated glass. On the left: curved pieces of glass vials samples; on the right: flat glass slide samples.

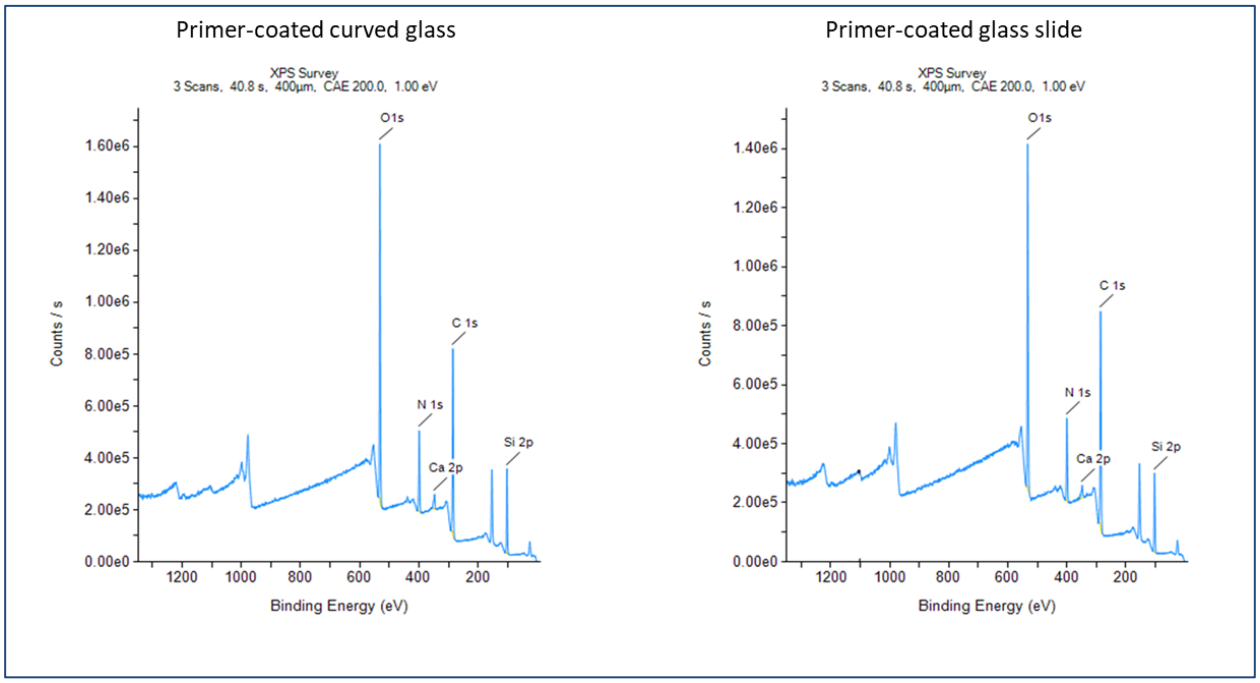

Figure 4.15 XPS survey spectra of primer-coated glass. On the left: curved pieces of glass vials samples; on the right: flat glass slide samples.

4.2.2.2 Tribological Analysis

Tribological tests were conducted to investigate the influence of surface coatings on the coefficient of friction (COF) in coated glass samples. The linear configuration of the test instrumentation allowed these measurements to be performed on curved pieces of glass vials. The results, presented in *Figure 4.16*, reveal distinct behavior between the various sample types.

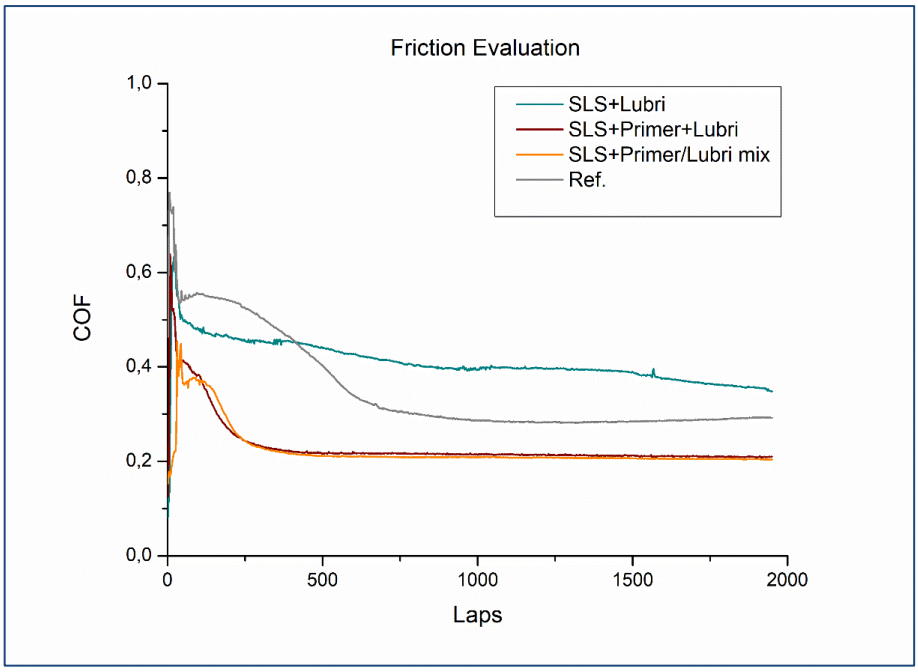

Figure 4.16 Representative curves of the COF evolution as a function of the number of Laps (2000). In grey the uncoated Ref. glass sample; in red the coated samples with primer and lubricant in sequence; in orange the coated sample with primer and lubricant in mixture; and in blue the coated sample with only lubricant.

The uncoated sample showed a high COF, indicating that, without coating, the reciprocal movement of the ceramic ball causes an increase in adhesion between the alumina ball and the glass, leading to high friction. In contrast, the Lubri-coated sample showed stabilisation with a similarly high COF, suggesting that the lubricating coating is not sufficient to reduce friction. This limitation probably stems from the inability of the lubricant to form a continuous lubricating film, resulting in persistent adhesion between the ball and the surface. In contrast, samples with Primer + Lubricants and Primer/Lubricants coatings showed the lowest COF values, confirming their effectiveness in reducing friction even under reciprocal motion conditions. This result can

be attributed to chemical interactions and optimised lubricant distribution, which contribute to the long-term stability of low-friction performance. Two primary mechanisms of COF reduction are likely at play: (i) adhesion reduction, in which the coating materials form both chemical and physical barriers on the glass surface, decreasing adhesion between the ceramic ball and the glass over time. The reciprocal movement favours the formation and distribution of lubricating layers, minimising adhesion on contact between the alumina sphere and the glass; (ii) surface smoothing, where the reciprocal movement of the sphere progressively 'smooths' surface irregularities, improving contact with the coating and further reducing friction. The observed reduction in COF over time suggests that thin lubricant coatings, in combination with reciprocal ball movement, are critical to improving the tribological performance of the system. Careful evaluation and optimisation of these coatings is essential to achieve optimal performance characteristics. The interaction between the movement of the alumina ceramic ball on the coated glass surface could facilitates a significant reduction in COF as investigated in some studies [193]. This movement favours the 'smoothing' of surface roughness, improving contact with the coating and creating a more stable lubricating film [54], which in turn reduces adhesive forces, enabling better sliding and reduced friction. Although this behavior is cited in some studies, in the specific case of this work further investigations are needed to support this hypothesis. Thin coatings, with their adhesion-reducing properties, also help optimise lubricant distribution, creating an ideal tribological environment for stable, long-term performance in tribological processes.

5. Conclusions and Future Perspectives

The pharmaceutical packaging industry faces a critical challenge in maintaining the strength and integrity of glass containers, which requires the application of coatings to ensure surface smoothness and functionality during production and filling processes. Current coating methods involve a two-stage process using a metal oxide primer and a lubricating layer, with the hot-end coating requiring specific equipment to handle toxic emissions. This PhD research, conducted in collaboration with Bormioli Pharma S.p.A., focuses on developing a sustainable alternative to the traditional hot-end coating. The study explores organosilane-based solutions, specifically aqueous-based aminosilanes as adhesion promoters and one-component organosilanes in water, aiming to achieve both environmental and economic advantages.

The study of the aminosilane primer coating, deposited using a dip-coating method, highlighted the importance of optimizing various deposition parameters to achieve strong mechanical performance of the final lubricating coating. In particular, for the primer coating, the rinsing step proved effective in removing physisorbed molecules, while low concentrations were found to be more effective for achieving uniform coverage of the glass substrate. Additionally, immersion time proved to be a critical factor in optimizing lubricant adhesion, with times of 30 and 120 minutes yielding the best results in terms of wear resistance and maintaining a low coefficient of friction (COF) under higher applied stress, as demonstrated by scratch testing in multipass mode. These results underscore the importance of the primer's structural network in effectively interacting with the lubricant, ultimately optimizing coating performance for industrial applications. Additional investigations are necessary to clarify whether the adhesion-promoting mechanism is driven by chemical bonding involving the amine functional groups in denser layers or by the formation of an interpenetrating network between the primer and polymer, facilitated by the gradual stratification of the siloxane network.

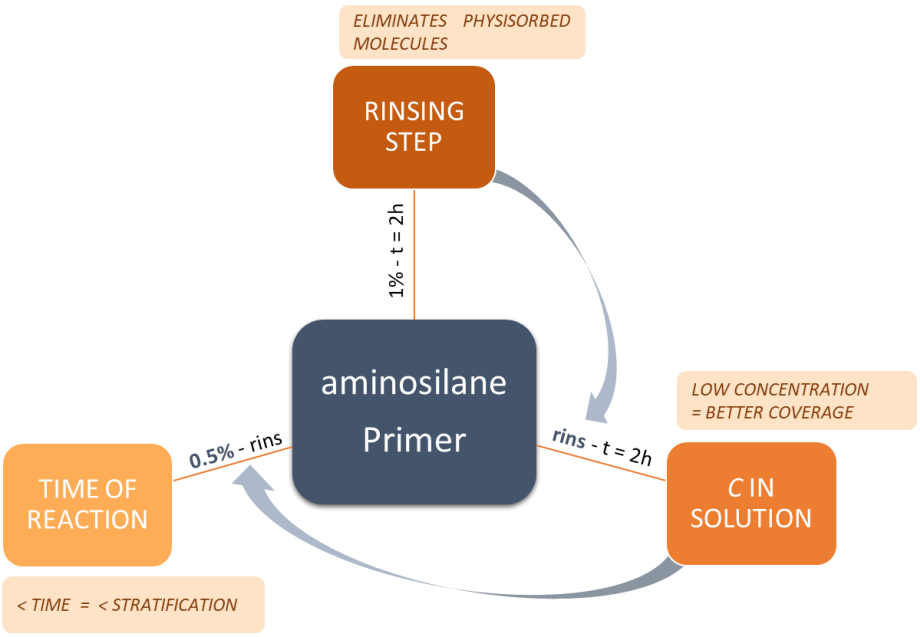

The study of coatings applied using spray techniques confirmed the feasibility of this method, which aligns with the intended industrial application on production lines for vial manufacturing. Mechanical analyses, including scratch and tribology tests, demonstrated the effectiveness of sprayed coatings in both abrasion protection and friction coefficient reduction. Additionally, the results highlighted the potential for a one-step deposition process, where the aminosilane primer can be mixed directly with the lubricant. This approach simplifies application and reinforces the industrial scalability of the coating process, offering a practical and efficient solution for large-scale implementation.

The investigation of the organosilane (SIA), applied via both dip and spray methods as a potential one-component coating, demonstrated promising scratch protection in mechanical scratch tests, although the sliding angle measurements were marginally below industrial acceptability criteria. Further studies are certainly needed; however, this research paves the way for the advantageous possibility of using a single molecule that provides both covalent adhesion to the glass substrate and surface lubrication functionality. This dual capability could simplify the coating process, representing a significant advancement toward more efficient and scalable coating solutions in industrial applications.

Overall, replacing the traditional hot-end process with a silane-based primer offers several industrial advantages. Firstly, it enables a more sustainable alternative to the hot-end coating by using an aqueous primer with low VOC content, without supplementary equipment needed for the toxic releases in the case of tin oxide primer deposition, which can be applied in a single step alongside the lubricant. This innovative approach not only reduces the environmental impact but also lowers production costs for pharmaceutical vials. Importantly, it allows for the elimination of the hot-end coating step without requiring a change in the currently used lubricant, which is pharmacopeia-approved and safe. This solution thus meets both regulatory and operational requirements, supporting a streamlined, cost-effective, and environmentally friendly coating process suitable for large-scale pharmaceutical production.

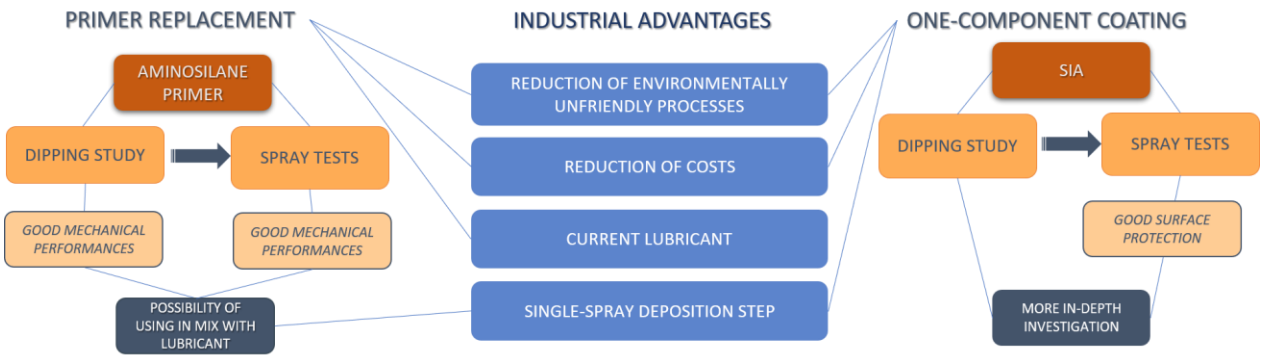

Future research will focus on a deeper investigation of the molecular interaction between primer and lubricant and of the functionality of one-component lubrication through the exploration of additional organosilane solutions. Additionally, efforts will be directed toward refining mechanical testing methods to more accurately simulate the movement of vials on production and filling lines. The tribological behavior of these systems is complex, as it depends not only on the surface properties of the coating but also on the specific instrumental configuration used for analysis. A key future objective is to establish a standardized approach for analysing the tribological behavior of vials moving along production lines. Standardizing this method would

provide a more precise tool not only for research in this field but also for quality control at an industrial level, ensuring consistent performance and reliability across production batches. We finally recall that this activity has been carried out in the framework of the IMEM-Bormioli Pharma joint laboratory and that the promising results obtained in this work have led to further invest in this laboratory that now is equipped with a nano-mechanical tester, a tilting table and a customized spray coating device at laboratory scale.

Bibliography

[1] R. A. Schaut and W. P. Weeks, 'Historical Review of Glasses Used for Parenteral Packaging', *PDA J. Pharm. Sci. Technol.*, vol. 71, no. 4, pp. 279–296, 2017, doi: 10.5731/pdajpst.2016.007377.

[2] Kuehn, S. E., 'Clash of the Titans: Super-Rivals Glass and Plastic Square Off for Patient Safety', *Pharmaceutical Manufacturing*, pp. 3–9, 2014.

[3] *The National Formulary.American Pharmaceutical Association.*, vol. IV. Washington, DC: American Pharmaceutical Association, 1916.

[4] E. Guadagnino, M. Guglielmi, and F. Nicoletti, 'Glass: The best material for pharmaceutical packaging', *Int. J. Appl. Glass Sci.*, vol. 13, no. 3, pp. 281–291, Jul. 2022, doi: 10.1111/ijag.16559.

[5] R. A. Schaut, K. C. Hoff, S. E. Demartino, W. K. Denson, and R. L. Verkleeren, 'Enhancing Patient Safety through the Use of a Pharmaceutical Glass Designed To Prevent Cracked Containers', *PDA J. Pharm. Sci. Technol.*, vol. 71, no. 6, pp. 511–528, 2017, doi: 10.5731/pdajpst.2017.007807.

[6] Robert Swift, *Pharmaceutical Dosage Forms - Parenteral Medications. Chapter: Glass containers for parenteral products.*, 3rd ed., vol. 1 Formulation and Packaging. Boca Raton: Sandeep Nema, John D. Ludwig, 2010.

[7] A. K. Varshneya and J. C. Mauro, 'Chapter 1 - Introduction', in *Fundamentals of Inorganic Glasses (Third Edition)*, Third Edition., A. K. Varshneya and J. C. Mauro, Eds., Elsevier, 2019, pp. 1–18. doi: https://doi.org/10.1016/B978-0-12-816225-5.00001-8.

[8] A. K. Varshneya and J. C. Mauro, 'Chapter 2 - Fundamentals of the glassy state', in *Fundamentals of Inorganic Glasses (Third Edition)*, Third Edition., A. K. Varshneya and J. C. Mauro, Eds., Elsevier, 2019, p. 15. doi: https://doi.org/10.1016/B978-0-12-816225-5.00002-X.

[9] G. Sacha, W. Clemmer, K. Abram, and M. Akers, 'Practical fundamentals of glass, rubber, and plastic sterile packaging systems', *Pharm. Dev. Technol.*, vol. 15, pp. 6–34, Feb. 2010, doi: 10.3109/10837450903511178.

[10] G. Scarinci, T. Toninato, and B. Locardi, *Vetri*, vol. Capitolo 1. in Quaderni di chemica applicata, vol. Capitolo 1. Casa editrice ambrosiana, 1977. [Online]. Available: https://books.google.it/books?id=hnJ0GwAACAAJ

[11] Dr. Juliane Brandt-Slowik, SCHOTT Technical Glass Solutions Jena, Germany, 'Structure-property correlations in borosilicate in comparison to soda-lime glass.', presented at the GPD 2023, [Online]. Available: glassonweb.com/article/structure property-correlations-borosilicate-comparison-soda-lime-glass.

[12] S. A. Pillai, D. Chobisa, D. Urimi, and N. Ravindra, 'Pharmaceutical Glass Interactions: A Review of Possibilities', *J Pharm Sci*, vol. 8, 2016.

[13] R. D. Ennis *et al.*, 'Glass Vials for Small Volume Parenterals: Influence of Drug and Manufacturing Processes on Glass Delamination', *Pharm. Dev. Technol.*, vol. 6, no. 3, pp. 393–405, Jan. 2001, doi: 10.1081/PDT-100002248.

[14] R. G. Iacocca *et al.*, 'Factors Affecting the Chemical Durability of Glass Used in the Pharmaceutical Industry', *AAPS PharmSciTech*, vol. 11, no. 3, pp. 1340–1349, Sep. 2010, doi: 10.1208/s12249-010-9506-9.

[15] J. E. Lee, E. Kim, J. B. Hwang, J. C. Choi, and J. K. Lee, 'Flake formation and composition in soda-lime-silica and borosilicate glasses', *Heliyon*, vol. 9, no. 6, p. e16333, Jun. 2023, doi: 10.1016/j.heliyon.2023.e16333.

[16] 'Assessment of drug product leachables associated with packaging/delivery systems.', presented at the USP-NF, United States Pharmacopeia (2023), Rockville, MD, 2020. doi: doi.org/10.31003/USPNF_M7127_02_01.

[17] V. Dimbleby, 'GLASS FOR PHARMACEUTICAL PURPOSES', *J. Pharm. Pharmacol.*, vol. 5, no. 1, pp. 969–989, 1953, doi: https://doi.org/10.1111/j.2042-7158.1953.tb14064.x.

[18] L. Lachman, H. A. Lieberman, and J. L. Kanig, *The Theory and Practice of Industrial Pharmacy*. Lippincott Williams & Wilkins, 1986. [Online]. Available: https://books.google.it/books?id=p_VsAAAAMAAJ

[19] F. R. Bacon and O. G. Burch, 'EFFECT OF TIME AND TEMPERATURE ON ACCELERATED CHEMICAL DURABILITY TESTS MADE ON COMMERCIAL GLASS BOTTLES', *J. Am. Ceram. Soc.*, vol. 23, no. 1, pp. 1–9, 1940, doi: https://doi.org/10.1111/j.1151-2916.1940.tb14184.x.

[20] Haines, D. et al., 'Glass Delamination Mechanisms: An Update.', presented at the PDA/FDA Glass Quality Conference, Washington DC, 2012.

[21] V. Rupertus, B. Hladik, U. Rothhaar, and V. Scheumann, 'A Quick Test To Monitor the Delamination Propensity of Glass Containers', *PDA J. Pharm. Sci. Technol. PDA*, vol. 68, pp. 373–80, Jul. 2014, doi: 10.5731/pdajpst.2014.00990.

[22] T. J. Roseman, J. A. Brown, and W. W. Scothorn, 'Glass for Parenteral Products: A Surface View Using the Scanning Electron Microscope', *J. Pharm. Sci.*, vol. 65, no. 1, pp. 22–29, 1976, doi: https://doi.org/10.1002/jps.2600650103.

[23] E. Guadagnino and D. Zuccato, 'Delamination Propensity of Pharmaceutical Glass Containers by Accelerated Testing with Different Extraction Media', *PDA J. Pharm. Sci. Technol.*, vol. 66, pp. 116–125, 2012.

[24] Sanga S. V., 'Review of glass types available for packaging parenteral solutions.', *Journal of the Parenteral Drug Association*, vol. 33(2), pp. 61–67, 1979.

[25] M. Guglielmi *et al.*, 'Laboratory intercomparison for the evaluation of the delamination propensity of glass containers for pharmaceutical use', *Int. J. Appl. Glass Sci.*, vol. 12, no. 1, pp. 135–144, 2021, doi: https://doi.org/10.1111/ijag.15795.

[26] 'PDA Technical Report 43. Identification and Classification of Nonconformities in Molded and Tubular Glass Containers for Pharmaceutical Manufacturing: Covering Ampoules, Bottles, Cartridges, Syringes and Vials.', presented at the Parenteral Drug Association, Bethesda, MD, 2013.

[27] '<1207> Package Integrity Evaluation—Sterile Products.', presented at the The United States Pharmacopeia Thirty-ninth Revision; USP Committee of Revision, U.S. Pharmacopeial Convention, Rockville, MD, 2016, pp. 7764–7772. [Online]. Available: https://doi.usp.org/USPNF/USPNF_M99926_01_01.html

[28] S. Bhakdi, I. Krämer, E. Siegel, B. Jansen, and M. Exner, 'Use of quantitative microbiological analyses to trace origin of contamination of parenteral nutrition solutions', *Med. Microbiol. Immunol. (Berl.)*, vol. 201, pp. 231–237, 2012.

[29] K. Marsh and B. Bugusu, 'Food Packaging?Roles, Materials, and Environmental Issues', *J. Food Sci.*, vol. 72, pp. R39-55, May 2007, doi: 10.1111/j.1750-3841.2007.00301.x.

[30] T. Gallucci, G. Lagioia, P. Piccinno, A. Lacalamita, A. Pontrandolfo, and A. Paiano, 'Environmental performance scenarios in the production of hollow glass containers for food packaging: an LCA approach', *Int. J. Life Cycle Assess.*, vol. 26, no. 4, pp. 785–798, Apr. 2021, doi: 10.1007/s11367-020-01797-7.

[31] S. Balzarotti, B. Maviglia, F. Biassoni, and M. R. Ciceri, 'Glass vs. Plastic: Affective Judgments of Food Packages After Visual and Haptic Exploration', *Procedia Manuf.*, vol. 3, pp. 2251–2258, 2015, doi: 10.1016/j.promfg.2015.07.369.

[32] F. Welle, 'Twenty years of PET bottle to bottle recycling—An overview', *Resour. Conserv. Recycl.*, vol. 55, no. 11, pp. 865–875, 2011, doi: https://doi.org/10.1016/j.resconrec.2011.04.009.

[33] Technavio Research Institute, 'Pharmaceutical Glass Packaging Market Analysis North America, APAC, Europe, South America, Middle East and Africa - US, Russia, China, UK, India - Size and Forecast 2024-2028.', p. 176, May 2024.

[34] A. Singh, P. K. Sharma, and R. Malviya, 'Eco Friendly Pharmaceutical Packaging Material', 2011.

[35] 'Reusable glass packaging As an inert and robust material, glass is particularly suitable for reuse. This promising decarbonisation lever is a key element of Verallia's strategy', [Online]. Available: https://fr.verallia.com/s/reemploi-emballage?language=en_US

[36] R. Stefanini, G. Borghesi, A. Ronzano, and G. Vignali, 'Plastic or glass: a new environmental assessment with a marine litter indicator for the comparison of pasteurized milk bottles', *Int. J. Life Cycle Assess.*, vol. 26, no. 4, pp. 767–784, Apr. 2021, doi: 10.1007/s11367-020-01804-x.

[37] S. A. Wang *et al.*, 'Enterobacter cloacae Bloodstream Infections Traced to Contaminated Human Albumin', *Clin. Infect. Dis.*, vol. 30, no. 1, pp. 35–40, Jan. 2000, doi: 10.1086/313585.

[38] N. Jackson and J. Ford, 'Experience in the control and evaluation of coatings on glass containers', *Thin Solid Films*, vol. 77, no. 1–3, pp. 23–40, Mar. 1981, doi: 10.1016/0040-6090(81)90357-6.

[39] A. A. Griffith and G. I. Taylor, 'VI. The phenomena of rupture and flow in solids', *Philos. Trans. R. Soc. Lond. Ser. Contain. Pap. Math. Phys. Character*, vol. 221, no. 582–593, pp. 163–198, 1921, doi: 10.1098/rsta.1921.0006.

[40] A. K. Varshneya and J. C. Mauro, 'Strength and toughness', in *Fundamentals of Inorganic Glasses*, Elsevier, 2019, pp. 487–535. doi: 10.1016/B978-0-12-816225-5.00018-3.

[41] 'Piattaforma EZ-fill®' [Online]. Available: https://www.stevanatogroup.com/it/offerta/packaging-primario-in-vetro/piattaforma-ez-fill/

[42] R. Gardon, 'Thermal Tempering of Glass', *Glass Sci. Technol.*, vol. 5, pp. 145–216, 1980.

[43] R. Tandon and S. Glass, 'Controlling the Fragmentation Behavior of Stressed Glass', in *Fracture Mech. Ceram.*, vol. 14, 2005, pp. 77–91. doi: 10.1007/978-0-387-28920-5_7.

[44] R. Gy, 'Ion Exchange for Glass Strengthening', *Mater. Sci. Eng. B*, vol. 149, pp. 159–165, Mar. 2008, doi: 10.1016/j.mseb.2007.11.029.

[45] D. Green, '64th Conference on Glass Problems: Ceramic Engineering and Science Proceedings, Volume 25, Issue 1', in *Ceramic Engineering and Science Proceedings*, vol. 25, 2008, pp. 253–266. doi: 10.1002/9780470294857.ch20.

[46] R. V. Ramaswamy and R. Srivastava, 'Ion-exchanged glass waveguides: a review', *J. Light. Technol.*, vol. 6, no. 6, pp. 984–1000, 1988, doi: 10.1109/50.4090.

[47] A. K. Varshneya and J. C. Mauro, 'Chapter 14 - Permeation, diffusion, and ionic conduction in glass', in *Fundamentals of Inorganic Glasses (Third Edition)*, Third Edition., A. K. Varshneya and J. C. Mauro, Eds., Elsevier, 2019, pp. 383–424. doi: https://doi.org/10.1016/B978-0-12-816225-5.00014-6.

[48] A. Varshneya, 'Chemical Strengthening of Glass: Lessons Learned and Yet To Be Learned', *Int. J. Appl. Glass Sci.*, vol. 1, pp. 131–142, Mar. 2010, doi: 10.1111/j.2041-1294.2010.00010.x.

[49] G. Pintori and V. M. Sglavo, 'Electric-field assisted ion-exchange of innovative float glass', *J. Non-Cryst. Solids*, vol. 600, p. 121994, 2023, doi: https://doi.org/10.1016/j.jnoncrysol.2022.121994.

[50] G. L. Smay, 'Interactions of organic coatings with metal oxide coatings and glass surfaces', *Glass Technol.*, vol. 26, pp. 46–59, 1985.

[51] S. M. Budd, 'Abrasion-resistant coatings for use on returnable glass containers', *Thin Solid Films*, vol. 77, no. 1–3, pp. 13–20, Mar. 1981, doi: 10.1016/0040-6090(81)90355-2.

[52] R. D. Southwick, J. S. Wasylyk, G. L. Smay, J. B. Kepple, E. C. Smith, and B. O. Augustsson, 'The mechanical properties of films for the protection of glass surfaces', *Thin Solid Films*, vol. 77, no. 1–3, pp. 41–50, Mar. 1981, doi: 10.1016/0040-6090(81)90358-8.

[53] A. Bhargava, F. Wang, B. Wood, G. Higginbotham, and I. Gentle, 'Studies of polyethylene-coated tin oxide films on glass bottles', *Surf. Interface Anal.*, vol. 29, no. 10, pp. 663–670, Oct. 2000, doi: 10.1002/1096-9918(200010)29:10<663::AID-SIA919>3.0.CO;2-A.

[54] M. Beauvais *et al.*, 'Film formation mechanism in glass lubrication by polymer latex dispersions', *Thin Solid Films*, vol. 518, no. 6, pp. 1689–1697, Jan. 2010, doi: 10.1016/j.tsf.2009.11.061.

[55] J. C. Manifacier, 'Thin metallic oxides as transparent conductors', *Thin Solid Films*, vol. 90, no. 3, pp. 297–308, 1982, doi: https://doi.org/10.1016/0040-6090(82)90381-9.

[56] Dawar, A.L., Joshi, J.C., 'Semiconducting transparent thin films: their properties and applications.', *J Mater Sci*, vol. 19, pp. 1–23, 1984, doi: https://doi.org/10.1007/BF00552989.

[57] A. M. B. van Mol, Y. Chae, A. H. McDaniel, and M. D. Allendorf, 'Chemical vapor deposition of tin oxide: Fundamentals and applications', *Thin Solid Films*, vol. 502, no. 1, pp. 72–78, 2006, doi: https://doi.org/10.1016/j.tsf.2005.07.247.

[58] S.-M. Lee, D.-L. Kim, H.-J. Youn, and K. S. Hong, 'Tin Oxide Films by Chemical Vapor Deposition Using a Monobutyltin Trichloride Source: The Effect of H2O on Deposition Behavior and Electrical Properties', *Jpn. J. Appl. Phys.*, vol. 39, no. 2R, p. 407, Feb. 2000, doi: 10.1143/JJAP.39.407.

[59] J. D. J. Jackson, B. Rand, and H. Rawson, 'Glass surface coatings resistant to mechanical damage', *Thin Solid Films*, vol. 77, no. 1, pp. 5–12, 1981, doi: https://doi.org/10.1016/0040-6090(81)90354-0.

[60] J. Giersberg, G. Eisen, P. Marchesi Elf Atochem, Dusseldorf, (Germany), 'The CERTINCOAT and TEGOGLAS SYSTEM for the protection of glass bottles and containers'', *International Glass Journal*, p. 104, 1999.

[61] G. L. Smay, 'Surface-Energy Determinations of Tin Oxide-Coated Soda–Lime–Silica Glass', *J. Am. Ceram. Soc.*, vol. 71, no. 4, p. C-217-C-219, 1988, doi: https://doi.org/10.1111/j.1151-2916.1988.tb05882.x.

[62] H. De Waal, 'Pointers for research and development in the glass container industry', *J. Non-Cryst. Solids*, vol. 87, no. 3, pp. 366–375, Nov. 1986, doi: 10.1016/S0022-3093(86)80010-2.

[63] P. G. Pape, 'Adhesion Promoters: Silane Coupling Agents', in *Applied Plastics Engineering Handbook*, Elsevier, 2017, pp. 555–572. doi: 10.1016/B978-0-323-39040-8.00026-2.

[64] G. L. Witucki, 'A Silane Primer: Chemistry and Applications of AIkoxy Silanes'.

[65] K. Glosz, A. Stolarczyk, and T. Jarosz, 'Siloxanes—versatile materials for surface functionalisation and graft copolymers', *Int. J. Mol. Sci.*, vol. 21, no. 17, pp. 1–21, 2020, doi: 10.3390/ijms21176387.

[66] P. G. Pape, 'Adhesion Promoters', in *Applied Plastics Engineering Handbook*, Elsevier, 2011, pp. 503–517. doi: 10.1016/B978-1-4377-3514-7.10029-7.

[67] M.-L. Abel, 'Organosilanes: Adhesion Promoters and Primers', in *Handbook of Adhesion Technology*, L. F. M. da Silva, A. Öchsner, and R. D. Adams, Eds., Berlin, Heidelberg: Springer Berlin Heidelberg, 2011, pp. 237–258. doi: 10.1007/978-3-642-01169-6_11.

[68] H. H. Nguyen, A. K. Tieu, S. Wan, H. Zhu, S. T. Pham, and B. Johnston, 'Surface characteristics and wettability of superhydrophobic silanized inorganic glass coating surfaces textured with a picosecond laser', *Appl. Surf. Sci.*, vol. 537, no. May 2020, p. 147808, 2021, doi: 10.1016/j.apsusc.2020.147808.

[69] H. Yan, W. Yuanhao, and Y. Hongxing, 'TEOS/silane coupling agent composed double layers structure: A novel super-hydrophilic coating with controllable water contact angle value', *Appl. Energy*, vol. 185, pp. 2209–2216, 2017, doi: 10.1016/j.apenergy.2015.09.097.

[70] S. Sriram, R. K. Singh, and A. Kumar, 'Silica and Silane based polymer composite coating on glass slide by dip- Coating Method', *Surf. Interfaces*, vol. 19, no. November 2019, p. 100472, 2020, doi: 10.1016/j.surfin.2020.100472.

[71] T. Dey and D. Naughton, 'Cleaning and anti-reflective (AR) hydrophobic coating of glass surface: a review from materials science perspective', *J. Sol-Gel Sci. Technol.*, vol. 77, no. 1, pp. 1–27, 2016, doi: 10.1007/s10971-015-3879-x.

[72] K. Pacaphol and D. Aht-Ong, 'The influences of silanes on interfacial adhesion and surface properties of nanocellulose film coating on glass and aluminum substrates', *Surf. Coat. Technol.*, vol. 320, pp. 70–81, 2017, doi: 10.1016/j.surfcoat.2017.01.111.

[73] R. J. Hand, B. Ellis, B. R. Whittle, and F. H. Wang, 'Epoxy based coatings on glass: Strengthening mechanisms', *J. Non-Cryst. Solids*, vol. 315, no. 3, pp. 276–287, 2003, doi: 10.1016/S0022-3093(02)01611-3.

[74] R. J. Hand, F. H. Wang, B. Ellis, and A. B. Seddon, 'Glass Strengthening Using Ormosil Polymeric Coatings', *J. Sol-Gel Sci. Technol.*, vol. 13, no. 1–3, pp. 695–699, 1998, doi: 10.1023/a:1008692922196.

[75] R. Briard, C. Heitz, and E. Barthel, 'Crack bridging mechanism for glass strengthening by organosilane water-based coatings', *J. Non-Cryst. Solids*, vol. 351, no. 4, pp. 323–330, 2005, doi: 10.1016/j.jnoncrysol.2004.11.004.

[76] G. Mariggiò, S. Dalle Vacche, R. Bongiovanni, C. Louter, and M. Corrado, 'Enhancing the design bending strength of new and aged glass with a functional coating', *Glass Struct. Eng.*, vol. 5, no. 2, pp. 135–146, 2020, doi: 10.1007/s40940-019-00114-5.

[77] G. Mariggiò, S. Dalle Vacche, R. Bongiovanni, C. Louter, and M. Corrado, 'A durable coating to prevent stress corrosion effects on the surface strength of annealed glass', *Glass Struct. Eng.*, no. Grenet 1899, 2021, doi: 10.1007/s40940-021-00161-x.

[78] W. Pathanatecha, 'A Study of Various Parameters Affecting Adhesion of Coatings to Metal Substrates'.

[79] R. L. De Rosa and S. R. Wagner, 'Scratch resistant polyimide coatings for aluminosilicate glass surfaces', *J. Adhes.*, vol. 78, no. 2, pp. 113–127, Feb. 2002, doi: 10.1080/00218460210385.

[80] B. I. Johnson, C. V. Cushman, B. M. Lunt, M. Kaykhaii, and M. R. Linford, 'https://www.researchgate.net/publication/303486340_An_Introduction_to_Silanes_their_Chemical_Vapor_Deposition_onto_SiSiO2_and_Characterization_of_the_Resulting_Monolayers', *Vac. Technol. Coat.*, no. June, pp. 1–9, 2016.

[81] W. M. Munief *et al.*, 'Silane Deposition via Gas-Phase Evaporation and High-Resolution Surface Characterization of the Ultrathin Siloxane Coatings', *Langmuir*, vol. 34, no. 35, pp. 10217–10229, 2018, doi: 10.1021/acs.langmuir.8b01044.

[82] W. Wang and M. W. Vaughn, 'Morphology and amine accessibility of (3-aminopropyl) triethoxysilane films on glass surfaces', *Scanning*, vol. 30, no. 2, pp. 65–77, 2008, doi: 10.1002/sca.20097.

[83] H. Y. Park, D. P. Kang, M. K. Na, H. W. Lee, H. H. Lee, and D. S. Shin, 'Characteristics of organic-inorganic hybrid coating films synthesized from colloidal silica-silane sol', *J. Electroceramics*, vol. 22, no. 1–3, pp. 309–314, 2009, doi: 10.1007/s10832-007-9355-4.

[84] M. Y. Tsai, C. C. Hsu, P. H. Chen, C. S. Lin, and A. Chen, 'Surface modification on a glass surface with a combination technique of sol-gel and air brushing processes', *Appl. Surf. Sci.*, vol. 257, no. 20, pp. 8640–8646, 2011, doi: 10.1016/j.apsusc.2011.05.041.

[85] J. Kron, G. Schottner, and K. J. Deichmann, 'Glass design via hybrid sol-gel materials', *Thin Solid Films*, vol. 392, no. 2, pp. 236–242, 2001, doi: 10.1016/S0040-6090(01)01034-3.

[86] Gelest, 'What is a Silane Coupling Agent?', *Technical Brochure*, [Online]. Available: https://technical.gelest.com/brochures/silane-coupling-agent/what-is-a-silane-coupling-agent/

[87] L. F. M. Da Silva, A. Öchsner, and R. D. Adams, Eds., *Handbook of Adhesion Technology*. Berlin, Heidelberg: Springer Berlin Heidelberg, 2011. doi: 10.1007/978-3-642-01169-6.

[88] Gelest, 'How Does a Silane Coupling Agent Work?', *Technical Brochure*, [Online]. Available: https://technical.gelest.com/brochures/silane-coupling-agent/my-test-section-3/

[89] R. M. Pasternack, S. Rivillon Amy, and Y. J. Chabal, 'Attachment of 3-(Aminopropyl)triethoxysilane on Silicon Oxide Surfaces: Dependence on Solution Temperature', *Langmuir*, vol. 24, no. 22, pp. 12963–12971, Nov. 2008, doi: 10.1021/la8024827.

[90] J. Huser, S. Bistac, M. Brogly, C. Delaite, T. Lasuye, and B. Stasik, 'Investigation on the Adsorption of Alkoxysilanes on Stainless Steel', *Appl. Spectrosc.*, vol. 67, no. 11, pp. 1308–1314, Nov. 2013, doi: 10.1366/13-07073.

[91] C. Cai, Z. Shen, S. Ma, and Y. Xing, 'Growth behavior and surface topography of different silane coupling agents adsorbed on the silicon dioxide substrate (0001) for vapor phase deposition', *J. Mater. Sci.*, vol. 42, no. 15, pp. 6108–6116, Aug. 2007, doi: 10.1007/s10853-006-1152-y.

[92] J. A. Howarter and J. P. Youngblood, 'Optimization of Silica Silanization by 3-Aminopropyltriethoxysilane', *Langmuir*, vol. 22, no. 26, pp. 11142–11147, 2006, doi: 10.1021/la061240g.

[93] H. J. Kang and F. D. Blum, 'Structure and dynamics of amino functional silanes adsorbed on silica surfaces', *J. Phys. Chem.*, vol. 95, no. 23, pp. 9391–9396, 1991, doi: 10.1021/j100176a065.

[94] M. Sypabekova, A. Hagemann, D. Rho, and S. Kim, 'Review: 3-Aminopropyltriethoxysilane (APTES) Deposition Methods on Oxide Surfaces in Solution and Vapor Phases for Biosensing Applications', *Biosensors*, vol. 13, no. 1, p. 36, Dec. 2022, doi: 10.3390/bios13010036.

[95] A. Issa and A. Luyt, 'Kinetics of Alkoxysilanes and Organoalkoxysilanes Polymerization: A Review', *Polymers*, vol. 11, no. 3, p. 537, Mar. 2019, doi: 10.3390/polym11030537.

[96] E. Metwalli, D. Haines, O. Becker, S. Conzone, and C. G. Pantano, 'Surface characterizations of mono-, di-, and tri-aminosilane treated glass substrates', *J. Colloid Interface Sci.*, vol. 298, no. 2, pp. 825–831, Jun. 2006, doi: 10.1016/j.jcis.2006.03.045.

[97] J. H. Moon, J. W. Shin, S. Y. Kim, and J. W. Park, 'Formation of Uniform Aminosilane Thin Layers: An Imine Formation To Measure Relative Surface Density of the Amine Group', *Langmuir*, vol. 12, no. 20, pp. 4621–4624, Jan. 1996, doi: 10.1021/la9604339.

[98] N. Graf, E. Yeğen, A. Lippitz, D. Treu, T. Wirth, and W. E. S. Unger, 'Optimization of cleaning and amino- silanization protocols for Si wafers to be used as platforms for biochip microarrays by surface analysis (XPS, ToF-SIMS and NEXAFS spectroscopy)', *Surf. Interface Anal.*, vol. 40, no. 3–4, pp. 180–183, Mar. 2008, doi: 10.1002/sia.2621.

[99] P. A. Heiney, K. Grüneberg, J. Fang, C. Dulcey, and R. Shashidhar, 'Structure and Growth of Chromophore-Functionalized (3-Aminopropyl)triethoxysilane Self-Assembled on Silicon', *Langmuir*, vol. 16, no. 6, pp. 2651–2657, 2000, doi: 10.1021/la990557w.

[100] Y. Uetsuji, N. Fukui, T. Yagi, and Y. Nakamura, 'The effect of number of chemical bonds on intrinsic adhesive strength of a silane coupling agent with metals: A first-principles study', *J. Mater. Res.*, vol. 37, no. 4, pp. 923–932, Feb. 2022, doi: 10.1557/s43578-022-00496-3.

[101] S. Altmann and J. Pfeiffer, 'The Hydrolysis/Condensation Behaviour of Methacryloyloxyalkylfunctional Alkoxysilanes: Structure-Reactivity Relations', *Monatshefte Fuer ChemieChemical Mon.*, vol. 134, pp. 1081–1092, Aug. 2003, doi: 10.1007/s00706-003-0615-y.

[102] B. Kannan, D. Higgins, and M. Collinson, 'Aminoalkoxysilane Reactivity in Surface Amine Gradients Prepared by Controlled-Rate Infusion', *Langmuir ACS J. Surf. Colloids*, vol. 28, Nov. 2012, doi: 10.1021/la303580c.

[103] M.-C. Brochier-Salon, P.-A. Bayle, M. Abdmouleh, and N. Belgacem, 'Kinetics of hydrolysis and self-condensation reaction of silanes by NMR spectroscopy', *Colloids Surf. Physicochem. Eng. Asp.*, vol. 312, pp. 83–91, Jan. 2008, doi: 10.1016/j.colsurfa.2007.06.028.

[104] H.-J. K. Frank D. Blum Wiriya Meesiri and J. E. Gambogi, 'Hydrolysis, adsorption, and dynamics of silane coupling agents on silica surfaces', *J. Adhes. Sci. Technol.*, vol. 5, no. 6, pp. 479–496, 1991, doi: 10.1163/156856191X00611.

[105] Y. Abe and T. Gunji, 'Oligo- and polysiloxanes', *Prog. Polym. Sci.*, vol. 29, no. 3, pp. 149–182, 2004, doi: https://doi.org/10.1016/j.progpolymsci.2003.08.003.

[106] G. Jia and Q.-H. Wan, 'Separation and identification of oligomeric vinylmethoxysiloxanes by gradient elution chromatography coupled with electrospray ionization mass spectrometry', *J. Chromatogr. A*, vol. 1395, pp. 129–135, 2015, doi: https://doi.org/10.1016/j.chroma.2015.03.079.

[107] M.-C. Brochier Salon and M. N. Belgacem, 'Competition between hydrolysis and condensation reactions of trialkoxysilanes, as a function of the amount of water and the nature of the organic group', *Colloids Surf. Physicochem. Eng. Asp.*, vol. 366, no. 1–3, pp. 147–154, Aug. 2010, doi: 10.1016/j.colsurfa.2010.06.002.

[108] R. Pietschnig and S. Spirk, 'The chemistry of organo silanetriols', *Coord. Chem. Rev.*, vol. 323, pp. 87–106, Sep. 2016, doi: 10.1016/j.ccr.2016.03.010.

[109] B. Arkles, J. R. Steinmetz, J. Zazyczny, and P. Mehta, 'Factors contributing to the stability of alkoxysilanes in aqueous solution', *J. Adhes. Sci. Technol.*, vol. 6, no. 1, pp. 193–206, Jan. 1992, doi: 10.1163/156856192X00133.

[110] B. Arkles, J. Steinmetz, J. Zazyczny, and M. Zolotnitsky, 'Stable, Water-Borne Silane Coupling Agents', Feb. 1991.

[111] M. Masmoudi, C. Rahal, M. Abdelmouleh, and R. Abdelhedi, 'Hydrolysis process of γ-APS and characterization of silane film formed on copper in different conditions', *Appl. Surf. Sci.*, vol. 286, pp. 71–77, Dec. 2013, doi: 10.1016/j.apsusc.2013.09.018.

[112] B. Arkles, 'Silane Coupling Agents'.

[113] Gelest, 'Aqueous Systems & Water-Borne Silanes', *Technical Brochure*, [Online]. Available: https://technical.gelest.com/brochures/silane-coupling-agent/special-topics/#aqueous-systems-water-borne-silanes

[114] 'Products. Gelest', [Online]. Available: https://www.gelest.com/

[115] H. K. Pulker, 'Chapter 5 - Glass and Thin Films', in *Coatings on Glass (Second Edition)*, Second Edition., H. K. Pulker, Ed., Amsterdam: Elsevier, 1999, pp. 73–102. doi: https://doi.org/10.1016/B978-044450103-5/50008-X.

[116] G. C. Allen, F. Sorbello, C. Altavilla, A. Castorina, and E. Ciliberto, 'Macro-, micro- and nano-investigations on 3-aminopropyltrimethoxysilane self-assembly-monolayers', *Thin Solid Films*, vol. 483, no. 1–2, pp. 306–311, Jul. 2005, doi: 10.1016/j.tsf.2004.12.062.

[117] X. Liu, J. L. Thomason, and F. R. Jones, 'XPS and AFM Study of Interaction of Organosilane and Sizing with E-Glass Fibre Surface', *J. Adhes.*, vol. 84, no. 4, pp. 322–338, Apr. 2008, doi: 10.1080/00218460802004386.

[118] J. Kim, P. Seidler, C. Fill, and L. S. Wan, 'Investigations of the effect of curing conditions on the structure and stability of amino-functionalized organic films on silicon substrates by Fourier transform infrared spectroscopy, ellipsometry, and fluorescence microscopy', *Surf. Sci.*, vol. 602, no. 21, pp. 3323–3330, Nov. 2008, doi: 10.1016/j.susc.2008.09.001.

[119] Y. Xie, C. A. S. Hill, Z. Xiao, H. Militz, and C. Mai, 'Silane coupling agents used for natural fiber/polymer composites: A review', *Compos. Part Appl. Sci. Manuf.*, vol. 41, no. 7, pp. 806–819, Jul. 2010, doi: 10.1016/j.compositesa.2010.03.005.

[120] Wang, D., Jones, F.R., 'Surface analytical study of the interaction between y-amino propyl triethoxysilane and E-glass surface. Part II X-ray photoelectron spectroscopy.', *J Mater Sci*, vol. 28, pp. 2481–2488, 1993, doi: https://doi.org/10.1007/BF01151683.

[121] Wang, D., Jones, F.R. & Denison, P., 'Surface analytical study of the interaction between γ-amino propyl triethoxysilane and E-glass surface.', *J Mater Sci*, vol. 27, pp. 36–48, 1992, doi: https://doi.org/10.1007/BF02403641.

[122] P. H. Harding and J. C. Berg, 'The adhesion promotion mechanism of organofunctional silanes', *J. Appl. Polym. Sci.*, vol. 67, no. 6, pp. 1025–1033, Feb. 1998, doi: 10.1002/(SICI)1097-4628(19980207)67:6<1025::AID-APP9>3.0.CO;2-K.

[123] X. M. Liu, J. Thomason, and F. R. Jones, 'The concentration of hydroxyl groups on glass surfaces and their effect on the structure of silane deposits', in *Silanes and other Coupling Agents*, 2009, pp. 25–38.

[124] 'Surface Preparation for Film and Coating Deposition Processes', in *Handbook of Deposition Technologies for Films and Coatings*, Elsevier, 2010, pp. 93–134. doi: 10.1016/B978-0-8155-2031-3.00003-X.

[125] J. J. Cras, C. A. Rowe-Taitt, D. A. Nivens, and F. S. Ligler, 'Comparison of chemical cleaning methods of glass in preparation for silanization', *Biosens. Bioelectron.*, vol. 14, no. 8–9, pp. 683–688, Dec. 1999, doi: 10.1016/S0956-5663(99)00043-3.

[126] F. J. Fuchs, '19 - Ultrasonic cleaning and washing of surfaces', in *Power Ultrasonics*, J. A. Gallego-Juárez and K. F. Graff, Eds., Oxford: Woodhead Publishing, 2015, pp. 577–609. doi: https://doi.org/10.1016/B978-1-78242-028-6.00019-3.

[127] F. J. Fuchs, 'New Ultrasonic Technology Improves Cleaning and Prevents Surface Damage Due to Cavitation Erosion Effects'.

[128] G. A. C. M. Spierings, 'Wet chemical etching of silicate glasses in hydrofluoric acid based solutions', *J. Mater. Sci.*, vol. 28, no. 23, pp. 6261–6273, Dec. 1993, doi: 10.1007/BF01352182.

[129] E. Kondoh, M. R. Baklanov, F. Jonckx, and K. Maex, 'Characterisation of HF-last cleaning of ion-implanted Si surfaces', *Mater. Sci. Semicond. Process.*, vol. 1, no. 2, pp. 107–117, Sep. 1998, doi: 10.1016/S1369-8001(98)00014-6.

[130] A. Poulon-Quintin *et al.*, 'Chemical surface modification of lithium disilicate needles of a silica-based ceramic after HF-etching and ultrasonic bath cleaning: Impact on the chemical bonding with silane', *Dent. Mater.*, vol. 37, no. 5, pp. 832–839, May 2021, doi: 10.1016/j.dental.2021.02.006.

[131] K. Terpilowski and D. Rymuszka, 'Surface properties of glass plates activated by air, oxygen, nitrogen and argon plasma', *Glass Phys. Chem.*, vol. 42, no. 6, pp. 535–541, Nov. 2016, doi: 10.1134/S1087659616060195.

[132] S. Sihelník *et al.*, 'Atmospheric-pressure air plasma sources for cleaning and activation of float soda-lime glass: Effects and comparison', *Surf. Interfaces*, vol. 40, p. 103080, Aug. 2023, doi: 10.1016/j.surfin.2023.103080.

[133] D. Li, M. Xiong, S. Wang, X. Chen, S. Wang, and Q. Zeng, 'Effects of low-temperature plasma treatment on wettability of glass surface: Molecular dynamic simulation and experimental study', *Appl. Surf. Sci.*, vol. 503, p. 144257, Feb. 2020, doi: 10.1016/j.apsusc.2019.144257.

[134] B. R. Gupta, 'Friction and wear mechanism of polymers, their composites and nanocomposites', in *Tribology of Polymers, Polymer Composites, and Polymer Nanocomposites*, Elsevier, 2023, pp. 51–117. doi: 10.1016/B978-0-323-90748-4.00012-1.

[135] I. Hutchings and P. Shipway, 'Lubricants and lubrication', in *Tribology*, Elsevier, 2017, pp. 79–105. doi: 10.1016/B978-0-08-100910-9.00004-0.

[136] Carlo G Pantano, Distinguished Professor of Materials, Science and Engineering, and Penn State University, 'Glass Surface Treatments: Commercial Processes Used in Glass Manufacture', *Lecture 10*, [Online]. Available: https://www.lehigh.edu/imi/teched/GlassProcess/Lectures/Lecture10_Pantano_Surface_Treatments

[137] X. Wang, J. Huang, and Z. Guo, 'Overview of the development of slippery surfaces: Lubricants from presence to absence', *Adv. Colloid Interface Sci.*, vol. 301, p. 102602, Mar. 2022, doi: 10.1016/j.cis.2022.102602.

[138] D. H. Lee and R. A. Condrate, 'FTIR spectral characterization of thin film coatings of oleic acid on glasses: I. Coatings on glasses from ethyl alcohol', 1998.

[139] 'Tegoglas® OL80 cold-end container glass coating', [Online]. Available: https://www.arkema.com/global/en/products/product-finder/product/organicperoxide/glass-coating/tegoglasol80/

[140] 'Tegoglas® RP40 cold-end container glass coating', [Online]. Available: https://www.arkema.com/global/en/products/product-finder/product/organicperoxide/glass-coating/tegoglasrp40/

[141] N. Dixit and D. S. Kalonia, 'Silicone Oil in Biopharmaceutical Containers: Applications and Recent Concerns', in *Concise Encyclopedia of High Performance Silicones*, 1st ed., A. Tiwari and M. D. Soucek, Eds., Wiley, 2014, pp. 381–394. doi: 10.1002/9781118938478.ch25.

[142] 'US Patent for Glass articles with low-friction coatings Patent', [Online]. Available: https://patents.justia.com/patent/11737951

[143] K. Chaudhary, 'Thin Film Deposition: Solution Based Approach', 2021. doi: 10.5772/intechopen.94455.

[144] T. Carey, C. Jones, F. Le Moal, D. Deganello, and F. Torrisi, 'Spray-Coating Thin Films on Three-Dimensional Surfaces for a Semitransparent Capacitive-Touch Device', *ACS Appl. Mater. Interfaces*, vol. 10, no. 23, pp. 19948–19956, 2018, doi: 10.1021/acsami.8b02784.

[145] L. Filipovic *et al.*, 'A Method for Simulating Spray Pyrolysis Deposition in the Level Set Framework', *Eng. Lett.*, vol. 21, pp. 224–240, Nov. 2013.

[146] Z. Wu, Y. Chen, H. Liu, W. Hua, J. Duan, and L. Kong, 'A Review of the Developments of the Characteristics and Mechanisms of Airless Spraying on Complex Surfaces', *Coatings*, vol. 13, p. 2095, Dec. 2023, doi: 10.3390/coatings13122095.

[147] T. Huhtamäki, X. Tian, J. Korhonen, and R. Ras, 'Surface-wetting characterization using contact-angle measurements', *Nat. Protoc.*, vol. 13, Jul. 2018, doi: 10.1038/s41596-018-0003-z.

[148] D. Y. Kwok and A. W. Neumann, 'Contact angle measurement and contact angle interpretation', *Adv. Colloid Interface Sci.*, vol. 81, no. 3, pp. 167–249, 1999, doi: https://doi.org/10.1016/S0001-8686(98)00087-6.

[149] 'https://www.exactoinc.com/blog/2022/11/07/what-contact-angle-reveals-about-wetting-agents-surfactants/'.

[150] D. Leonard, G. Chandler, and S. Seraphin, 'Scanning Electron Microscopy', vol. 2, 2012. doi: 10.1002/0471266965.com081.pub2.

[151] 'https://www.technologynetworks.com/analysis/articles/sem-vs-tem-331262'.

[152] 'https://myscope.training/SEM_Beam_specimen_interactions'.

[153] G. Binnig, C. F. Quate, and Ch. Gerber, 'Atomic Force Microscope', *Phys Rev Lett*, vol. 56, no. 9, pp. 930–933, Mar. 1986, doi: 10.1103/PhysRevLett.56.930.

[154] S. Magonov and M. Whangbo, *Surface Analysis with STM and AFM: Experimental and Theoretical Aspects of Image Analysis*. 2007. doi: 10.1002/9783527615117.

[155] B. Alunda and Y. Lee, 'Review: Cantilever-Based Sensors for High Speed Atomic Force Microscopy', *Sensors*, vol. 20, p. 4784, Aug. 2020, doi: 10.3390/s20174784.

[156] S. Akhtar, 'Applications of Atomic Force Microscopy in Corrosion Research', in *Recent Developments in Analytical Techniques for Corrosion Research*, I. ulhaq Toor, Ed., Cham: Springer International Publishing, 2022, pp. 187–201. doi: 10.1007/978-3-030-89101-5_9.

[157] 'Fourier Transforms', in *Fourier Transform Infrared Spectrometry*, John Wiley & Sons, Ltd, 2007, pp. 75–95. doi: https://doi.org/10.1002/9780470106310.ch4.

[158] I. S. A. W. Committee, D. R. Brezinski, J. M. Julian, ed Brezinski, and C. S. for C. T. I. S. Committee, *An Infrared Spectroscopy Atlas for the Coatings Industry*. Federation of Societies for Coatings Technology, 1991. [Online]. Available: https://books.google.it/books?id=7opCPwAACAAJ

[159] 'https://www.edinst.com/blog/what-is-ftir-spectroscopy/'.

[160] 'Attenuated Total Reflection', in *Fourier Transform Infrared Spectrometry*, John Wiley & Sons, Ltd, 2007, pp. 321–348. doi: https://doi.org/10.1002/9780470106310.ch15.

[161] Nefedov, V.I., *X-Ray Photoelectron Spectroscopy of Solid Surfaces*, 1 st. CRC Press., 1988. [Online]. Available: https://doi.org/10.1201/9780429070587

[162] 'https://www.coretechint.com/en/technical_info/theory_detail/1/'.

[163] O. S. Heavens, 'Some factors influencing the adhesion of films produced by vacuum evaporation', *J. Phys. Radium*, vol. 11, pp. 355–360, 1950.

[164] A. J. Perry, 'Scratch adhesion testing of hard coatings', *Thin Solid Films*, vol. 107, no. 2, pp. 167–180, 1983, doi: https://doi.org/10.1016/0040-6090(83)90019-6.

[165] P. J. Burnett and D. S. Rickerby, 'The relationship between hardness and scratch adhession', *Thin Solid Films*, vol. 154, no. 1, pp. 403–416, 1987, doi: https://doi.org/10.1016/0040-6090(87)90382-8.

[166] N. X. Randall, 'The current state-of-the-art in scratch testing of coated systems', *Surf. Coat. Technol.*, vol. 380, p. 125092, 2019, doi: https://doi.org/10.1016/j.surfcoat.2019.125092.

[167] K. G. Budinski, 'Laboratory Testing Methods for Solid Friction', in *Friction, Lubrication, and Wear Technology*, ASM International, 2017. doi: 10.31399/asm.hb.v18.a0006361.

[168] J. Hintikka, A. Mäntylä, J. Vaara, T. Frondelius, and A. Lehtovaara, 'Stable and unstable friction in fretting contacts', *Tribol. Int.*, vol. 131, pp. 73–89, Oct. 2018, doi: 10.1016/j.triboint.2018.10.014.

[169] J. K. Lancaster, '"Introduction to friction", ASM handbook, volume 18, friction, lubrication and wear technology: Volume chairman, Peter J. Blau', *Tribol. Int.*, vol. 26, no. 4, pp. 25–26, 1992, doi: https://doi.org/10.1016/0301-679X(93)90010-X.

[170] M. J. Valdes, J. G. Ardila Marín, M. A. Rodriguez-Cabal, and J. D. Betancur, 'TRIBOMETRY: How is friction research quantified? A review', *Int. J. Eng. Res. Technol.*, vol. 13, no. 10, p. 2596, Oct. 2020, doi: 10.37624/IJERT/13.10.2020.2596-2610.

[171] 'ASTM G99-17 . Standard Test Method for Wear Testing with a Pin-on-Disk Apparatus', doi: 10.1520/G0099-17.

[172] 'https://wiki.anton-paar.com/en/basics-of-tribology/'.

[173] 'ASTM G133-22. Standard Test Method for Linearly Reciprocating Ball-on-Flat Sliding Wear', doi: 10.1520/G0133-22.

[174] R. Falcone, F. Licenziati, E. Orsega, and M. Verità, 'The dependence of the weathering of soda-lime-silica glass on environmental parameters: A preliminary investigation', *Glass Technol. - Eur. J. Glass Sci. Technol. Part A*, vol. 52, pp. 23–29, Feb. 2011.

[175] N. J. Smith and C. G. Pantano, 'Leached Layer Formation on Float Glass Surfaces in the Presence of Acid Interleave Coatings', *J. Am. Ceram. Soc.*, vol. 91, no. 3, pp. 736–744, 2008, doi: https://doi.org/10.1111/j.1551-2916.2007.02079.x.

[176] M. Ouis, W. Abd-Allah, and O. Sallam, 'Gamma ray interaction with soda lime silicate glasses doped with V2O5, CuO or SrO', *Appl. Phys. A*, vol. 128, Apr. 2022, doi: 10.1007/s00339-022-05522-z.

[177] R. Peña-Alonso, F. Rubio, J. Rubio, and J. Oteo, 'Study of the hydrolysis and condensation of gamma- Aminopropyltriethoxysilane by FT-IR spectroscopy', *J. Mater. Sci. - J MATER SCI*, vol. 42, pp. 595–603, Jan. 2007, doi: 10.1007/s10853-006-1138-9.

[178] C.-H. Chiang, H. Ishida, and J. L. Koenig, 'The structure of γ-aminopropyltriethoxysilane on glass surfaces', *J. Colloid Interface Sci.*, vol. 74, no. 2, pp. 396–404, 1980, doi: https://doi.org/10.1016/0021-9797(80)90209-X.

[179] E. Metwalli, D. Haines, O. Becker, S. Conzone, and C. G. Pantano, 'Surface characterizations of mono-, di-, and tri-aminosilane treated glass substrates', *J. Colloid Interface Sci.*, vol. 298, no. 2, pp. 825–831, Jun. 2006, doi: 10.1016/j.jcis.2006.03.045.

[180] D. V. Okhrimenko *et al.*, 'Hydrolytic Stability of 3-Aminopropylsilane Coupling Agent on Silica and Silicate Surfaces at Elevated Temperatures', *ACS Appl. Mater. Interfaces*, vol. 9, no. 9, pp. 8344–8353, Mar. 2017, doi: 10.1021/acsami.6b14343.

[181] B. Roy, F. Baier, A. Rosin, T. Gerdes, and S. Schafföner, 'Structural characterization of the near-surface region of soda–lime–silica glass by X-ray photoelectron spectroscopy', *Int. J. Appl. Glass Sci.*, vol. 14, no. 2, pp. 229–239, 2023, doi: https://doi.org/10.1111/ijag.16604.

[182] C. Luo *et al.*, 'Role of Interfacial Bonding in Tribochemical Wear', *Front. Chem.*, vol. 10, p. 852371, Apr. 2022, doi: 10.3389/fchem.2022.852371.

[183] B. Juretzka, S. Wieber, R. Wilkens, M. Hagemann, R. E. Kolb, and R. Riedel, 'Tribological Behavior of Film Forming Organosilane/-Siloxane Oil Additives: Film Characterization and Influences on Lubrication', *Tribol. Lett.*, vol. 68, 2019, [Online]. Available: https://api.semanticscholar.org/CorpusID:208279020

[184] L. Yang, L. Bin, H. Yichuan, D. Yuncheng, and W. Shiguo, 'Effect of silane coating surface treatment on friction and wear properties of carbon fiber/PI composites', *Mater. Sci.-Pol.*, vol. 40, no. 2, pp. 214–222, Aug. 2022, doi: 10.2478/msp-2022-0022.

[185] C. Panagopoulos, E. Georgiou, G. Tradas, and K. Giannakopoulos, 'Wear Behaviour of Nanostructured Polymer-Based Safety Films on Soda-Lime Glass', *Coatings*, vol. 6, no. 3, p. 26, Jul. 2016, doi: 10.3390/coatings6030026.

[186] L. G. Yu, E. S. Yamaguchi, M. Kasrai, and G. M. Bancroft, 'Study of silane-based antiwear additives: Wear and chemistry', *Tribol. Int.*, vol. 44, no. 6, pp. 692–701, Jun. 2011, doi: 10.1016/j.triboint.2010.03.005.

[187] W. Morales, R. L. Fusaro, M. Siebert, T. Keith, R. Jansen, and P. Herrera-Fierro, 'A New Antiwear Additive/Surface Pretreatment for PFPE Liquid Lubricants', *Tribol. Trans.*, vol. 40, no. 2, pp. 321–329, Jan. 1997, doi: 10.1080/10402009708983661.

[188] B. Kafle *et al.*, 'Fourier-transform infrared spectroscopy for characterization of liquid protein solutions: A comparison of two sampling techniques', *Vib. Spectrosc.*, vol. 124, p. 103490, 2023, doi: https://doi.org/10.1016/j.vibspec.2022.103490.

[189] V. Houérou, J.-C. Sangleboeuf, and T. Rouxel, 'Scratchability of Soda-Lime Silica (SLS) Glasses: Dynamic Fracture Analysis', *Key Eng. Mater. - KEY ENG MAT*, vol. 290, pp. 31–38, Jul. 2005, doi: 10.4028/www.scientific.net/KEM.290.31.

[190] V. L. Houérou, J.-C. Sangleboeuf, S. Dériano, T. Rouxel, and G. Duisit, 'Surface damage of soda–lime–silica glasses: indentation scratch behavior', *J. Non-Cryst. Solids*, vol. 316, no. 1, pp. 54–63, 2003, doi: https://doi.org/10.1016/S0022-3093(02)01937-3.

[191] P. Bandyopadhyay, A. Dey, S. Roy, and A. K. Mukhopadhyay, 'Effect of load in scratch experiments on soda lime silica glass', *J. Non-Cryst. Solids*, vol. 358, no. 8, pp. 1091–1103, 2012, doi: https://doi.org/10.1016/j.jnoncrysol.2012.02.006.

[192] I. Zakiev, G. A. Gogotsi, M. Storchak, and V. Zakiev, 'Glass Fracture during Micro-Scratching', *Surfaces*, vol. 3, no. 2, pp. 211–224, Jun. 2020, doi: 10.3390/surfaces3020016.

[193] B. Li, P. Li, R. Zhou, X.-Q. Feng, and K. Zhou, 'Contact mechanics in tribological and contact damage-related problems: A review', *Tribol. Int.*, vol. 171, p. 107534, Jul. 2022, doi: 10.1016/j.triboint.2022.107534.

Acknowledgements

I would like to extend my gratitude to my academic supervisor, Dr. Giovanna Trevisi (IMEM-CNR, Parma), and the director, Dr. Andrea Zappettini (IMEM-CNR, Parma), for their invaluable guidance throughout my doctoral journey and for fostering a strong collaboration with Bormioli Pharma S.p.A. I am also grateful to my industrial supervisors, Eng. Davide Faverzani, Dr. Michele Poncini, and Dr. Davide Costa (Bormioli Pharma S.p.A.), who welcomed me into their facilities, providing invaluable insights into production processes and associated challenges.

A special thank you to Dr. Francesca Casoli and Dr. Lucia Nasi (IMEM-CNR, Parma) for their support with AFM microscopy training and analyses, and again to Dr. Giovanna Trevisi for guidance in SEM microscopy. My sincere thanks go to Dr. Davide Calestani (IMEM-CNR, Parma) for his assistance with sample metallization and to Dr. Francesca Rossi and Dr. Filippo Vurro for their help with the plasma cleaner, and Dr. Giulia Spaggiari for her assistance with preliminary Raman spectroscopy analyses. I am grateful to Dr. Letizia Savio (IMEM-CNR, Genoa) for her expertise in XPS measurement analysis and to Dr. Valentina Sinisi (IMEM-CNR, Parma) for her contributions to FT-IR solution measurements and her support during the thesis writing process. I am also thankful to Prof. Matteo Tegoni and Prof. Lara Righi (University of Parma) for access to FT-IR equipment, with particular appreciation to Prof. Righi for her interest in my research. I would like to thank all my colleagues at IMEM-CNR in Parma who have accompanied and supported me over the years and with whom I have shared unforgettable moments. Thanks to all of them, my workplace has become a second home, where moments of conviviality are pleasant and constructive. Here I have found true friendships.

I would like to acknowledge Dr. Giovanna Gautier, Dr. Maria Giulia Faga and Dr. Mattia Di Maro (STEMS-CNR, Turin) for welcoming me into their institute to conduct mechanical analyses on the samples.

During my time abroad at CEITEC in Brno, I was fortunate to work with Dr. Ladislav Čelko, Dr. Michaela Remešová, and Dr. Vendula Bednaříková (CEITEC, Brno), whose mentorship was invaluable. A special thanks to Eng. Marek Doubrava (University of Technology, Brno) for his

guidance with scratch measurements and data interpretation—his generosity and availability left a lasting impression.

I am also deeply appreciative of Prof. Amirhossein Pakseresht and Dr. Omid Sharifahmadian (FunGlass Institute, Trencin), who warmly supported me during my stay at their institute. Thanks as well to Eng. Michal Krbaťa (Alexander Dubček University of Trenčín) for conducting mechanical measurements on the samples. These international experiences greatly enriched my personal and professional growth. I would especially like to thank Zina Pavloušková, Senior Reserchер (CEITEC-Brno) and all the wonderful friends I found along the way, who made me feel unexpectedly at home.